EPRASHEED
signature series

2011 – Issue 21

Saudi Arabia oil & gas

Saudi Arabia Oil & Gas (Print) ISSN 2045-6670
www.saudiarabiaoilandgas.com
Saudi Arabia Oil & Gas (Online) ISSN 2045-6689

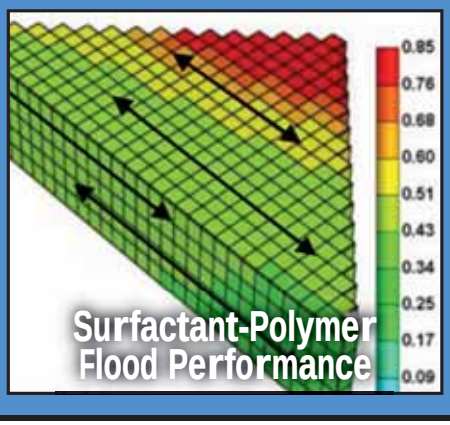

Surfactant-Polymer Flood Performance

Inside

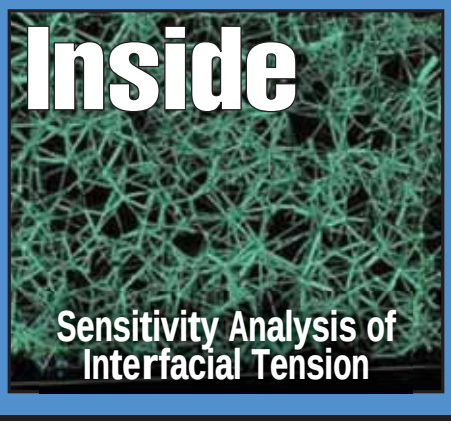

Sensitivity Analysis of Interfacial Tension

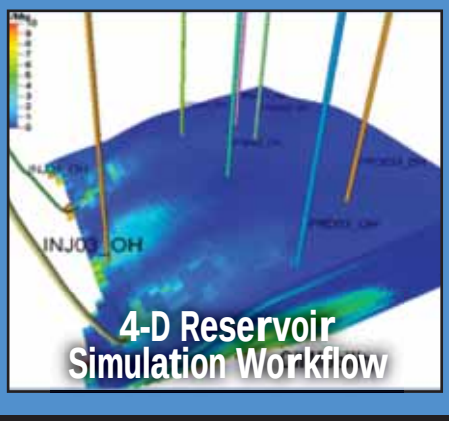

4-D Reservoir Simulation Workflow

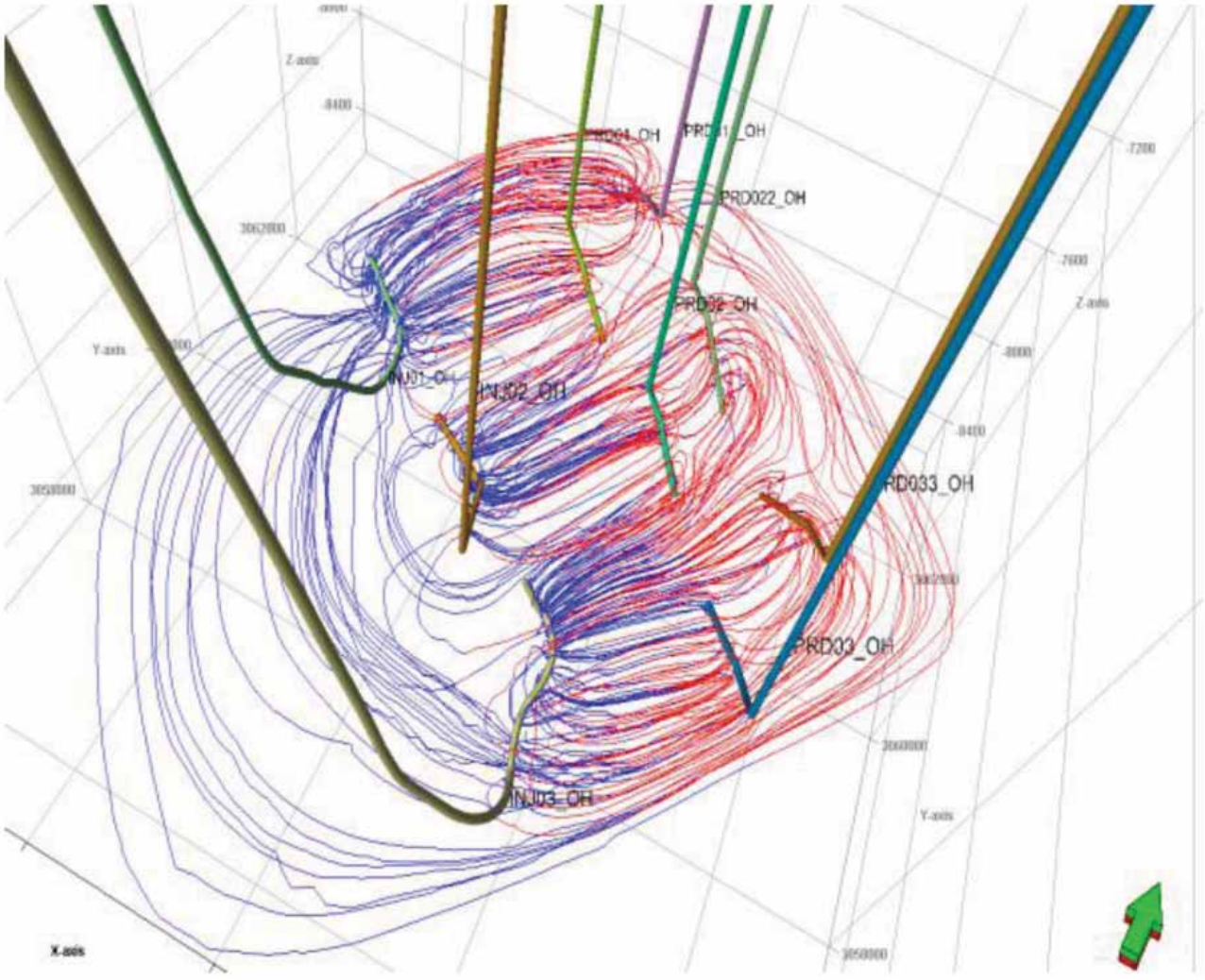

Streamline simulation pattern of polymer flooding.

مدينة الملك عبدالعزيز
للعلوم والتقنية KACST
Oil and Gas Research Institute

Seismic Analysis Center

Our Vision Is to be the leading soultion provider for seismic processing and imaging in the arabian peninsula

SAC - KACST - P.O. Box. 6086 Riyadh 11442
Tel. : +966 1 4814324 - FAx : +966 1 4814314

www.sac.edu.sa

Who is going to help discover the energy for a global population expected to grow 20% by 2025?

Join us, and you will.

At Chevron, we're dedicated to providing the energy the world needs to keep moving forward. Here you can be part of a diverse team of professionals from different disciplines and skill sets working together. A team that welcomes tomorrow's challenges and believes the best way to solve them is through collaboration. So no matter what your expertise, you'll have the tools and support to make a difference every day. Find out how far your skills and talents can take you. For local and global opportunities, visit us online today.

Chevron

Human Energy®

An equal opportunity employer that values diversity and fosters a culture of inclusion.

مدينة الملك عبدالعزيز
للعلوم والتقنية KACST

Oil and Gas Research Institute

Hydrocarbon resources (crude oil and gas) are the main source of world energy, and as the international demand increases, the technical challenges increase to meet that demand. Hydrocarbon production optimization at minimum cost and the need to serve the national petroleum industry has been the driving force behind the establishment of the Oil and Gas Research Institute (OGRI) at King Abdulaziz City for Science and Technology (KACST). OGRI is a governmental research and development entity. Its applied research activities concentrate on the upstream sector of the petroleum industry. Fields of interest cover most of the petroleum science and engineering aspects through four main divisions:

- Reservoir Characterization and Numerical Simulation,
- Drilling Engineering,
- Rock Mechanics,
- Production and Enhanced Recovery.

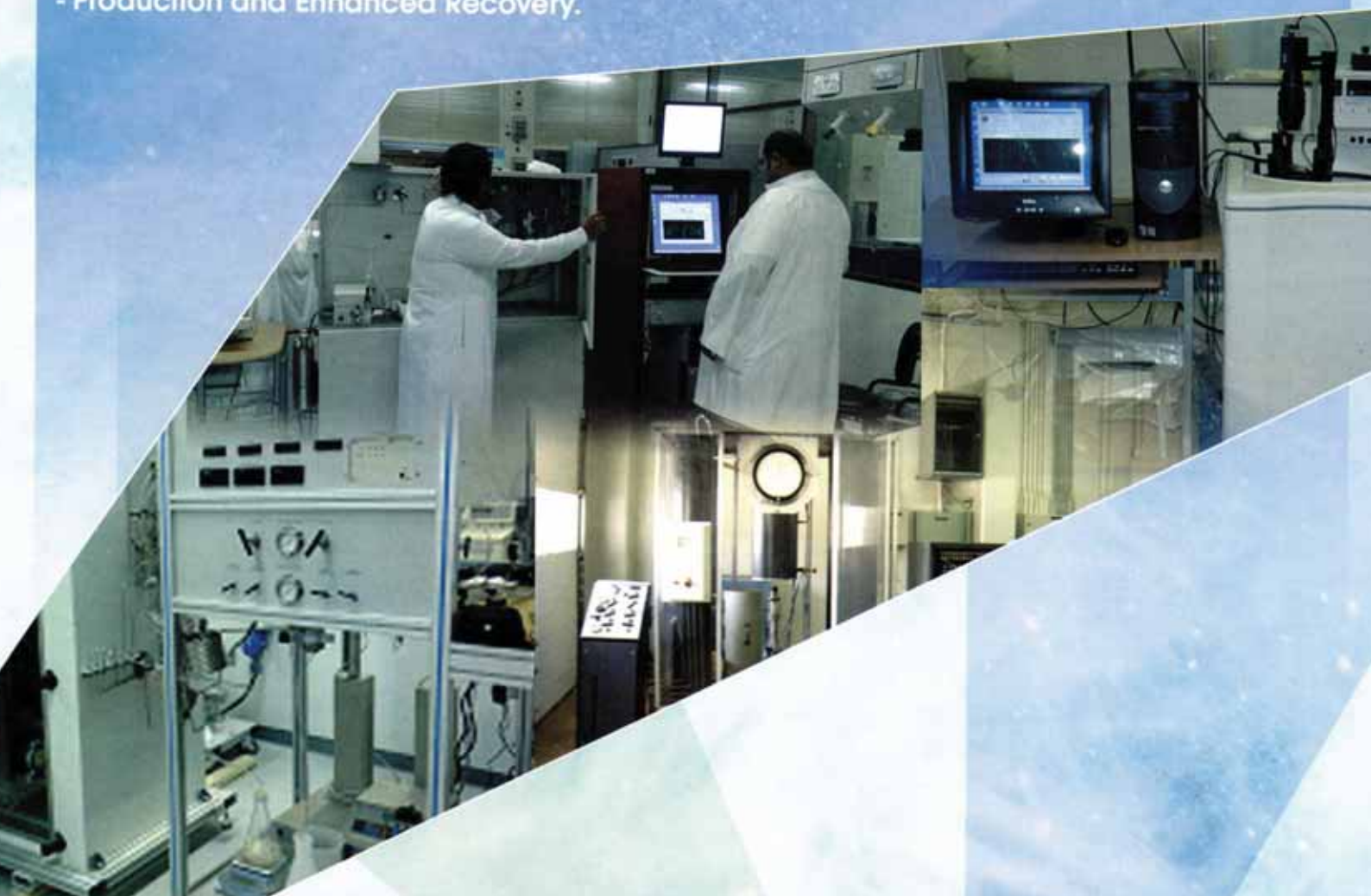

Services Provided

Service	Techniques
CONVENTIONAL CORE ANALYSIS	➤ Helium Porosity (Ambient Conditions) ➤ Gas Permeability & Porosity (Low and Reservoir Overburden Stress) ➤ Klinkenberg Correction ➤ Liquid Permeability (Reservoir Conditions)
SPECIAL CORE ANALYSIS (SCAL)	**CAPILLARY PRESSURE TESTS** ➤ Centrifuge Techniques (Reservoir Conditions) ➤ Low and High Pressure Mercury Injection and Withdrawal Technique ➤ Pore Size Distribution (PSD) **RELATIVE PERMEABILITY MEASUREMENTS** ➤ Unsteady State Flooding Technique (Reservoir Conditions) ➤ Centrifuge Technique (Reservoir Conditions) **WETTABILITY TESTS** ➤ Centrifuge USBM Method ➤ Contact angle Measurement (Ambient and Reservoir Conditions) ➤ Interfacial Tension Measurements **PETROGRAPHIC SERVICES** ➤ Sieve Analysis ➤ Particle Size Analysis ➤ Thin section
RESERVOIR FLUID ANALYSIS	➤ Interfacial & Surface tension ➤ Gas and Gas Condensate Viscosity ➤ Refractive index and pH ➤ Contact angle
ADVANCED RESERVOIR ENGINEERING	➤ Water-Oil /Water-Gas Displacement ➤ Gas Flooding and WAG ➤ Chemical Flooding
PETROLEUM RELATED ROCK MECHANICS	➤ Uniaxial, Triaxial, and Hydrostatic Compressive strength ➤ Stress-Strain Behavior ➤ Failure Envelope ➤ Elastic moduli ➤ Bulk and Pore Compressibility ➤ Fracture Toughness

OGRI - KACST - K.S.A - P.O. Box. 6086 Riyadh 11442
Tel. : +966 1 4813307 Fax : +966 1 4813526

EPRASHEED
signature series
2011 – Issue 21
Saudi Arabia oil & gas
www.saudiarabiaoilandgas.com

Contents

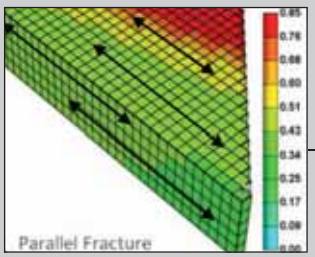

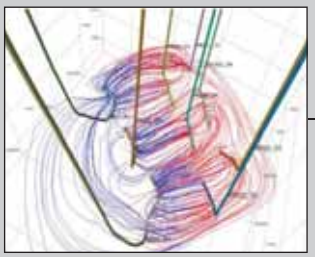

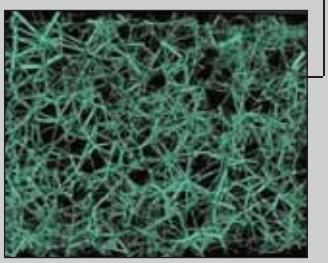

CEO and Founder
EPRasheed
Wajid Rasheed
wajid.rasheed@eprasheed.com

Editors
Majid Rasheed
Mauro Martins

Design
Sue Smith
sue.smith@eprasheed.com

United Kingdom
► Head Office
Tel: (44) 207 193 1602

► Adam Mehar
adam.mehar@saudiarabiaoilandgas.com
Main: (44) 1753 708872
Fax: (44) 1753 725460
Mobile: (44) 777 2096692

Saudi Arabia
► Akram ul Haq
PO BOX 3260, Jeddah 21471
akram.ul.haq@saudiarabiaoilandgas.com
Tel: (966) 557 276 426

► Mohanned AlSagri
mohanned.alsagri@saudiarabiaoilandgas.com

Brazil
► Ana Felix
afelix@braziloilandgas.com
Tel: (55) 21 9714 8690

► Fabio Jones
fabio.jones@braziloilandgas.com
Tel: (55) 21 9392 7821

► Roberto S. Zangrando
rzangrando@braziloilandgas.com
Tel: (55) 22 8818 8507

MASTERGEAR UK

The **Stainless Steel** Gearbox Range.

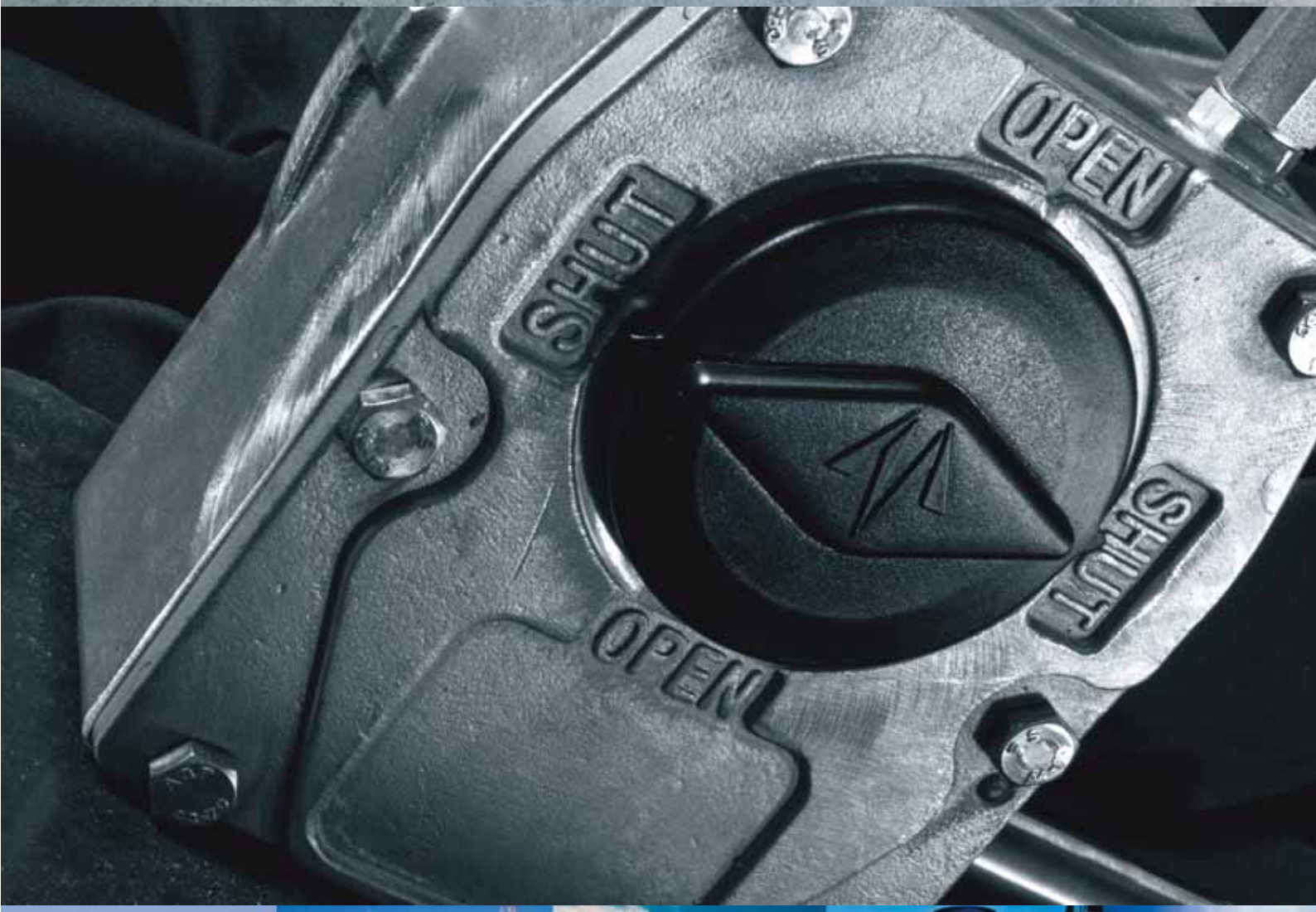

Built to withstand the World's most **extreme environments.**

www.mastergearworldwide.com

New Complex Sets Course for Future

By Saudi Aramco Staff.

Al-Midra Complex is unique, dynamic, technologically advanced and environmentally aware. The complex can be described as an "intelligent building." The focus was on flexibility of design, personnel circulation and flow, energy efficiency and open plan layout.

Like those of many international companies, the offices are an open-plan layout, with common areas for networking and conference rooms that seat 15–60 persons.

The services center contains a gymnasium for women, while the nearby multi-purpose facility, which is also part of the Al-Midra Complex, has a gymnasium for men, so that everyone has a convenient place for exercise before or after work. The multipurpose facility also houses a 500-seat auditorium and multipurpose room. The auditorium is world-class and can be used for meetings, presentations and conventions.

Consideration of the environment was paramount, and many "green" options were implemented. In seeking an energy efficient approach, another primary condition was also to provide a healthy and comfortable environment for employees.

Elevators: The 16 elevators in the office tower are controlled by a group control system that maximizes efficiency and gets passengers to their destinations faster with less crowding.

Solar shaded parking: Revolutionary new technology uses solar panels, doubling as sunshades over the 4,500 parking spaces, to supply 10 megawatts of energy.

Reflective exterior glass: Reflective, low-emissivity glass on Al-Midra Tower's exterior, together with the silver aluminum cladding, provides internal thermal control.

CO_2 sensors: CO_2 sensors measure carbon dioxide levels and monitor indoor air quality. This enables fresh-air intake tailored to the needs of the occupants.

Interior design: Great efforts were made in planning the interior design of Al-Midra to ensure it provided a sustainable office environment. Employees will enjoy the efficiency in space planning, high-quality materials and an ergonomic design that allows personnel to feel comfortable and safe in every aspect of their workplace. Work stations are oriented around the periphery of each floor, affording privacy and a light, airy atmosphere in which to work. The open-plan layout promotes collaboration between personnel, a necessity for project-based work. Small and large conference rooms are designed for maximum comfort in seating and high levels of interactivity. The rooms also feature technology such as plasma screens for video conferencing.

As a company, Saudi Aramco will never remain static. The company's future depends on a desire to grow, on visionary planning, commitment to excellence and hard work. These ingredients went into the construction of the Al-Midra Complex.

SRAK

شركة جنوب الربع الخالي المحدودة

South Rub Al-Khali Company Ltd.

ارامكو السعودية
Saudi Aramco

A Shell-Saudi Aramco Joint Venture

We Seek To Fuel A Better Future

www.srak.co

Under the patronage of His Royal Highness Prince Khalifa bin Salman Al Khalifa
Prime Minister of the Kingdom of Bahrain

Society of Petroleum Engineers

ufi Approved Event

MEOS 2011

17th Middle East Oil & Gas Show and Conference

Conference: 25-28 September 2011
Exhibition: 26-28 September 2011

Bahrain International Exhibition and Convention Centre

www.MEOS2011.com

NEW DATES ANNOUNCED

AN ALLWORLD EXHIBITIONS EVENT

Organisers

ادارة المعارض العربية
Arabian Exhibition Management

fawzi@aeminfo.com.bh

Worldwide Co-ordinator

oes

meos@oesallworld.com

Conference Organisers

SPE International

spedub@spe.org

Reservoir Quality, Completion Quality and Operational Efficiency in Horizontal Organic Shale Wells: Observations from a Recent Study of Production Log Data

By Camron Miller and George Waters, Schlumberger.

Abstract

Production logs from more than 100 horizontal shale wells in multiple basins have been acquired and interpreted. An evaluation of this data set confirms that production is highly variable along the length of the wellbores. In some basins, two-thirds of gas production is coming from only one third of the perforation clusters. Furthermore, when looking at all basins, almost one third of all perforation clusters are not contributing to production. This highlights a significant opportunity to improve overall completion effectiveness and economics in these high profile projects.

Observations of near-wellbore reservoir quality and completion efficiency can be attained from the analysis of this data. Rock properties such as mineralogy, natural fracture density, and closure stress in the near wellbore region impact reservoir quality and hydraulic fracture conductivity. Completion parameters such as the staging of stimulation treatments, the number of perforation clusters per frac stage, and perforation cluster spacing can all impact the productivity of an individual perforation cluster. Correlations between productivity and key geologic, petrophysical and completion parameters can be made. The result is a better understanding of the parameters that are controlling completion effectiveness, and corresponding productivity in horizontal organic shale wells.

Introduction

Operators have been drilling horizontal wells within organic shale for a number of years, with favorable economics. However, not all of these projects have been a complete success as some wells are failing to meet performance expectations. When considering the heightened risk associated with the exploration and development of unconventional gas, success rates are being watched closely and highly scrutinized. This paper reviews a recent evaluation of over 100 production logs collected within horizontal gas shale wells and attempts to explain the variability in production in terms of Reservoir Quality (RQ), Completion Quality (CQ) and Operational Efficiency (OE). Reservoir Quality is defined by those petrophysical parameters of organic

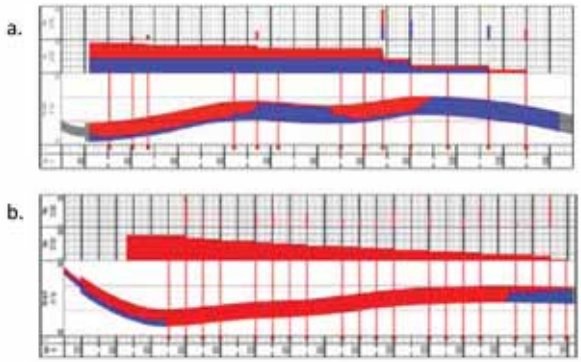

Figs 1a & 1b –Production log comparison of two Woodford Shale wells illustrating the typical variability observed in perforation performance (a) along the length of the lateral vs. the more desirable, uniform production performance (b), which can be linked to heterogeneity, well trajectory, RQ and CQ. The red color represents gas production, while blue indicates water. The red tick marks in the track from the bottom in both examples represent perforation cluster locations.

Basin	Well Count
Woodford Shale	57
Barnett Shale	34
Fayetteville Shale	7
Eagle Ford Shale	5
Haynesville Shale	5
Marcellus Shale	4
Total Wells	112

Table 1 –Shale basins represented in study and horizontal production log count by basin

shales that make them viable candidates for development. The key petrophysical parameters are: organic content, thermal maturation, effective porosity, fluid saturations, pore pressure, and Gas-In-Place.

Completion Quality is defined by those geomechanical parameters that are required to effectively stimulate organic shales. The key geomechanical parameters are: near-wellbore and far-field stresses, mineralogy, specifically clay content and type, and the presence, orientation, and nature of natural fractures. In the context of this work Operational Efficiency is defined as the completion techniques that improve the connection between the reservoir and the wellbore. This study focuses primarily on OE parameters such as perforation cluster number, length and spacing, and fracture stage number and spacing. Where data is available, RQ and CQ are evaluated to aid in the interpretation of the impact of OE parameters on production. The goal is to better understand the parameters that are controlling completion effectiveness, and corresponding productivity in horizontal organic shale wells.

Today, most laterals are drilled based on the evaluation of 3D seismic and extensive log data sets collected within offset vertical wellbores, or pilot holes. In most

cases the well is steered using a logging while drilling (LWD) gamma ray measurement which can identify significant structural changes, and in many cases vertical variations in bedding. Mud logs are also used to determine mineralogy and identify gas shows.

Production data has indicated that lateral placement has significant impact on well performance (Miller et al, 2010). While 3D seismic, offset well logs, LWD gamma ray logs and mud logs all have application, they do not address the small scale vertical variability that exists within shale reservoirs. To optimize productivity, reservoir heterogeneity must be accounted for either during drilling or stimulation.

Analysis of a large number of production logs acquired along horizontal wellbores in six U.S. gas shale basins suggests that some stimulation stages are underperforming. Figures 1a and 1b portray production log results from two horizontal Arkoma Basin Woodford Shale wells. In Figure 1a, only approximately 50% of the perforation clusters are contributing to the overall production. Figure 1b illustrates an ideal scenario where all perforation clusters are contributing, a phenomenon that only occurs in one out of every five horizontal shale wells. The authors are suggesting that well placement and stimulation with respect to RQ and CQ will result in more uniform production across perforation stages and overall better well performance. Rocks having superior RQ and CQ should be targeted as they will impart better drilling and completion efficiency.

Lateral Heterogeneity

Heterogeneity in lateral wellbores is primarily controlled by wellbore geometry and vertical variations in rock characteristics, which occur at an extremely small scale in shale reservoirs. Small scale lateral variability in reservoir properties related to diagenetic processes have been noted, but the impact on well performance is not yet clear. In general, rock properties at a log scale change slowly in a lateral direction. An exception to this would be natural fracture density, which can change rapidly. Larger scale lateral variability is primarily controlled by shale depositional processes (Bohacs, 2009). Rock properties and natural fracture distribution within shales have significant implications to horizontal stimulation. Strong relationships between natural fractures, minimum horizontal stress (σh) and mineralogy have been observed (Miller, et al, 2010). These data can be inte- grated and used to subdivide the reservoir based on lateral heterogeneity and should guide stage organization and perforation placement. Vertical and lateral variability must be addressed, preferably during drilling, in order to increase the potential for an economic success. Doing so has shown to positively impact shale productivity (Baihly, et al, 2010).

Horizontal Log Data Set

Most of the production logs used for this study are FlowScan Imager* (FSI) datasets which provide more accurate flow measurements than possible with conventional production logging tools in horizontal wells and unambiguous flow profiling regardless of phase mixing or recirculation. There are a limited number of PS Platform* (PSP) logs included in the dataset. These wells were included only when log quality data was high, essentially, when water volume is low, in order to improve the statistical significance of the dataset.

No effort has been made to compare the time at which the production logs were run. Production results may also be impacted by varying wellhead flowing pressures among the wells at the time of logging. The impact of water production on the production log results was not assessed, yet most wells were producing little fluid at the time of logging. Wells with very high water production were eliminated from this dataset. These wells are either producing fracturing fluid shortly after the stimulation treatments, or extraneous formation water. This is inferred to be fracturing fluid in most cases, although some wells were eliminated because they indeed are producing water from surrounding formations. Other wells were eliminated due to the inability of the logging tool to reach the furthest perforations.

There are six basins represented within the dataset under review in this paper. The basins and well count are shown in Table 1. The Woodford Shale and Barnett Shale make up the majority of the wells in the dataset. For this reason, basin specific correlations are constrained to these two basins in most cases as the small number of horizontal production logs in the other basins does not provide statistical significance.

Production Normalization

To respect the proprietary nature of the actual production from the wells in the dataset all production data was normalized by basin. The best producing well was assigned a normalized rate of 1.0. The flow rate from lesser producing wells is shown as a fraction relative to the best producing well. Therefore, for figures shown in this paper in which all six basins are displayed, there will be six wells showing a normalized rate of one. This was done so that wells from the Haynesville Shale did not skew the dataset, as the Haynesville Shale wells all produce at the high end of the complete well dataset.

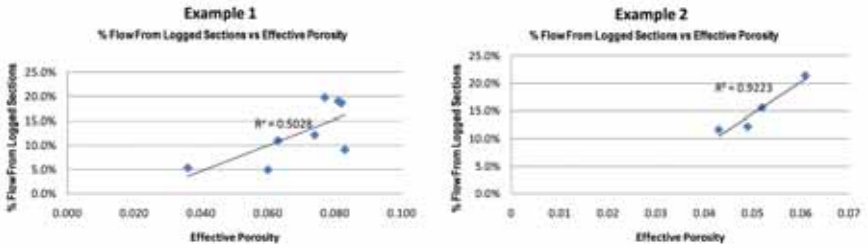

Figs 2a and 2b Plots for two wells that show a correlation between % of flow from logged sections and effective porosity

Where appropriate, figures are shown for given basins to demonstrate a particular point being made. This allows basin specific trends to be seen that may not be clearly visible when assessing the complete dataset.

Observations: RQ and CQ

Porosity and other RQ parameters from two horizontal shale wells were analyzed and compared to production log results in the same wellbore. Successful correlations between effective porosity and production were estab-lished and are shown in Figures 2a and 2b. These graphs plot effective porosity against the percent of flow from logged sections. This is used to account of the production logging tool failing to log the entire stimulated interval. Each point represents the average effective porosity over a range that is equal to the perforation cluster length, plus 10 ft on either side of the cluster. In most cases as effective porosity increases the volume of clay decreases, especially smectitic clays. The absence of expandable clays dramatically improves RQ and CQ as it generally results in higher matrix permeability and lower in-situ stresses. A higher permeability will directly impact well productivity. Low in-situ stress promotes efficient hydraulic fracturing, particularly with respect to fracture conductivity. Two wells do not make a trend, but unfortunately limited RQ data is available on wells with production logs. These two wells are from different shale basins though, so the correlation is not isolated to only a single basin.

Borehole micro-resistivity images respond to mineralogy. Resistive minerals, such as silica and calcite, appear light colored on the image log, while conductive minerals, such as clay minerals and pyrite, appear dark in color. This qualitative indication of mineralogy is very useful when landing and stimulating lateral shale wellbores. Low clay intervals are the targets in most shale plays due to their superior RQ and CQ parameters. These intervals typically contain more gas, are easier to drill and can be stimulated more easily. In silica-rich shales, such as the Barnett Shale, Fayetteville Shale and Woodford Shale, where carbonate content is relatively low, stress is inversely proportional to the resistivity of an interval when no tectonics are present (Waters, et al, 2006). In addition, the resistivity of the interval is directly related to clay volume (Waters, et al, 2006, and Miller, et al, 2010). These relationships become more complicated in shales where carbonate content is higher, such as the Haynesville shale and Eagle Ford Shale.

This paper reviews two wells which have borehole micro-resistivity images and a production log along the lateral. For these wells, production from each stimulation stage and perforation cluster was evaluated and compared to horizontal image logs in order to define relationships between production, RQ and CQ. In both examples, an inverse relationship between shallow formation resistivity and hydraulic fracture initiation pressure exists (Figs. 3a and 3b). In one of the examples, zones having more resistive mineralogy and lower fracture initiation pressures contributed greater than nominal production while those having poor RQ and CQ parameters contributed minimally (Fig. 3b). The other well also showed the same production trends, but more detailed explanation was needed since it is an infill well that was drilled across hydraulically induced fractures from offset wellbores. There are clear benefits

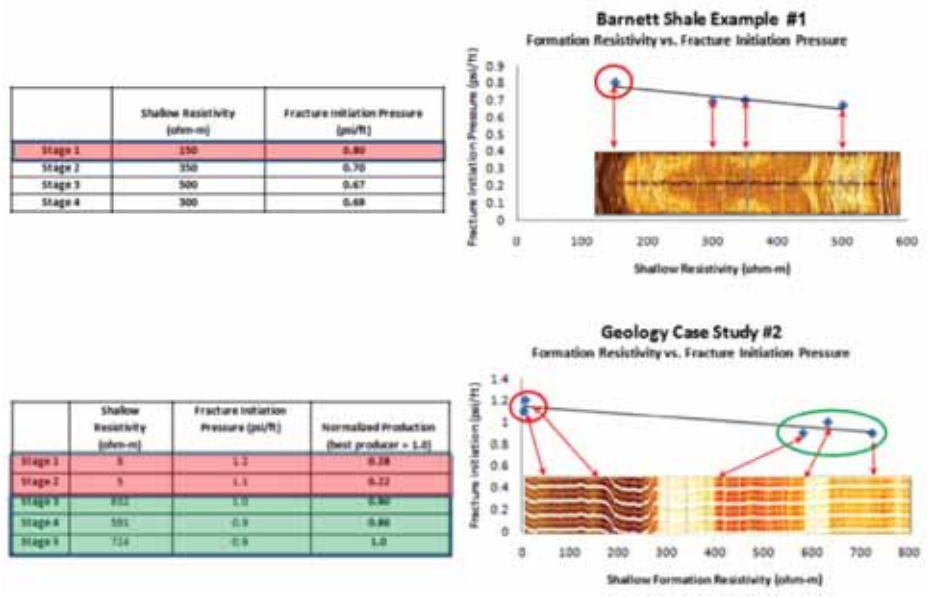

	Shallow Resistivity (ohm-m)	Fracture Initiation Pressure (psi/ft)
Stage 1	150	0.80
Stage 2	350	0.70
Stage 3	500	0.67
Stage 4	300	0.68

	Shallow Resistivity (ohm-m)	Fracture Initiation Pressure (psi/ft)	Normalized Production (best producer = 1.0)
Stage 1	5	1.2	0.18
Stage 2	5	1.1	0.22
Stage 3	832	1.0	0.80
Stage 4	581	0.9	0.86
Stage 5	714	0.9	1.0

Figs 3a and 3b – Comparison of shallow formation resistivity to hydrauic fracture initiation pressures, by stage interval, in a horizontal Barnett Shale well (top: Modified from Waters (2006)) and another US shale basin (bottom).

associated with landing horizontal shale wells within high RQ and CQ interval and minimizing exposure to poor quality rock.

Observations: Operational Efficiency

When available, wellbore trajectory information (deviation and azimuth) and completion parameters such as number, length and spacing of both stages and perforation clusters were evaluated with respect to production. Particular attention was paid to the variability in production from these stages and perforation clusters. Numerous relationships were defined and some were basin specific.

The best Barnett Shale wells have deviations of less than 90 degrees. The opposite trend occurs for the Woodford Shale. It is inconclusive why the results vary, but good Barnett Shale production from wells deviated less than 90% demonstrates that fluids can be unloaded from laterals that are less than horizontal. The dataset size was insufficient to determine whether deviations greater or less than 90 degrees is beneficial to production in a specific reservoir.

The best wells in the Woodford Shale occur when the lateral is not aligned with σh. The Woodford Shale has a large spacing between perforation clusters and fracture lengths are commonly long and narrow. Thus, the closer fracture spacing achieved in the reservoir for wells misaligned with σh appears to be beneficial to production.

Wells completed with fracture stage lengths in the range of 300 ft to 400 ft appear to be optimum. As the likelihood of fracture complexity goes up the stage length can increase accordingly. The Barnett Shale generates the most complexity during stimulation and produces effectively at wider spacing, with the best wells producing from stage spacings of 400 ft and greater.

Production within 10% of the theoretical average occurs on as little as 39% of all wells in the Fayetteville Shale and as many as 49% of wells in the Eagle Ford Shale. Twenty percent of stages in all wells are producing less than half of their theoretical average. No production was seen on 6.5% of the stages in all of the wells analyzed.

Production from the heel section of the lateral is greatest in the Woodford Shale, Barnett Shale and Fayetteville Shale. The toe section produces the best in the Eagle Ford Shale. This production is not associated with wellbore deviation. Further analysis is required

once the horizontal production log dataset has grown sufficiently large.

The best perforation cluster spacing within shale reservoirs is between 75 ft and 175 ft. Wider cluster spacing is effective in the Barnett Shale where a wide fracture network is common due to the low horizontal stress anisotropy and natural fracture azimuth oblique to the hydraulic fracture. Larger perforation cluster spacing between stages than within stages is detrimental to production. This is no apparent stress alteration from stimulation justifying a larger spacing although a larger spacing is observed in the dataset.

For all wells in the dataset, 29.6% of all perforation clusters are not producing. The range is from 21% in the Eagle Ford Shale to 32% in the Woodford Shale. Even in the best wells, 19% of all perforation clusters are not producing. This varies from 6% in the Haynesville Shale to 22.5% in the Woodford Shale.

The best wells utilize two to six perforation clusters per stage, with fewer clusters per stage the better. The best Barnett Shale wells only have one or two perforation clusters per frac stage. Woodford Shale wells employing 8 clusters per stage significantly under produce their peers with fewer clusters per stage. Wells in which 6 clusters per stage were employed had approximately 50% of the clusters not contributing. Even on the best wells, 46% of the clusters are not appreciably flowing when placing 6 clusters per stage. Twenty percent of all clusters were not contributing when only two clusters per frac stage were used. This is a surprisingly high number and represents a significant opportunity to improve productivity if cost effective ways can be utilized to place laterals in intervals with the best CQ, and minimize near-wellbore fracture conductivity damage due to overflushing.

Conclusions

The variability observed in the 70% of perforation clusters which are producing is likely the result of the wellbore cutting across layers of differing RQ and CQ, but could also be the result of issues encountered during the stimulation process, possibly the overflushing of stimulation treatments. Perforations which are still cleaning up will appear as non-productive or producing poorly, but could start contributing with time. Time lapse production logging would identify this issue. Comingling production from multiple perforation clusters can create variability as well. Most variability can be explained by evaluating RQ and CQ parameters in the shale reservoir. Poor CQ is the worst case scenario. Good CQ and poor RQ may work, but is not desirable. Good RQ combined with good CQ, in the absence of geohazards, maximizes the potential for an economic success within organic shale wells. Further work is recommended, once more production logs are run within horizontal shale wells having either borehole images or other sophisticated data sets so that similar comparisons can be made and understood.

*Mark of Schlumberger

Acknowledgements

The authors would like to acknowledge the work of Brian Dupuis and Jason Sprinkle for assisting with the interpretation of the production logs, Sergio Jerez-Vera, Jenna Salamah, Karthik Srinivasan and Irewole Olukoya for their work in compiling the database, and Helena Gamero Diaz for her technical insight. The authors also wish to thank Schlumberger for the opportunity to publish this work.

References

1. Arthur, M. 2010. Plumbing the Depths in Pennsylvania: A Primer on Marcellus Shale Geology and Technology. The Pennsylvania State University College of Agricultural Sciences Cooperative Extension, Marcellus Shale Educational Webinar Series, October, 2010.

2. Baihly, J., Malpani, R., Edwards, C., Yen Han, S., Kok, J., Tollefsen, E. and Wheeler, W. 2010. Unlocking the Shale Mystery: How Lateral Measurements and Well Placement Impact Completions and Resultant Production. Paper SPE138427 presented at the 2010 SPE Tight Gas Completions Conference, San Antonio,Texas, 2-3 November.

3. Baihly, J., Altman, R., Malpani, R., and Luo, F. 2010. Shale Gas Production Decline Trend Comparison over Time and Basins. Paper SPE135555 presented at the 2010 SPE Annual Technical Conference and Exhibition, Florence, Italy, 19-22 September.

4. Bazan, L.W., Larkin, S.D, Lattibeaudiere, M.G., and Palisch, T.T. 2010. Improving Production in the Eagle Ford Shale with Fracture Modeling, Increased Conductivity and Optimized Stage and Cluster Spacing Along the Horizontal Wellbore. Paper SPE138425 presented at the 2010 SPE Tight Gas Completions Conference, San Antonio, Texas, 2-3 November.

5. Bohacs, K.M., The Devil in the Details: What Controls Vertical and Lateral Variation of Hydrocarbon Source and Shale-Gas Reservoir Potential at Millimeter

to Kilometer Scales?, Houston Geological Society Bulletin, Volume 52, No. 01, September 2009, pp 17-17.

6. Crosby, D.G., Yang, Z., Rahman, S.S. 1998. Transversely Fractured Horizontal Wells: A Technical Appraisal of Gas Production in Australia. Paper SPE50093 presented at the 1998 Asia Pacific Oil & Gas Conference and Exhibition, Perth, Australia, 12-14, October.

7. El Rabaa,W. 1989. Experimental Study of Hydraulic Fracture Geometry Initiated From Horizontal Wells. Paper SPE19720 presented at the 1989 SPE Annual Technical Conference and Exhibition, San Antonio, Texas, 8-11 October.

8. Fisher, M.K., Wright, C.A., Davidson, B.M., Goodwin, A.K., Fielder, E.O., Buckler, W.S., and Steinsberger, N.P. 2002. Integrating Fracture-Mapping Technologies To Improve Stimulations in the Barnett Shale. Paper SPE77441 presented at the 2002 SPE Annual Technical Conference and Exhibition, San Antonio, Texas, 29 September – 2 October.

9. Inamdar, A., Malpani, R., Atwood, K., Brook, K., Erwemi, A., Ogundare, T., and Purcell, D. 2010. Evaluation of Stimulation Techniques Using Microseismic Mapping in the Eagle Ford Shale. Paper SPE136873 presented at the 2010 SPE Tight Gas Completions Conference, San Antonio, Texas, 2-3 November.

10. Miller, C., Rylander, E., Le Calvez, J. 2010. Detailed Rock Evaluation and Strategic Reservoir Stimulation Planning For Optimal Production in Horizontal Gas Shale Wells. Abstract and poster presented at the 2010 AAPG International Conference and Exhibition, Calgary, AB, Cana- da, 12-15 September.

11. Plahn, S.V., Nolte, K.G., Thompson, L.G., and Miska, S. 1995. A Quantitative Investigation of the Fracture Pump-In/Flowback Test. Paper SPE30504 presented at the 1995 SPE Annual Technical Conference and Exhibition, Dallas, Texas, 22-25, October.

12. Ramsay, J.G., Folding and Fracturing of Rocks. Book published with permission of McGraw-Hill Book Company, New York, copyright 1967.

13. Rich, J.P., and Ammerman, M. 2010. Unconventional Geophysics for Unconventional Plays. Paper SPE131779 presented at the 2010 SPE Unconventional Gas Conference, Pittsburgh, Pennsylvania, 23-25, February.

14. Vulgamore, T., Clawson, T., Pope, C., Wolhort, S., Mayerhofer, M., Machovoe, S. and Waltman, C. 2007. Applying Hydraulic Fracture Diagnostics To Optimize Stimulations in the Woodford Shale. Paper SPE110029 presented at the 2007 SPE Annual Conference and Technical Exhibition, Anaheim, California, 11-14 November.

15. Warpinski, N. and Branagan, P., "Altered-Stress Fracturing," Journal of Petroleum Technology, September 1989, pp 990-997.

16. Waters, G., Dean B., Downie, R., Kerrihard, K., Austbo, L. and McPherson, B. 2009. Simultaneous Hydraulic Fracturing of Adjacent Horizontal Wells in the Woodford Shale. Paper SPE119635 presented at the 2009 SPE Hydraulic Fracturing Technology Conference, The Woodlands, Texas, 19-21 January.

17. Waters G., Heinze, J., Jackson, R., and Ketter, A. 2006. Use of Horizontal Well Image Tools To Optimize Barnett Shale Reservoir Exploitation. Paper SPE103202 presented at the 2006 SPE Annual Technical Conference and Exhibition, San Antonio, Texas, 24-27 September.

18. Weng, X. 1993. Fracture Initiation and Propagation From Deviated Wellbores. Paper SPE26597 presented at the 1993 SPE Annual Conference and Technical Exhibition, Houston, Texas, 3-6 October.

Triple-porosity Models: One Further Step Towards Capturing Fractured Reservoirs Heterogeneity

By Hasan A. Al-Ahmadi, SPE, Saudi Aramco, and R. A. Wattenbarger, SPE, Texas A&M University.

This paper was prepared for presentation at the 2011 SPE Saudi Arabia Section Technical Symposium and Exhibition held in AlKhobar, Saudi Arabia, 15–18 May 2011.

Abstract

Fractured reservoirs present a challenge in terms of characterization and modeling. Due to the fact that they consist of two coexisting and interacting media: matrix and fractures, not only we need to characterize the intrinsic properties of each medium but also accurately model how they interact. Dual-porosity models have been the norm in modeling fractures reservoirs. However, these models assume uniform matrix and fractures properties all over that medium. One further step into capturing the reservoir heterogeneity is to subdivide each medium and assign each one different property. In this paper, fractures are considered to have different properties and hence the triple-porosity model is introduced.

The triple-porosity model presented in this paper consists of three contiguous porous media: a matrix, less permeable microfractures and more permeable macrofractures. These media coexist and interact differently in the reservoir. It is assumed that flow is sequential following the direction of increased permeability and only macrofractures provide the conduit for fluids flow. Different solutions were derived based on different assumptions governing the flow between the fractures and matrix systems; i.e., pseudosteady state or transient flow in addition to different flow geometry; i.e., linear and radial. Some of these solutions are original. The model was confirmed mathematically by reducing it to dual-porosity system and numerically with reservoir simulation and applied to field cases. In addition, the solutions were modified to account for gas flow due to changing gas properties and gas adsorption in fractured unconventional reservoirs.

Introduction

A naturally fractured reservoir (NFR) can be defined as a reservoir that contains a connected network of fractures created by natural processes that have or predicted to have an effect on the fluid flow (Nelson 2001). Naturally fractured reservoirs contain more than 20% of the World's hydrocarbon reserves (Sarma and Aziz 2006). Moreover, most of the unconventional resources such as shale gas are also contained in fractured reservoirs.

Traditionally, dual-porosity models have been used to model NFRs where all fractures are assumed to have identical properties. Many dual-porosity models have

been developed starting by Warren and Root (1963) sugar cube model in which matrix provides the storage while fractures provide the flow medium. The model assumed pseudosteady state fluid transfer between matrix and fractures. Since then several models were developed mainly as variation of the Warren and Root model assuming different matrix-fracture fluid transfer conditions.

However, it is more realistic to assume fractures having different properties. Thus, triple-porosity models have been developed as more realistic models to capture reservoir heterogeneity in NFRs. Models for more than three interacting media are also available in the literature. However, no triple-porosity model has been developed for linear flow system in fractured reservoirs. In addition, no triple-porosity (dual fracture) model is available for either linear or radial geometry that considers transient fluid transfer between matrix and fractures. These limitations are overcome in this paper.

Literature Review

Dual-Porosity Models. Naturally fractured reservoirs are usually characterized using dual-porosity models. The foundations of dual-porosity models were first introduced by Barenblatt et al., (1960). The model assumes pseudosteady state fluid transfer between matrix and fractures. Later, Warren and Root (1963) extended Barenblatt et al., model to well test analysis and introduced it to the petroleum literature. The Warren and Root model was mainly developed for transient well test analysis in which they introduced two dimensionless parameters, ω and λ. ω describes the storativity of the fractures system and λ is the parameter governing fracture-matrix flow. Dual-porosity models can be categorized into two major categories based on the interporosity fluid transfer assumption: pseudosteady state models and unsteady state models.

Pseudosteady State Models. Warren and Root (1963) based their analysis on sugar cube idealization of the fractured reservoir, Fig. 1. They assumed pseudo-steady state flow between the matrix and fracture systems. That is, the pressure at the middle of the matrix block starts changing at time zero. In their model, two differential forms (one for matrix and one for fracture) of diffusivity equations were solved simultaneously at a mathematical point. The fracture-matrix interaction is related by

$$q = \alpha \frac{k_m}{\mu}\left(p_m - p_f\right) \qquad (1)$$

where q is the transfer rate, α is the shape factor, k_m is the matrix permeability, μ is the fluid viscosity and (p_m – p_f) is the pressure difference between the matrix and the fracture.

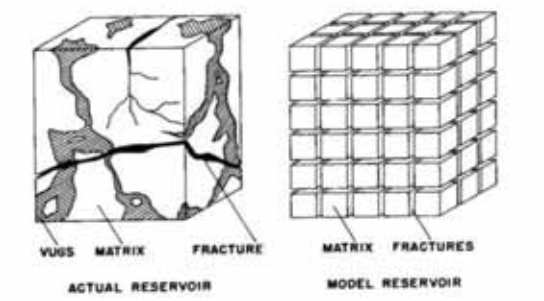

Fig. 1 – Idealization of the heterogeneous porous medium (Warren and Root 1963).

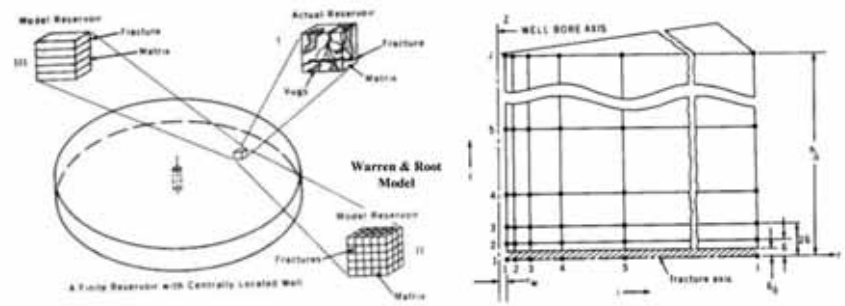

Fig. 2 – Idealization of the heterogeneous porous medium (Kazemi 1969).

Unsteady State Models. Other models (Kazemi 1969; de Swaan 1976; Ozkan et al., 1987) assume unsteady-state (transient) flow condition between matrix and fracture systems. Kazemi (1969) proposed the slab dual-porosity model, Fig. 2, and provided a numerical solution for dual-porosity reservoirs assuming transient flow between matrix and fractures. His solution, however, was similar to that of Warren and Root except for the transition period between the matrix and fractures systems.

Triple-Porosity Models. The dual-porosity models assume uniform matrix and fractures properties throughout the reservoir which may not be true in actual reservoirs. An improvement to this drawback is to consider two matrix systems with different properties. This system is a triple-porosity system. Another form of triple-porosity is to consider two fractures systems with different properties in addition to the matrix. The latter is sometimes referred to as dual fracture model.

The first triple-porosity model was developed by Liu (1981, 1983). Liu developed his model for radial flow of slightly compressible fluids through a triple-porosity reservoir under pseudosteady state interporosity flow. This model, however, is rarely referenced as it was not published in the petroleum literature. In petroleum literature, the first triple-porosity model was introduced by Abdassah and Ershaghi (1986). Two geometrical configurations were considered: strata model and uniformly distributed blocks model. In both models, two matrix systems have different properties flowing to a single fracture under gradient (unsteady state) interporosity flow. The solutions were developed for the radial system.

Jalali and Ershaghi (1987) investigated the transition zone behavior of the radial triple porosity system. They extended the Abdassah and Ershaghi strata (layered) model by allowing the matrix systems to have different properties and thickness.

Al-Ghamdi and Ershaghi (1996) was the first to introduce the dual fracture triple-porosity model for radial system. Their model consists of a matrix and two fracture systems; more permeable macrofracture and less permeable microfracture. Two sub models were presented. The first is similar to the triple-porosity layered model where microfractures replace one of the matrix systems. The second is where the matrix feeds the microfractures under pseudosteady state flow which in turns feed the macrofractures under pseudosteady state flow condition as well. The macrofractures and/or microfractures are allowed to flow to the well.

Liu et al., (2003) presented a radial triple-continuum model. The system consists of fractures, matrix and cavity media.

Only the fractures feed the well but they receive flow from both matrix and cavity systems under pseudo-steady state condition.

Unlike previous triple-porosity models, the matrix and cavity systems are exchanging flow (under pseudosteady state condition) and thus it is called triple-continuum. Their solution was an extension of Warren and Root solution.

Wu et al., (2004) used the triple-continuum model for modeling flow and transport of tracers and nuclear waste in the unsaturated zone of Yucca Mountain. The system consists of large fractures, small fractures and matrix. They confirmed the validity of the analytical solution with numerical simulation for injection well injecting at constant rate in a radial system. In addition, they demonstrated the usefulness of the triple-continuum model for estimating reservoir parameters.

Dreier (2004) improved the triple-porosity dual fracture model originally developed by Al-Ghamdi and Ershaghi (1996) by considering transient flow condition between microfractures and macrofractures. Flow between matrix and microfractures is still under pseudosteady state condition. His main work (Dreier et al., 2004) was the development of new quadruple-porosity sequential feed and simultaneous feed models. He also addressed the need for nonlinear regression to match well test data and estimate reservoir properties in case of quadruple porosity model.

Linear Flow in Fractured Reservoir. Linear flow occurs at early time (transient flow) when flow is perpendicular to any flow surface. Wattenbarger (2007) identified different causes for linear transient flow including hydraulic fracture draining a square geometry, high permeability layers draining adjacent tight layers and early-time constant pressure drainage from different geometries.

El-Banbi (1998) developed new linear dual-porosity solutions for fluid flow in linear fractured reservoirs. Solutions were derived in Laplace domain for several inner and outer boundary conditions. These include constant rate and constant pressure inner boundaries and infinite and closed outer boundaries. Skin and wellbore storage effects have been incorporated as well. One important finding is that reservoir functions, f(s) , derived for ra-

dial flow can be used in linear flow solutions in Laplace domain and vice versa.

Bello (2009) demonstrated that El-Banbi solutions could be used to model horizontal well performance in tight fractured reservoirs. He then applied the constant pressure solution to analyze rate transient in horizontal multistage fractured shale gas wells.

Bello (2009) and Bello and Wattenbarger (2008, 2009, 2010) used the dual-porosity linear flow model to analyze shale gas wells. Five flow regions were defined based on the linear dual-porosity constant pressure solution. It was found that shale gas wells performance could be analyzed effectively by region 4 (transient linear flow from a homogeneous matrix). Skin effect was proposed to affect the early flow periods and a modified algebraic equation was proposed to account for it.

Ozkan et al., (2009) and Brown et al., (2009) proposed a trilinear model for analyzing well test in tight gas wells. Three contiguous media were considered: finite conductivity hydraulic fractures, dual-porosity inner reservoir between the hydraulic fractures and outer reservoir beyond the tip of the hydraulic fractures. Based on their analysis, the outer reservoir does not contribute significantly to the flow.

Al-Ahmadi et al., (2010) presented procedures to analyze shale gas wells using the slab and cube dual-porosity idealizations demonstrated by field examples.

New Analytical Triple-Porosity Solutions

As stated earlier, to the best of our knowledge, no triple-porosity model has been developed for linear flow system. In addition, no triple-porosity (dual fracture) model is available for either linear or radial geometry that considers transient fluid transfer between matrix and fractures in fractured reservoirs. Therefore, a triple-porosity model is developed (Al-Ahmadi 2010) in this paper and new solutions are derived for linear flow in fractured reservoirs. The triple-porosity system consists of three contiguous porous media: the matrix, less permeable microfractures and more permeable macrofractures. The main flow is through the macrofractures, which feed the well while they receive flow from the microfractures only. Consequently, the matrix feeds the microfractures only. Therefore, the flow is sequential from one medium to the other. In the petroleum literature, this type of model is sometimes called dual-fracture model.

To facilitate deriving the solution, it is chosen to model the fluid flow toward a horizontal well in a triple-porosity reservoir. El-Banbi (1998) solutions for linear flow in dual-porosity reservoirs will be used. However, new reservoir functions will be derived that pertain to the triple-porosity system and can be used in El-Banbi's solutions. Throughout this paper, matrix, microfractures and macrofractures are identified with subscripts m, f and F, respectively.

Linear Flow Solutions for Fractured Linear Reservoirs. El-Banbi (1998) was the first to present solutions to the fluid flow in fractured linear reservoirs. The analytical solutions for constant rate and constant pressure cases in Laplace domain are given by

Constant rate case:

$$\overline{p_{wDL}} = \frac{2\pi}{s\sqrt{s\,f(s)}}\left[\frac{1+\exp\left(-2\sqrt{s\,f(s)}y_{De}\right)}{1-\exp\left(-2\sqrt{s\,f(s)}y_{De}\right)}\right] \quad (2)$$

Constant pressure case:

$$\frac{1}{\overline{q_{DL}}} = \frac{2\pi\, s}{\sqrt{s\,f(s)}}\left[\frac{1+\exp\left(-2\sqrt{s\,f(s)}y_{De}\right)}{1-\exp\left(-2\sqrt{s\,f(s)}y_{De}\right)}\right] \quad (3)$$

Complete list of solutions are available in El-Banbi (1998). These solutions can be used to model horizontal wells in dual-porosity reservoirs (Bello, 2009). Accordingly, as will be shown later, they are equally applicable to triple-porosity reservoirs considered in this work since linear flow is the main flow regime. The fracture function, *f(s)* however, is different depending on the type of reservoir and imposed assumptions.

Derivations of the Triple-Porosity Analytical Solutions. A sketch of the triple-porosity dual-fracture model is shown in Fig. 3. The arrows indicate the flow directions where fluids flow from matrix to microfractures to the macrofractures - following the direction of increased permeability - and finally to the well.

Model Assumptions. The analytical solutions are derived under the following assumptions:

1. Fully penetrating horizontal well at the center of a closed rectangular reservoir producing at a constant rate
2. Triple-porosity system made up of matrix, less permeable microfractures and more permeable macrofractures
3. Each medium is assumed to be homogenous and isotropic
4. Matrix blocks are idealized as slabs
5. Flow is sequential from one medium to the other; form matrix to microfractures to macrofractures
6. Flow of slightly compressible fluid with constant viscosity

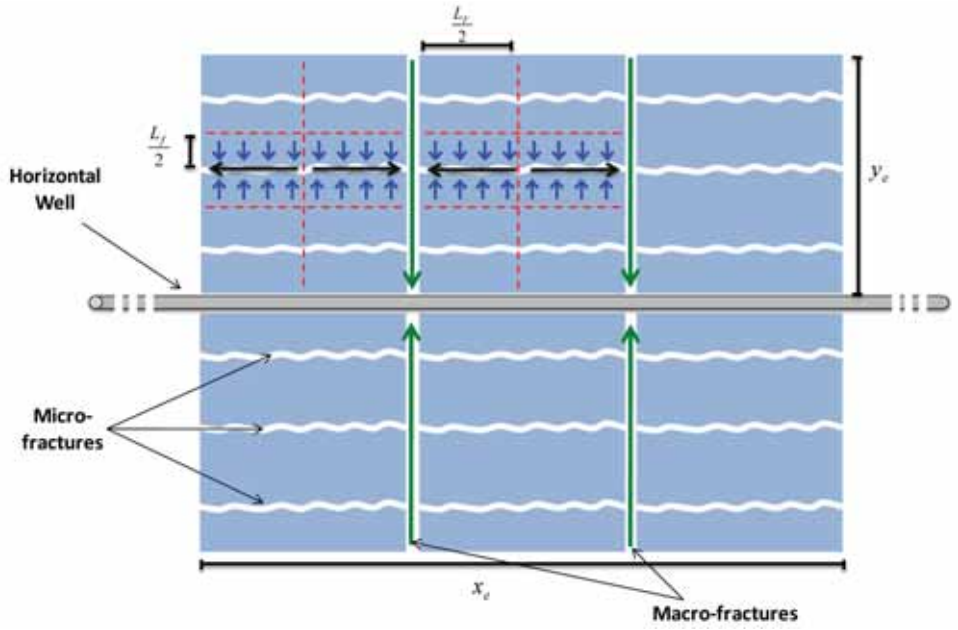

Fig. 3 – Top view of a horizontal well in a triple-porosity system with sequential flow. Arrows indicate flow directions (Al-Ahmadi 2010).

Four Sub-models of the triple-porosity model are derived (Al-Ahmadi, 2010). The main difference between the models is the assumption of interporosity flow condition, i.e., pseudosteady state or transient. These models are shown graphically in Fig. 4. The analytical solution derivation for the fully transient (Model 1) is shown in this paper. More detailed solutions derivations for the other models are available in Al-Ahmadi (2010).

Definitions of Dimensionless Variables. Before proceeding with the derivations, the dimensionless variables are defined.

$$t_{DAc} = \frac{0.00633\,k_F t}{[\varphi c_t]_t\,\mu\,A_{cw}} \tag{4}$$

$$p_{DL} = \frac{k_F\sqrt{A_{cw}}(p_i - p)}{141.2\,qB\mu} \tag{5}$$

$$\omega_F = \frac{[\varphi V c_t]_F}{[\varphi V c_t]_t} \tag{6}$$

$$\omega_f = \frac{[\varphi V c_t]_f}{[\varphi V c_t]_t} \tag{7}$$

$$\omega_m = \frac{[\varphi V c_t]_m}{[\varphi V c_t]_t} = 1 - \omega_F - \omega_f \tag{8}$$

$$\lambda_{Ac,Ff} = \frac{12}{L_F^2}\frac{k_f}{k_F}A_{cw} \tag{9}$$

$$\lambda_{Ac,fm} = \frac{12}{L_f^2}\frac{k_m}{k_F}A_{cw} \tag{10}$$

$$z_D = \frac{z}{L_f/2} \tag{11}$$

$$x_D = \frac{x}{L_F/2} \tag{12}$$

$$y_D = \frac{y}{\sqrt{A_{cw}}} \tag{13}$$

ω and λ are the storativity ratio and interporosity flow parameter, respectively. k_F and k_f are the bulk (macroscopic) fractures permeabilities. Detailed parameters definitions are available in the nomenclature section in this paper.

Model 1: Fully Transient Triple-Porosity Model. The first Sub-model, Model 1, is the fully transient model. The flow between matrix and microfractures and that between microfractures and macrofractures are under transient condition. This model is an extension to the dual-porosity transient slab model (Kazemi 1969 Model). The derivation starts by writing the differential equations describing the flow in each medium.

Matrix:

$$\frac{\partial^2 p_{DLm}}{\partial z_D^2} = (1 - \omega_f - \omega_F)\frac{3}{\lambda_{Ac,fm}}\frac{\partial p_{DLm}}{\partial t_{DAc}} \tag{14}$$

Microfractures:

$$\frac{\partial^2 p_{DLf}}{\partial x_D^2} = \omega_f\frac{3}{\lambda_{Ac,Ff}}\frac{\partial p_{DLf}}{\partial t_{DAc}} + \frac{\lambda_{Ac,fm}}{\lambda_{Ac,Ff}}\frac{\partial p_{DLm}}{\partial z_D}\bigg|_{z_D=1} \tag{15}$$

Macrofractures:

$$\frac{\partial^2 p_{DLF}}{\partial y_D^2} = \omega_F\frac{\partial p_{DLF}}{\partial t_{DAc}} + \frac{\lambda_{Ac,Ff}}{3}\frac{\partial p_{DLf}}{\partial x_D}\bigg|_{x_D=1} \tag{16}$$

The initial and boundary conditions in dimensionless form are as follows:

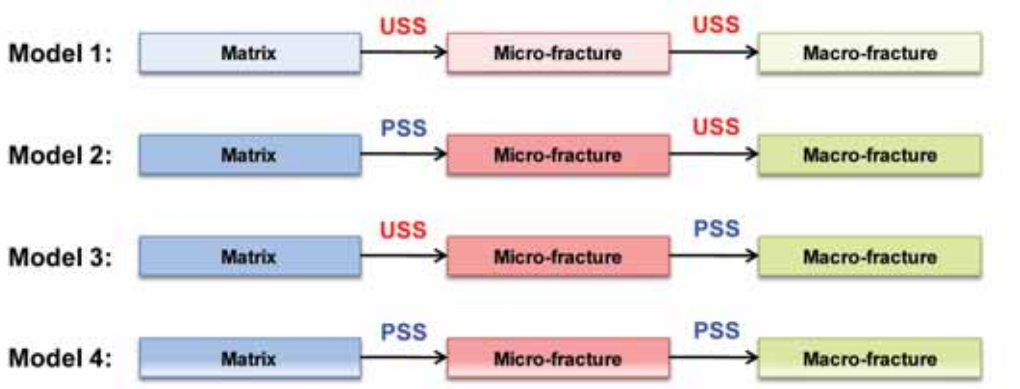

Fig. 4 – Sub-models of the triple-porosity model based on different interporosity flow condition assumptions. PSS: pseudosteady state. USS: unsteady state or transient. Arrows indicate flow directions.

Matrix:

Initial condition: $p_{DLm}(z_D,0)=0$

Inner boundary: $\dfrac{\partial p_{DLm}}{\partial z_D}=0 \qquad @\ z_D=0$

Outer boundary: $p_{DLm}=p_{DLf} \qquad @\ z_D=1$

Microfractures:

Initial condition: $p_{DLf}(x_D,0)=0$

Inner boundary: $\dfrac{\partial p_{DLf}}{\partial x_D}=0 \qquad @\ x_D=0$

Outer boundary: $p_{DLf}=p_{DLF} \qquad @\ x_D=1$

Macrofractures:

Initial condition: $p_{DLF}(y_D,0)=0$

Inner boundary: $\left.\dfrac{\partial p_{DLF}}{\partial y_D}\right|_{y_D=0}=-2\pi$

Outer boundary: $\dfrac{\partial p_{DLF}}{\partial y_D}=0 \qquad @\ y_D=y_{De}=y_e/\sqrt{A_{cw}}$

The system of differential equations, Eqs. 14 to 16, can be solved using Laplace transformation as detailed in the Appendix. The fracture function, *f(s)*, for this model is given by

$$f(s)=\omega_F+\frac{\lambda_{Ac,Ff}}{3s}\sqrt{s\,f_f(s)}\,\tanh\left(\sqrt{s\,f_f(s)}\right) \qquad (17)$$

$$f_f(s)=\frac{3\omega_f}{\lambda_{Ac,Ff}}+\frac{\lambda_{Ac,fm}}{s\,\lambda_{Ac,Ff}}\sqrt{\frac{3s\,\omega_m}{\lambda_{Ac,fm}}}\,\tanh\left(\sqrt{\frac{3s\,\omega_m}{\lambda_{Ac,fm}}}\right)$$

Using the fracture function, Eq. 17 in Eqs. 2 or 3 will give the triple-porosity fully transient model response for constant rate or constant pressure cases, respectively in Laplace domain. The solution can then be inverted to real (time) domain using inverting algorithms like Stehfest Algorithm (Stehfest 1970).

Model 2: Mixed Flow Triple-Porosity Model. The second sub-model, Model 2, is where the interporosity flow between matrix and microfractures is under pseudosteady state while it is transient between microfractures and macrofractures. A similar model was derived by Dreier et al., (2004) for radial flow. However, their fracture function is different since they had different definitions of dimensionless variables and used intrinsic properties for the transient flow.

Model 3: Mixed Flow Triple-Porosity Model. The third sub-model, Model 3, is where the flow between the matrix and microfractures is transient while the flow between microfractures and macrofractures is pseudosteady state. It is the opposite of Model 2.

Model 4: Fully PSS Triple-Porosity Model. The fourth sub-model, Model 4, is the fully pseudosteady state model. The flow between all three media is under pseudosteady state. This model is an extension of the Warren and Root dual-porosity pseudosteady state model. This model is also a limiting case of Liu et al., (2000; Wu et al., 2004) triple-continuum model if considering sequential flow and ignoring the flow component between matrix and macrofractures.

Table 1 summarizes the fractures functions derived for each sub model. The detailed derivations for all models are available in Al-Ahmadi (2010).

Triple-Porosity Solutions Comparison. Models 1 through 4 cover all possibilities of fluid flow in triple-porosity system under sequential flow assumption. Comparison of the constant pressure solution based on these models is shown in Fig. 5. As can be seen on the figure, Models 1 and 4 represents the end members while Models 2 and 3 are combination of these models. Model 2 follows Model 1 at early time but follows Model 4 at later time while Model 3 is the opposite. Considering rate

Table 1 – Fracture functions derived for triple-porosity model (New Solutions)	
Model	**Fracture Function, $f(s)$**
Triple-Porosity Fully Transient (Model 1)	$f(s)=\omega_F+\frac{\lambda_{Ac,Ff}}{3s}\sqrt{s\,f_f(s)}\,\tanh\left(\sqrt{s\,f_f(s)}\right)$ $f_f(s)=\frac{3\omega_f}{\lambda_{Ac,Ff}}+\frac{\lambda_{Ac,fm}}{s\,\lambda_{Ac,Ff}}\sqrt{\frac{3s\,\omega_m}{\lambda_{Ac,fm}}}\,\tanh\left(\sqrt{\frac{3s\,\omega_m}{\lambda_{Ac,fm}}}\right)$
Triple-Porosity Mixed Flow (Model 2)	$f(s)=\omega_F+\frac{\lambda_{Ac,Ff}}{3s}\sqrt{s\,f_f(s)}\,\tanh\left(\sqrt{s\,f_f(s)}\right)$ $f_f(s)=\frac{3\omega_f}{\lambda_{Ac,Ff}}+\frac{3\omega_m\lambda_{Ac,fm}}{s\omega_m\lambda_{Ac,Ff}+\lambda_{Ac,fm}\lambda_{Ac,Ff}}$
Triple-Porosity Mixed Flow (Model 3)	$f(s)=\omega_F+\frac{3\omega_f\lambda_{Ac,Ff}+\frac{\lambda_{Ac,Ff}\lambda_{Ac,fm}}{s}\sqrt{\frac{3s\,\omega_m}{\lambda_{Ac,fm}}}\,\tanh\left(\sqrt{\frac{3s\,\omega_m}{\lambda_{Ac,fm}}}\right)}{3\lambda_{Ac,Ff}+3s\omega_f+\lambda_{Ac,fm}\sqrt{\frac{3s\,\omega_m}{\lambda_{Ac,fm}}}\,\tanh\left(\sqrt{\frac{3s\,\omega_m}{\lambda_{Ac,fm}}}\right)}$
Triple-Porosity Fully PSS (Model 4)	$f(s)=\omega_F+\frac{\lambda_{Ac,Ff}\left[\omega_m\lambda_{Ac,fm}+\omega_f\left(s\omega_m+\lambda_{Ac,fm}\right)\right]}{\left(\lambda_{Ac,Ff}+s\omega_f\right)\left(s\omega_m+\lambda_{Ac,fm}\right)+s\omega_m\lambda_{Ac,fm}}$

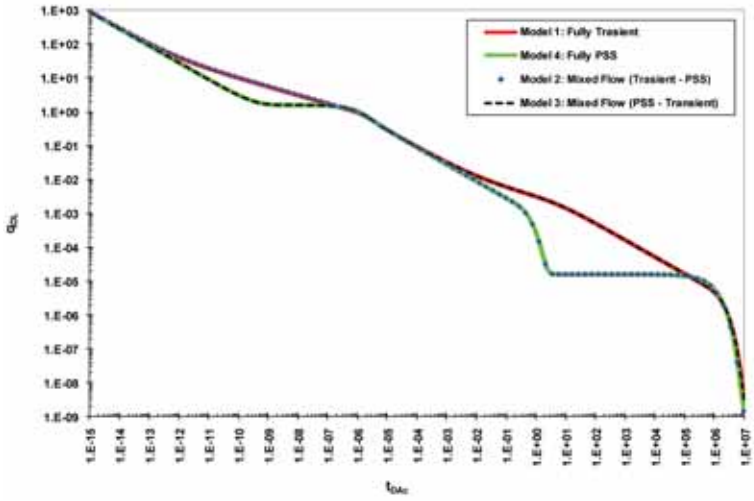

Fig. 5 – Comparison of the constant pressure solutions based on the four triple-porosity models assumptions (Al-Ahmadi, 2010).

transient analysis, Models 1 and 3 are more likely to be applicable to field data.

Flow Regions Based on the Analytical Solution. Since Model 1, the fully transient model, is the most general of all the four triple-porosity variations and shows all possible flow regions, the discussions in this paper will be limited to Model 1. Based on Model 1 constant pressure solution, six flow regions can be identified as the pressure propagates through the triple-porosity system (Al-Ahmadi, 2010). These flow regions are shown graphically on the log-log plot of dimensionless rate versus dimensionless time in Fig. 6. Regions 1 through 5 exhibit an alternating slopes of – 1/2 and – 1/4 indicating linear and bilinear transient flow, respectively. Region 6 is the boundary dominated flow and exhibits an expo-

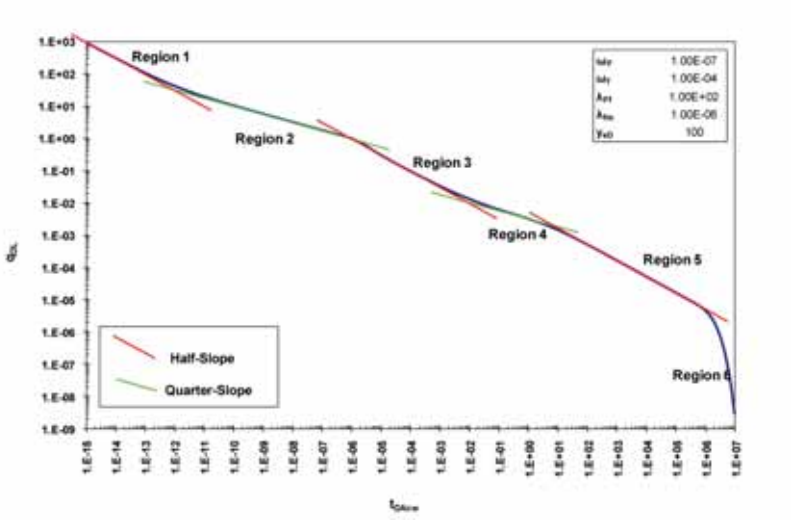

Fig. 6 – A log-log plot of triple-porosity solution. Six flow regions can be identified for Model 1 constant pressure solution. Slopes are labeled on the graph (Al-Ahmadi, 2010).

nential decline due to constant bottom-hole pressure. These flow regions are explained in details in the following sections.

Region 1. Region 1 represents the transient linear flow in the macrofractures only. The permeability of macrofractures is usually high and therefore, in most cases, this flow region will be very short. It may not be captured by most well rate measurement tools. This flow region exhibits a half-slope on the log-log plot of rate versus time.

Region 2. Region 2 is the bilinear flow in the macrofractures and microfractures. It is caused by simultaneous perpendicular transient linear flow in the microfractures and the macrofractures. This flow region exhibit a quarter-slope on the log-log plot of rate versus time.

Region 3. Region 3 is the linear flow in the microfractures system. It will occur once the transient flow in the macrofractures ends indicating the end of bilinear flow (region 2). This flow region exhibits a half-slope on the log-log plot of rate versus time.

Region 4. Region 4 is the bilinear flow in the microfractures and matrix. It is caused by the linear flow in the matrix while the microfractures are still in transient flow. This flow region exhibits a quarter-slope on the log-log plot of rate versus time. In most field cases, this flow region is the first one to be observed.

Region 5. Region 5 is the main and longest flow region in most field cases. It is the linear flow out of the matrix to the surrounding microfractures. This region exhibits a half-slope on the log-log plot of rate versus time. Analysis of this region will allow the estimation of fractures surface area available to flow, A_{cm}.

Region 6. Region 6 is the boundary dominated flow. It starts when the pressure at the center of the matrix blocks starts to decline. This flow is governed by exponential decline due to constant bottom-hole pressure.

Model verification

Mathematical Consistency of the Analytical Solutions. In this section, the solutions mathematical consistency is checked by reducing the triple-porosity model to its dual-porosity counterpart. This can be achieved by allowing the microfractures to dominate the flow and assigning to them the dual-porosity matrix properties

Table 2 – Input parameters for dual and triple-porosity solutions comparison

Dual-Porosity Parameters		Triple-Porosity Parameters	
ω	0.001	ω_F	0.001
λ	0.005	ω_f	0.999
y_{eD}	10	$\lambda_{Ac,Ff}$	0.005
		$\lambda_{Ac,fm}$	1×10^{-9}
		y_{eD}	10

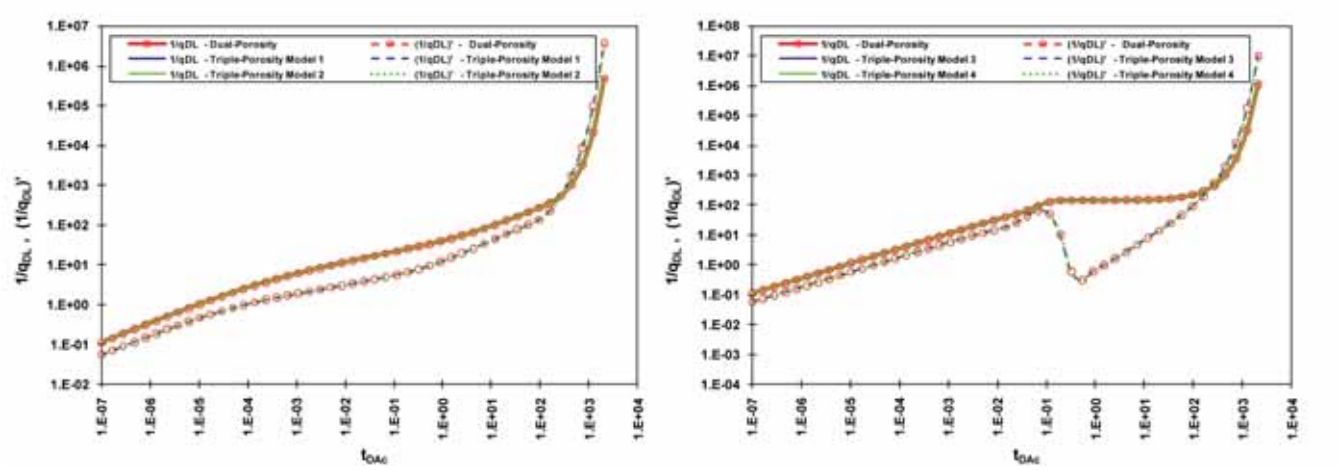

Fig. 7 –A log-log plot of transient dual-porosity (DP) and triple-porosity (TP) Models 1 and 2 solutions (on left) and pseudosteady state dual-porosity (DP) and triple-porosity (TP) Models 3 and 4 solutions (on right) for constant pressure linear flow case. In both figures, the two solutions are identical indicating the mathematical consistency of the new triple-porosity solutions.

from the dual-porosity system. In this case, the matrix-microfractures interporosity coefficient, $\lambda_{Ac,fm}$, is very small and the triple-porosity matrix storativity ratio, ω, is zero.

This comparison is shown for all models in the following figures. Table 2 shows the data used for comparison.

Models 1 and 2 are reduced to the transient slab dual-porosity model since the flow between microfractures and macrofractures is under transient conditions in the two models. Models 3 and 4, however, are reduced to the pseudosteady state dual-porosity model since the flow between microfractures and macrofractures is under pseudosteady state condition in the two models. As shown in Fig. 7, the triple-porosity solutions are identical to their dual-porosity counterpart. This confirms the mathematical consistency of the new triple-porosity solutions.

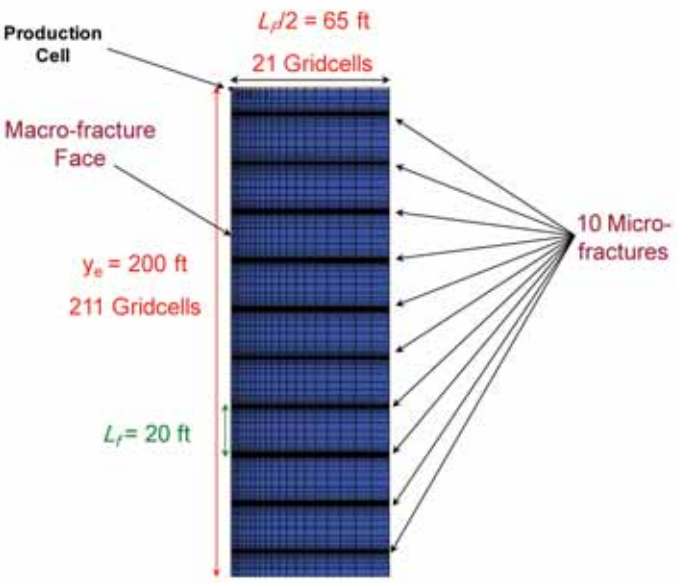

Fig. 8 – Top view of the CMG 2-D triple-porosity simulation model.

Comparison to Simulation Model. A triple-porosity simulation model was built explicitly using CMG reservoir simulator to understand the behavior of triple-porosity reservoirs and to verify the derived analytical solutions. The model considers the flow toward a horizontal well in a triple-porosity reservoir. One representative segment is modeled which represents one quadrant of the reservoir volume around a macrofracture. This segment contains ten microfractures orthogonal to the macrofractures at 20 ft fracture spacing. The model is a 2-D model with 21 gridcells in the x-direction, 211 gridcells in y-direction and only one cell in the z-direction. A top view of the model is shown in Fig. 8. All matrix, microfractures and macrofractures properties are assigned explicitly. In addition, the simulation model assumes constant connate water saturation.

The simulation model was run for many cases by changing the three porosities and permeabilities of the three media and the simulation results are compared to that of the analytical solutions for each case. All cases were matched with analytical solutions and thus confirming their validity. A result of one case for oil reservoir is shown in Fig. 9.

Applicability of Triple-Porosity Solutions for Radial Flow. Although the triple-porosity solutions derived in

this paper were for linear flow, they are equally applicable to radial flow following El-Banbi (1998) work. The differential equation in Laplace domain that governs the flow in the macrofractures in case of radial system is given by

$$\frac{1}{r_D}\frac{\partial}{\partial r_D}\left(r_D\frac{\partial\overline{p_{DF}}}{\partial r_D}\right)-s\,f(s)\overline{p_{DF}}=0 \qquad (18)$$

The constant pressure solution for a closed reservoir is given by (El-Banbi 1998)

$$\frac{1}{\overline{q_D}}=\frac{s\left[I_0\left(\sqrt{s\,f(s)}\right)K_1\left(\sqrt{s\,f(s)}r_{eD}\right)+I_1\left(\sqrt{s\,f(s)}r_{eD}\right)K_0\left(\sqrt{s\,f(s)}\right)\right]}{\sqrt{s\,f(s)}\left[I_1\left(\sqrt{s\,f(s)}r_{eD}\right)K_1\left(\sqrt{s\,f(s)}\right)+I_1\left(\sqrt{s\,f(s)}\right)K_1\left(\sqrt{s\,f(s)}r_{eD}\right)\right]} \qquad (19)$$

The fracture functions, *f(s)*, derived for all the models can be used in the radial flow solutions as well. Fig. 10 shows comparison between radial dual-porosity solutions and the new triple-porosity solutions reduced to their dual-porosity counterpart and applied to radial flow. Data used for comparison are shown in Table 3. The solutions are identical indicating the applicability of the new triple-porosity solutions derived in this work to radial flow.

Application to Gas Flow. It is important to note that the above solutions were derived for slightly compressible fluids and thus are applicable to liquid flow only. However, they can be applied to gas flow by using real gas pseudo-pressure, *m(p)*, instead of pressure to linearize the left-hand side of the diffusivity equation. Therefore, the dimensionless pressure variable will be defined in terms of real gas pseudo-pressure as:

$$m_{DL}=\frac{k_F\sqrt{A_{cw}}\left[m(p_i)-m(p)\right]}{1422\,q_g\,T} \qquad (20)$$

where *m(p)* is the real gas pseudo-pressure defined as (Al-Hussainy et al. 1966):

$$m(p)=2\int_{p_0}^{p}\frac{p}{z\,\mu}dp \qquad (21)$$

With the above linearization, the derived solutions are applicable to the transient flow regime for gas flow.

However, once the reservoir boundaries are reached and average reservoir pressure starts to decline, the gas properties will change considerably especially the gas viscosity and compressibility. Therefore, the solutions have to be corrected for changing fluid properties. This is usually achieved by using pseudo-time or material balance time. An example of these transformations is the Fraim and Wattenbarger (1987) normalized time defined as

Table 3 – Input parameters for dual and triple-porosity solutions comparison for radial flow

Dual-Porosity Parameters		Triple-Porosity Parameters	
ω	0.001	ω_F	0.001
λ	0.001	ω_f	0.999
r_{eD}	10	$\lambda_{Ac,Ff}$	0.001
		$\lambda_{Ac,fm}$	1×10^{-9}
		r_{eD}	10

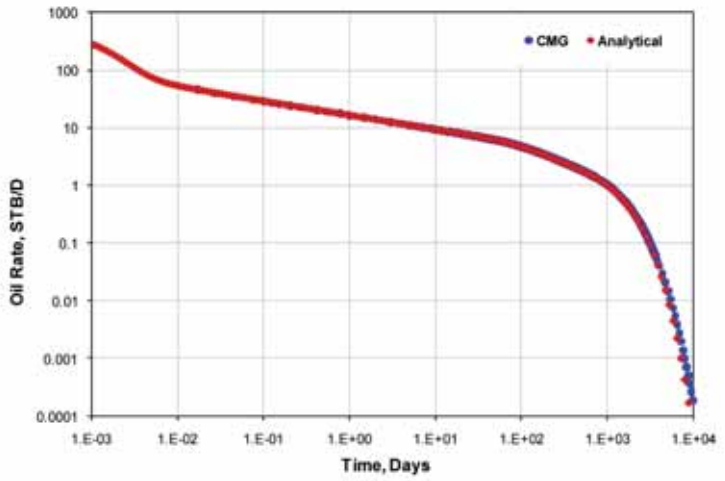

Fig. 9 – Match between simulation and analytical solution results for oil reservoir case. (kF,in = 1000 md, kf,in = 1 md and km = 1.5x10 md) (Al-Ahmadi 2010).

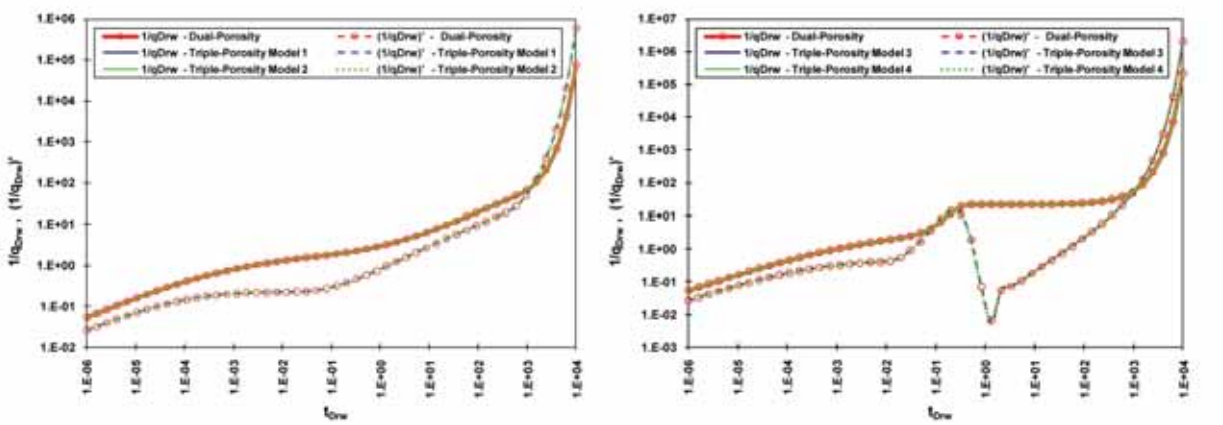

Fig. 10 – Log-log plot of dual-porosity and triple-porosity constant pressure solutions for radial flow. On the left is the transient solution and on right is the pseudosteady solution (Al-Ahmadi 2010).

$$t_n = \int_0^t \frac{(\mu c_t)_i}{\mu(\bar{p})c_t(\bar{p})} d\tau \qquad (22)$$

Thus, with these two modifications, the analytical solutions derived in this work are applicable to gas flow.

Accounting for Adsorbed Gas. Unlike tight gas reservoirs, gas in shale reservoirs is stored as compressed (free) gas and adsorbed gas. Adsorbed gas does not usually flow until the pressure drops below the sorption pressure. Adsorbed gas can be accounted for using Langmuir isotherm which defines the adsorbed gas volume as:

$$V = V_L \frac{p}{(p + p_L)} \qquad (23)$$

where

V: Volume of gas currently adsorbed (scf/cuf)
V_L: Langmuir's volume (scf/cuf)
p_L: Langmuir's pressure (psia)
p_{Lp}: Reservoir pressure (psia)

Therefore, the analytical solutions have to account for the adsorbed gas before applying them to shale gas wells. This can be achieved by modifying the gas compressibility definition to include adsorbed gas. Following Bumb and McKee (1988), the modified total compressibility is defined as:

$$c_t^* = c_f + c_g S_g + c_w S_w + c_d \qquad (24)$$

where c_d is the desorbed gas compressibility given by:

$$c_d = \frac{\rho_{g_{sc}} V_L p_L}{\varphi \bar{\rho}_g (p_L + \bar{p})^2} = \frac{B_g V_L p_L}{\varphi (p_L + \bar{p})^2} \qquad (25)$$

Thus, to account for adsorption, c^*_t instead of c_t will be used in the analytical solutions to be applicable to shale gas wells.

For material balance calculations, the modified compressibility factor (z^*) is used instead of z (King 1993). z^* is defined as:

$$z^* = \frac{z}{(1 - S_{wi}) + \frac{V_L T p_{sc} z}{\varphi (p + p_L) T_{sc} z_{sc}}} \qquad (26)$$

Then the gas material balance equation becomes:

$$\frac{\bar{p}}{z^*} = \frac{p_i}{z_i^*}\left(1 - \frac{G_p}{G}\right) \qquad (27)$$

The *OGIP* accounting for free and adsorbed gas can be calculated using the following volumetric equation (Samandarli 2011):

$$G = V_b\left[\left(\frac{\varphi S_{gi}}{B_{gi}}\right) + (1 - \varphi)\left(V_L \frac{p_i}{p_i + p_L}\right)\right] \qquad (28)$$

Field Application

Tight reservoirs such as shale oil or shale gas are perfect field case to apply this model due to the large contrast in the three porous media permeability values. Horizontal wells placed in these reservoirs are usually hydraulically fractured due to low matrix permeability. Natural fractures usually exist in these reservoirs as well. The case presented here is from a shale gas reservoir.

Shale Gas reservoirs play a major role in the United State natural gas supply as they are aggressively developed capitalizing on new technologies, namely horizontal wells with multistage fracturing. It has been observed that these wells behave as though they are controlled by transient linear flow (Bello 2009; Bello and Wattenbarger 2008, 2009, 2010; Al-Ahmadi et al., 2010). According to Medeiros et al., (2008) linear flow is the

dominant flow regime for fractured horizontal wells in tight formations for most of their productive lives. This behavior is characterized by a negative half-slope on the log-log plot of gas rate versus time and a straight line on the $[m(p_i) - m(p_{wf})]/q_g$ vs. $t^{0.5}$ plot (the square root of time plot).

Some shale gas wells, however, exhibit a bi-linear flow just before the linear flow is observed. This behavior is characterized by a negative quarter-slope on the log-log plot of gas rate versus time or a straight line on the [m(pi) – $m(p_{wf})]/q_g$ vs. $t^{0.25}$ plot. The bi-linear flow is due to two perpendicular transient linear flows occurring simultaneously in two contiguous systems. These could be microfractures and matrix or microfractures and macrofractures systems.

Previously, shale gas wells have been modeled using linear dual-porosity models (Bello 2009; Bello and Wattenbarger 2008, 2009, 2010; Al-Ahmadi et al., 2010). In these models, the matrix was assumed "homogeneous" although it might be enhanced by natural fractures by having high effective matrix permeability. In addition, orthogonal fractures are assumed to have identical properties. However, most if not all of horizontal wells drilled in shale gas reservoirs are hydraulically fractured. As the hydraulic fractures propagate, they re-activate the pre-existing natural fractures (Gale et al., 2007). The result will be two orthogonal fractures systems with different properties. Therefore, dual porosity model will not be sufficient to characterize these reservoirs. As a result, the triple-porosity model with fully transient flow assumption (Model 1) will be used to model horizontal shale gas wells. For this specific case, macrofractures are the hydraulic fractures while microfractures are the natural fractures.

Analysis Procedure. Due to the large number of variables involved in the triple-porosity model, nonlinear regression will be utilized to estimate a set of unknown parameters by matching the well's production rate. Other parameters may be assumed or estimated through other methods. Including many variables in the regression may lead to non-uniqueness of the converged solution. The parameters to be found by regression are fractures intrinsic permeabilities, drainage area half-width (hydraulic fracture half-length) and natural fractures spacing. After the match is obtained, the well model is fully defined. Hence, the OGIP can be calculated by volumetric method and well future production can be forecasted.

Nonlinear Regression. The triple-porosity model presented in this paper needs at most five parameters; namely two ω's, two λ's and y_{De}. In addition, these calculated parameters depend on reservoir properties which have to be estimated. This leads to estimation of many parameters that may not be known or needs to be calculated. Therefore, the need for regression arises in order to match field data and have a good estimate of the sought reservoir or well parameters. In automated well test interpretations, the common regression methods are the least squares (LS), least absolute value (LAV) and modified least absolute value minimization (Rosa and Horne 1995, 1996). It was found, however, that the least absolute value regression method is the most appropriate in matching noisy data and can be used effectively with triple-porosity model to match field data (Al-Ahmadi 2010).

However, in order to get the most accurate results with regression, data that shows special trends should be included in the regression. For example, if the data that shows linear flow was only included in the regression and the data that shows a bi-linear flow just before it was ignored, the data will be matched but the solutions will not be representative as if that data was also included. In short, as expected the more data included in the regression, the more accurate the results will be.

Field Case. A field case from the Barnett Shale will be used to demonstrate the application of the triple-porosity model. Gas rate history for these wells is shown in Fig. 11. The fully transient model (Model 1) with nonlinear regression and normalized time will be applied. Gas adsorption will be included in the analysis as well. The well is matched with the analytical solutions by first assuming no adsorbed gas and then including gas adsorption. Comparisons are made for each well. The following adsorption data are used for the Barnett Shale (Mengal 2010):

V_L = 96 scf/ton
p_L = 650 psi
Bulk Density = 2.58 gm/cc

Well 314 is a horizontal well with multistage hydraulic fracturing treatment producing at a constant bottomhole pressure.

The well production rate exhibits a half-slope on the log-log plot of rate versus time indicating a linear flow. However, the early and late data deviate from this trend. The early deviation may be due to skin effect due to the presence of fracturing job water in the hydraulic fractures making it difficult for the gas to start flowing to

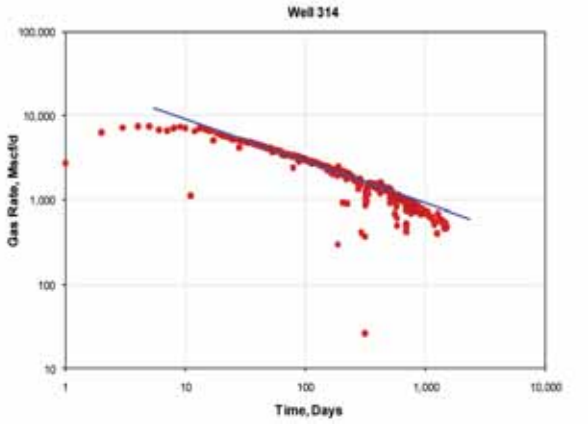

Fig. 11 – Log-Log plot of gas rate versus time for a horizontal shale gas wells. The well exhibits a linear flow for almost two log cycles. The blue and indicates a half-slope.

Table 4 – Well 314 data

"Known" Data			Assumed Data		
L_F	(ft)	106	φ_F		0.2
n_F		28	w_F	(ft)	0.1
φ_m		0.06	φ_f		0.01
k_m	(md)	1.5×10^{-4}	w_f	(ft)	0.01
h	(ft)	300			
x_e	(ft)	2968			
μ_{gi}	(cp)	0.0201	Unknown Data		
B_{gi}	(rcf/scf)	0.00509			
c_{ti}	(psi^{-1})	300×10^{-6}	$k_{F,in}$	(md)	
p_i	(psi)	2950	$k_{f,in}$	(md)	
p_{wf}	(psi)	500	y_e	(ft)	
$m(p_i)$	(psi^2/cp)	5.97×10^8	L_f	(ft)	
$m(p_{wf})$	(psi^2/cp)	2.03×10^7			
T	(°R)	610			
S_{wi}		0.3			

the well (Bello and Wattenbarger 2009; Al-Ahmadi et al., 2010). The later deviation is due to either start of boundary dominated flow (BDF) or reduction of well's drainage area due to drilling nearby well. In this work, no skin effect is considered and the later deviation will be dealt with as BDF. However, if the well is affected by skin, it results in a lower permeability value for the hydraulic fractures.

Table 4 summarizes well 314 data in addition to other assumed parameters. From the hydraulic fractures treatment, hydraulic fractures spacing is calculated assuming each perforation cluster corresponds to a hydraulic fracture. In addition, drainage area length, x_e, is the same as perforated interval. The matrix porosity and permeability used are the most available in the literature for the Barnett Shale. Representative values are assumed for fractures intrinsic porosity and width. Finally, the fractures intrinsic permeabilities, drainage area half-width and natural fractures spacing will be found by regression.

Regression results are shown in Table 5 and Fig. 12 with and without adsorption using LAV method.

From the regression results above, the hydraulic fractures intrinsic permeability is more than an order of magnitude compared to that of the natural fractures.

Table 5 – Regression results for Well 314			
	First Guess	LAV Results (Without Adsorption)	LAV Results (With Adsorption)
$k_{F,in}$	100	10.9	9.4
$k_{f,in}$	1	0.26	0.33
L_f	10	24	22.4
y_e	300	205	160
Iterations	–	18	21
OGIP, *Bscf*	–	3.01	4.05

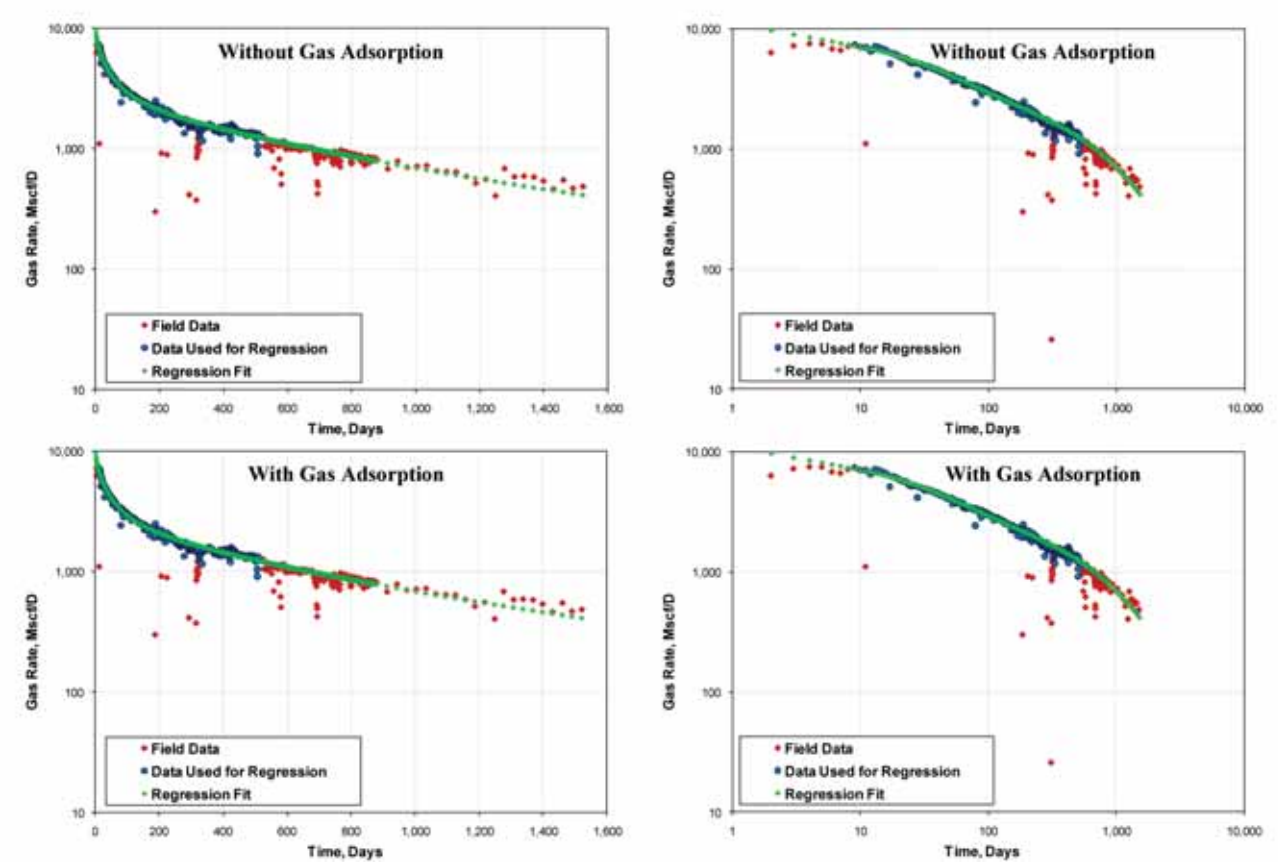

Fig. 12 – Matching Well 314 production history using the regression results without (top) and with (bottom) adsorption. On the left is the decline curve plot and log-log plot is on the right for gas rate vs. time.

In addition, the natural fractures permeability is about three orders of magnitude compared to the matrix permeability. Furthermore, the natural fracture spacing is about 23 ft indicating that matrix is in fact enhanced by natural fractures.

Including adsorption did not change the estimate of fractures intrinsic permeabilities or the natural fractures spacing but it had a big impact on drainage area half-width and consequently OGIP. Thus, including adsorption reduces the reservoir size while increasing its gas content by 35%. The same matrix porosity was used in both cases which may not be physically correct. The calculated *OGIP* is 3.01 *Bscf* if adsorbed gas is ignored. Al-Ahmadi et al., (2010) estimated 2.74 *Bscf* for *OGIP* for this well using linear dual-porosity model. The two estimates are within 10% relative error.

Knowing all the triple-porosity parameters, the whole well production history is forecasted as shown in Fig.

12 based on the regression results for the first 500 days. As can be seen, the model very well reproduced the well production trend with and without adsorption as shown on the log-log and decline curve plots.

Conclusions

The major conclusions from this work can be summarized as follows:

1. Triple-porosity models are proposed as a more practical technique for capturing fractured reservoir heterogeneity by allowing fractures to have different properties.
2. New triple-porosity (dual-fracture) solutions have been developed for fractured linear reservoirs and proved to be applicable to radial flow geometry as well.
3. Six flow regions can be identified for fully transient triple-porosity model (Model 1).
4. The new model has been verified by reducing it to simpler dual porosity models and by comparing it to reservoir simulation.
5. The derived solutions are also applicable to gas flow using gas real gas pseudo-pressure and normalized time.
6. Triple-porosity fully transient model (Model 1) is applicable to fractured shale gas horizontal wells when gas adsorption is incorporated. The model can be used to match field data, characterize well drainage area, determine reservoir size and *OGIP* and forecast future production.

Nomenclature

A_{cw}	cross-sectional area to flow defined as $2hx_e$, ft^2
A_{cm}	total matrix surface area draining into fracture system, ft^2
B_{gi}	formation volume factor at initial reservoir pressure, rcf/scf
c_t	total compressibility, psi^{-1}
E	objective function
$\bar{g}$	objective function gradient
h	reservoir thickness, ft
H	Hessian matrix
k_F	macrofractures bulk permeability, md
k_f	microfracture bulk permeability, md
$k_{F,in}$	macrofracture intrinsic permeability, md
$k_{f,in}$	microfracture intrinsic permeability, md
k_m	matrix permeability, md
L_F	macrofractures spacing, ft
L_f	microfractures spacing, ft
$m(p)$	real gas pseudo-pressure, psi^2/cp
p_D	dimensionless pressure (transient triple porosity model)
p_i	initial reservoir pressure, psi
p_L	Langmuir's pressure, psi
p_{wf}	wellbore flowing pressure, psi
q_D	dimensionless rate (transient triple porosity model)
q_{DL}	dimensionless rate based on $A_{cw}^{0.5}$ and k_F (rectangular geometry, triple porosity)
q_g	gas rate, Mscf/day
r_w	wellbore radius, ft
S_{gi}	initial gas saturation, fraction
S_{wi}	initial water saturation, fraction
T	absolute temperature, °R
t	time, days
t_{DAcw}	dimensionless time based on A_{cw} and k_F (rectangular geometry, triple-porosity)
t_{esr}	time to end of straight line on the square root of time plot, days
V_b	total system bulk volume, ft^3
V_L	Langmuir's volume, scf/ton (or scf/cuf)
V	bulk volume fraction, dimensionless
x_e	drainage area length (rectangular geometry), ft
y_{De}	dimensionless reservoir half-width (rectangular geometry)
y_e	drainage area half-width (rectangular geometry), equivalent to fracture half-length, ft

Greek symbols

α	Warren and Root shape factor
$\vec{\alpha}$	vector of unknown regression parameters
λ	dimensionless interporosity parameter
μ	viscosity, cp
ω	dimensionless storativity ratio
ϕ	porosity

Subscripts

i	initial
F	macrofracture (hydraulic fracture)
f	microfracture (natural fracture)
m	matrix
$t = F+f+m$	total system (macrofracture +microfracture + matrix)

Acknowledgement

Most of the contents of this paper is based on Hasan A. Al-Ahmadi M.S. degree work at Texas A&M University. The authors would like to thank Saudi Aramco Management for permission to publish this paper.

References

Abdassah, D. and Ershaghi, I. 1986. Triple-Porosity Systems for Representing Naturally Fractured Reservoirs. *SPE Form Eval* (April): 113–127. SPE-13409-PA.

Al-Ahmadi, H.A. 2010. A Triple-Porosity Model for Fractured Horizontal Wells. M.Sc. Thesis, Texas A&M U., College Station, Texas.

Al-Ahmadi, H.A., Almarzooq, A.M. and Wattenbarger, R.A. 2010. Application of Linear Flow Analysis to Shale Gas Wells – Field Cases. Paper SPE 130370 presented at the 2010 Unconventional Gas Conference, Pittsburgh, Pennsylvania, 23-25 February.

Al-Ghamdi, A. and Ershaghi, I. 1996. Pressure Transient Analysis of Dually Fractured Reservoirs. *SPE J.* (March): 93–100. SPE-26959-PA.

Al-Hussainy, R., Ramey Jr., H.J. and Crawford, P.B. 1966. The Flow of Real Gas Through Porous Media. *J. Pet Tech* (May): 624–636. SPE-1243A-PA

Anderson, D.M., Nobakht, M., Moghadam, S. and Mattar, L. 2010. Analysis of Production Data from Fractured Shale Gas Wells. Paper SPE 131787 presented at the SPE Unconventional Gas Conference, Pittsburgh, Pennsylvania, 23-25 February.

Barenblatt, G.I., Zhelto, I.P. and Kochina, I.N. 1960. Basic Concepts of the Theory of Seepage of Homogeneous Liquids in Fissured Rocks. *Journal of Applied Mathematical Mechanics* (USSR) 24 (5): 852–864.

Barrodale, I. and Roberts, F.D.K. 1974. Solution of an Overdetermined System of Equations in the l1 Norm. Communication of the ACM 17 (6): 319–320.

Bello, R.O. and Wattenbarger, R.A. 2008. Rate Transient Analysis in Naturally Fractured Shale Gas Reservoirs. Paper SPE 114591 presented at the CIPC/SPE Gas Technology Symposium 2008 Joint Conference, Calgary, Alberta, Canada, 16-19 June.

Bello, R.O. and Wattenbarger, R.A. 2009. Modeling and Analysis of Shale Gas Production with a Skin Effect. Paper CIPC 2009-082 presented at the Canadian International Petroleum Conference, Calgary, Alberta, Canada, 16-18 June.

Bello, R.O. and Wattenbarger, R.A. 2010. Multistage Hydraulically Fractured Shale Gas Rate Transient Analysis. Paper SPE 126754 presented at the SPE North Africa Technical Conference and Exhibition held in Cairo, Egypt, 14-17 February.

Bello, R.O. 2009. Rate Transient Analysis in Shale Gas Reservoirs with Transient Linear Behavior. Ph.D. Dissertation, Texas A&M U., College Station, Texas.

Brown, M., Ozkan, E., Raghavan, R. and Kazemi, H. 2009. Practical Solutions for Pressure Transient Responses of Fractured Horizontal Wells in Unconventional Reservoirs. Paper SPE 125043 presented at the Annual Technical Conference and Exhibition, New Orleans, Louisiana, 4-7 October.

Bumb, A.C. and McKee, C.R. 1988. Gas-Well Testing in the Pressure of Desorption for Coalbed Methane and Devonian Shale. *SPE Form Eval* (March): 179-185. SPE-15227-PA.

Cheney, E.W. and Kincaid, R.D. 1985. Numerical Mathematics and Computing, 2nd edition. Monterey, California: Brooks/Cole Publishing Company.

CMG Simulator. 2008. Computer Modeling Group, Calgary, Canada.

de Swaan, O.A. 1976. Analytic Solutions for Determining Naturally Fractured Reservoir Properties by Well Testing. *SPE J.* (June): 117– 122. SPE-5346-PA.

Dreier, J. 2004. Pressure-Transient Analysis of Wells in Reservoirs with a Multiple Fracture Network. M.Sc. Thesis, Colorado School of Mines, Golden, Colorado.

Dreier, J., Ozkan, E. and Kazemi, H. 2004. New Analytical Pressure-Transient Models to Detect and Characterize Reservoirs with Multiple Fracture Systems. Paper SPE 92039 presented at the SPE International Petroleum Conference in Mexico, Puebla, Mexico, 8-9 November.

El-Banbi, A.H. 1998. Analysis of Tight Gas Wells. Ph.D. Dissertation, Texas A&M U., College Station, Texas.

Fraim, M.L. and Wattenbarger, R.A. 1987. Gas Reservoir Decline-Curve Analysis Using Type Curve with Real Gas Pseudopressure and Normalized Time. *SPE Form Eval* (December): 671–682. SPE-14238-PA.

Gale, J.F., Reed, R.M. and Holder, J. 2007. Natural Fractures in the Barnett Shale and their Importance for Hydraulic Fracture Treatments. *AAPG Bulletin*. 91 (4): 603–622.

Jalali, Y. and Ershaghi, I. 1987. Pressure Transient Analysis of Heterogeneous Naturally Fractured Reservoirs. Paper SPE 16341 presented at the SPE California Regional Meeting, Ventura, California, 8-10 April.

Kazemi, H. 1969. Pressure Transient of Naturally Fractured Reservoirs with Uniform Fracture Distribution. *SPE J.* (December):451–462. SPE-2156A-PA.

King, G.R. 1993. Material-Balance Techniques for Coal-Seam and Devonian Shale Gas Reservoirs with Limited Water Influx. *SPE Res Eng* (February): 67–72. SPE-20730-PA.

Liu, C.Q. 1981. Exact Solution for the Compressible Flow Equations through a Medium with Triple-Porosity. *Applied Mathematics and Mechanics* 2 (4): 457–462.

Liu, C.Q. 1983. Exact Solution of Unsteady Axisymmetrical Two-Dimensional Flow through Triple Porous Media. *Applied Mathematics and Mechanics* 4 (5): 717–724.

Liu, J.C., Bodvarsson, G.S. and Wu, Y.S. 2003. Analysis of Flow Behavior in Fractured Lithophysal Reservoirs. *Journal of Contaminant Hydrology* 62-63: 189–211.

Mayerhofer, M.J., Lolon, E.P., Youngblood, J.E. and Heinze, J.R. 2006. Integration of Microseismic Fracture Mapping Results with Numerical Fracture Network Production Modeling in the Barnett Shale. Paper SPE 102103 presented at the Annual Technical Conference and Exhibition, San Antonio, Texas, 24-27 September.

Medeiros, F., Ozkan, E. and Kazemi, H. 2008. Productivity and Drainage Area of Fractured Horizontal Wells in Tight Gas Reservoirs. *SPE Res Eval & Eng* (October): 902–911. SPE-108110-PA.

Mengal, S.A. 2010. Accounting for Adsorbed Gas and Its Effect on Production Behavior of Shale Gas Reservoirs. M.Sc. Thesis, Texas A&M U., College Station, Texas.

Nelson, R.A. 2001. Geologic Analysis of Naturally Fractured Reservoirs, 2nd edition. Woburn, Massachusetts: Butterworth-Heinemann.

Ozkan, E., Brown, M., Raghavan, R. and Kazemi, H. 2009. Comparison of Fractured Horizontal-Well Performance in Conventional and Unconventional Reservoirs. Paper SPE 121290 presented at the SPE Western Regional Meeting, San Jose, California, 24-26 March.

Ozkan, E., Ohaeri, U. and Raghavan, R. 1987. Unsteady Flow to a Well Produced at a Constant Pressure in Fractured Reservoir. *SPE Form Eval* (June): 186-200. SPE-9902-PA.

Rosa, A.J. and Horne, R.N. 1995. Automated Well Test Analysis Using Robust (LAV) Nonlinear Parameter Estimation. *SPE Advanced Technology Series* 3 (1): 95–102. SPE-22679-PA.

Rosa, A.J. and Horne, R.N. 1996. New Approaches for Robust Nonlinear Parameter Estimation in Automated Well Test Analysis Using the Least Absolute Value Criterion. *SPE Advanced Technology Series* 4 (1): 21–27. SPE-26964-PA.

Samandarli, O. 2011. A New Method for History

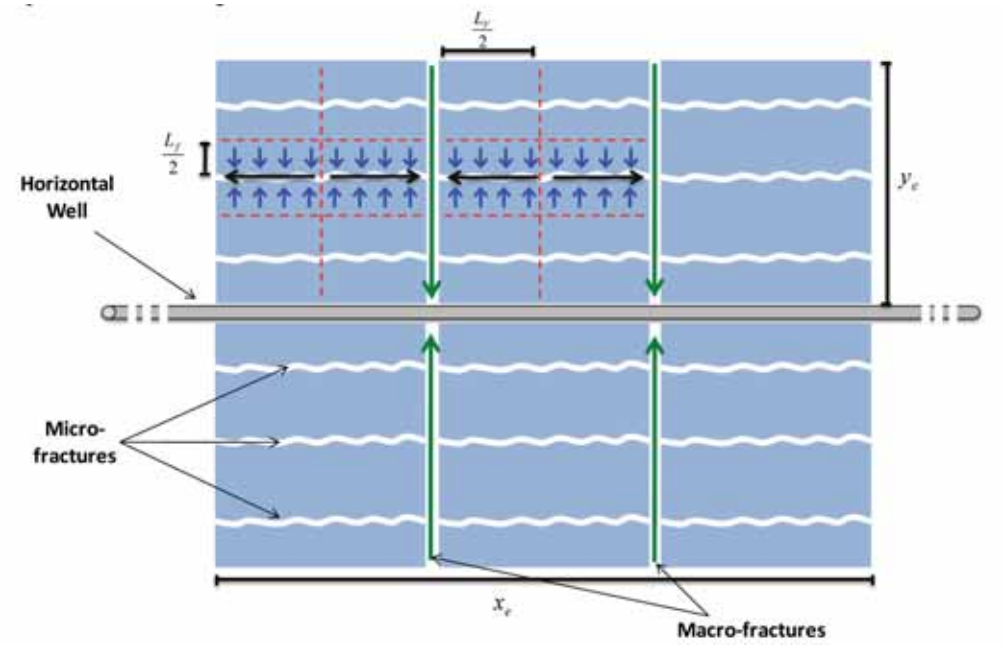

Fig. A-1 – A sketch of triple-porosity system under sequential feed assumption. Arrows show flow directions.

Matching and Forecasting of Shale Gas/Oil Reservoirs with Dual and Triple-Porosity Systems. M.Sc. Thesis, Texas A&M U., College Station, Texas.

Sarma, P. and Aziz, K. 2006. New Transfer Functions for Simulation of Naturally Fractured Reservoirs with Dual-Porosity Models. *SPE J.* (September): 328–340. SPE-90231-PA.

Stehfest, H. 1970. Algorithm 358 – Numerical Inversion of Laplace Transforms. Communication of the ACM 13 (1): 47 – 49.

Van Everdingen, A.F. and Hurst, W. 1949. The Application of the Laplace Transformation to Flow Problems in Reservoirs. Trans., AIME, 186: 305–324.

Warren, J.E. and Root, P.J. 1963. The Behavior of Naturally Fractured Reservoirs. *SPE J.* (September): 245–255. SPE-426-PA.

Wattenbarger, R.A. 2007. Some Reservoir Performance Aspects of Unconventional Gas Production. Private Conference Presentation.

Wu, Y.S., Liu, H.H. and Bodvarsson, G.S. 2004. A Triple-Continuum Approach for Modeling Flow and Transport Processes in Fractured Rock. *Journal of Contaminant Hydrology* 73: 145–179.

Appendix: Derivation of Linear Triple-Porosity Fully Transient Model

Model 1: Fully Transient Triple-Porosity Model. The first Sub-model, Model 1, is the fully transient model. The flow between matrix and microfractures and that between microfractures and macrofractures are under transient condition. This model is an extension to the dual-porosity transient slab model (Kazemi 1969 Model). The derivation starts by writing the differential equations describing the flow in each medium.

Matrix Equation

Since the flow transfer from matrix to fractures is under transient condition, the matrix equation is given by:

$$\frac{\partial^2 p_m}{\partial z^2} = \frac{[\varphi V \mu c_t]_m}{k_m} \frac{\partial p_m}{\partial t} \qquad \text{(A-1)}$$

Note: z here is a direction parallel to y-axis. It is not the vertical direction. Microfracture Equation

$$\frac{k_f}{\mu} \frac{\partial^2 p_f}{\partial x^2} + q_{source,m} = (\varphi V c_t)_f \frac{\partial p_f}{\partial t} \qquad \text{(A-2)}$$

$q_{source,m}$, is a source term of flow from matrix to the microfracture under transient flow and can be written as:

$$q_{source,m} = -\frac{1}{L_f/2} \frac{k_m}{\mu} \frac{\partial p_m}{\partial z}\bigg|_{z=L_f/2} \qquad \text{(A-3)}$$

Thus, the final form of microfractures equation is:

$$\frac{\partial^2 p_f}{\partial x^2} = \frac{[\varphi V \mu c_t]_f}{k_f} \frac{\partial p_f}{\partial t} + \frac{1}{L_f/2} \frac{k_m}{k_f} \frac{\partial p_m}{\partial z}\bigg|_{z=L_f/2} \qquad \text{(A-4)}$$

Macrofracture Equation

The macrofractures receive flow from the microfractures and the flow can be modeled using the equation:

$$\frac{k_F}{\mu} \frac{\partial^2 p_F}{\partial y^2} + q_{source,f} = (\varphi V c_t)_F \frac{\partial p_F}{\partial t} \qquad \text{(A-5)}$$

$q_{source,f}$, is the source term of flow from microfractures to the macrofracture under transient flow and can be written as:

$$q_{source,f} = -\frac{1}{L_F/2} \frac{k_f}{\mu} \frac{\partial p_f}{\partial x}\bigg|_{x=L_F/2} \qquad \text{(A-6)}$$

Thus, the final form of microfractures equation is:

$$\frac{\partial^2 p_F}{\partial y^2} = \frac{[\varphi V \mu c_t]_F}{k_F} \frac{\partial p_F}{\partial t} + \frac{1}{L_F/2} \frac{k_f}{k_F} \frac{\partial p_f}{\partial x}\bigg|_{x=L_F/2} \qquad \text{(A-7)}$$

System of Equations with Initial and Boundary Conditions

Matrix:

$$\frac{\partial^2 p_m}{\partial z^2} = \frac{[\varphi V \mu c_t]_m}{k_m} \frac{\partial p_m}{\partial t} \qquad \text{(A-1)}$$

Microfractures:

$$\frac{\partial^2 p_f}{\partial x^2} = \frac{[\varphi V \mu c_t]_f}{k_f} \frac{\partial p_f}{\partial t} + \frac{1}{L_f/2} \frac{k_m}{k_f} \frac{\partial p_m}{\partial z}\bigg|_{z=L_f/2} \qquad \text{(A-4)}$$

Macrofractures:

$$\frac{\partial^2 p_F}{\partial y^2} = \frac{[\varphi V \mu c_t]_F}{k_F} \frac{\partial p_F}{\partial t} + \frac{1}{L_F/2} \frac{k_f}{k_F} \frac{\partial p_f}{\partial x}\bigg|_{x=L_F/2} \qquad \text{(A-7)}$$

Initial and boundary conditions are:

Matrix:

Initial condition: $p_m(z,0) = p_i$

Inner boundary: $\frac{\partial p_m}{\partial z} = 0 \quad @\ z = 0$

Outer boundary: $p_m = p_f \quad @\ z = \frac{L_f}{2}$

Microfractures:

Initial condition: $p_f(x,0) = p_i$

Inner boundary: $\frac{\partial p_f}{\partial x}=0 \quad @\ x=0$

Outer boundary: $p_f = p_F \quad @\ x=\frac{L_F}{2}$

Macrofractures:

Initial condition: $p_F(y,0)=p_i$

Inner boundary: $q=-\frac{k_F A_{cw}}{\mu}\left.\frac{\partial p_F}{\partial y}\right|_{y=0}$

Outer boundary: $\frac{\partial p_F}{\partial y}=0 \quad @\ y=y_e$

System Dimensionless Equations with Initial and Boundary Conditions

Matrix:

$$\frac{\partial^2 p_{DLm}}{\partial z_D^2}=\frac{3\omega_m}{\lambda_{Ac,fm}}\frac{\partial p_{DLm}}{\partial t_{DAc}} \qquad \text{(A-8)}$$

Microfractures:

$$\frac{\partial^2 p_{DLf}}{\partial x_D^2}=\frac{3\omega_f}{\lambda_{Ac,Ff}}\frac{\partial p_{DLf}}{\partial t_{DAc}}+\frac{\lambda_{Ac,fm}}{\lambda_{Ac,Ff}}\left.\frac{\partial p_{DLm}}{\partial z_D}\right|_{z_D=1} \qquad \text{(A-9)}$$

Macrofractures:

$$\frac{\partial^2 p_{DLF}}{\partial y_D^2}=\omega_F\frac{\partial p_{DLF}}{\partial t_{DAc}}+\frac{\lambda_{Ac,Ff}}{3}\left.\frac{\partial p_{DLf}}{\partial x_D}\right|_{x_D=1} \qquad \text{(A-10)}$$

Dimensionless initial and boundary conditions are:

Matrix:

Initial condition: $p_{DLm}(z_D,0)=0$

Inner boundary: $\frac{\partial p_{DLm}}{\partial z_D}=0 \quad @\ z_D=0$

Outer boundary: $p_{DLm}=p_{DLf} \quad @\ z_D=1$

Microfractures:

Initial condition: $p_{DLf}(x_D,0)=0$

Inner boundary: $\frac{\partial p_{DLf}}{\partial x_D}=0 \quad @\ x_D=0$

Outer boundary: $p_{DLf}=p_{DLF} \quad @\ x_D=1$

Macrofractures:

Initial condition: $p_{DLF}(y_D,0)=0$

Inner boundary: $\left.\frac{\partial p_{DLF}}{\partial y_D}\right|_{y_D=0}=-2\pi$

Outer boundary: $\frac{\partial p_{DLF}}{\partial y_D}=0 \quad @\ y_D=y_{De}=y_e/\sqrt{A_{cw}}$

Laplace Transformation

In order to solve the above system of differential equations, they have to be transformed into Laplace domain for easier solving as detailed below.

Matrix equation:

$$\frac{\partial^2 \overline{p_{DLm}}}{\partial z_D^2}=\frac{3\omega_m}{\lambda_{Ac,fm}}\left[s\,\overline{p_{DLm}}-\overline{p_{DLm}}(z_D,0)\right] \qquad \text{(A-11)}$$

The initial and boundary conditions in Laplace domain are:

Initial condition: $\overline{p_{DLm}}(z_D,0)=0$

Inner boundary: $\frac{\partial \overline{p_{DLm}}}{\partial z_D}=0 \quad @\ z_D=0$

Outer boundary: $\overline{p_{DLm}}=\overline{p_{DLf}} \quad @\ z_D=1$

Using the initial condition, Eq. A-11 becomes:

$$\frac{\partial^2 \overline{p_{DLm}}}{\partial z_D^2}-\frac{3\omega_m}{\lambda_{Ac,fm}}s\,\overline{p_{DLm}}=0 \qquad \text{(A-12)}$$

The general solution for Eq. A-12 is given by:

$$\overline{p_{DLm}}=A\cosh\left(\sqrt{\frac{3s\,\omega_m}{\lambda_{Ac,fm}}}\,z_D\right)+B\sinh\left(\sqrt{\frac{3s\,\omega_m}{\lambda_{Ac,fm}}}\,z_D\right) \qquad \text{(A-13)}$$

The constants A and B are determined as:

$$B=0 \qquad \text{(A-14)}$$

$$A=\frac{\overline{p_{DLf}}}{\cosh\left(\sqrt{\frac{3s\,\omega_m}{\lambda_{Ac,fm}}}\right)} \qquad \text{(A-15)}$$

Therefore, the final solution for Eq. A-12 is

$$\overline{p_{DLm}}=\frac{\overline{p_{DLf}}}{\cosh\left(\sqrt{\frac{3s\,\omega_m}{\lambda_{Ac,fm}}}\right)}\cosh\left(\sqrt{\frac{3s\,\omega_m}{\lambda_{Ac,fm}}}\,z_D\right) \qquad \text{(A-16)}$$

Microfractures equation:

$$\frac{\partial^2 \overline{p_{DLf}}}{\partial x_D^2}=\frac{3\omega_f}{\lambda_{Ac,Ff}}\left[s\,\overline{p_{DLf}}-\overline{p_{DLf}}(x_D,0)\right]+\frac{\lambda_{Ac,fm}}{\lambda_{Ac,Ff}}\left.\frac{\partial \overline{p_{DLm}}}{\partial z_D}\right|_{z_D=1} \qquad \text{(A-17)}$$

The initial and boundary conditions in Laplace domain are:

Initial condition: $\overline{p_{DLf}}(x_D,0)=0$

Inner boundary: $\frac{\partial \overline{p_{DLf}}}{\partial x_D}=0 \quad @\ x_D=0$

Outer boundary: $\overline{p_{DLf}}=\overline{p_{DLF}} \quad @\ x_D=1$

Using the initial condition, Eq. A-17 becomes:

$$\frac{\partial^2 \overline{p_{DLf}}}{\partial x_D^2} = \frac{3\omega_f}{\lambda_{Ac,Ff}} s\,\overline{p_{DLf}} + \frac{\lambda_{Ac,fm}}{\lambda_{Ac,Ff}} \left.\frac{\partial \overline{p_{DLm}}}{\partial z_D}\right|_{z_D=1} \quad \text{(A-18)}$$

Now, differentiating Eq. A-16, we have:

$$\left.\frac{\partial \overline{p_{DLm}}}{\partial z_D}\right|_{z_D=1} = \overline{p_{DLf}} \sqrt{\frac{3s\,\omega_m}{\lambda_{Ac,fm}}} \tanh\left(\sqrt{\frac{3s\,\omega_m}{\lambda_{Ac,fm}}}\right) \quad \text{(A-19)}$$

Substituting Eq. A-19 in A-18:

$$\frac{\partial^2 \overline{p_{DLf}}}{\partial x_D^2} = s\,\overline{p_{DLf}}\left[\frac{3\,\omega_f}{\lambda_{Ac,Ff}} + \frac{\lambda_{Ac,fm}}{s\,\lambda_{Ac,Ff}} \sqrt{\frac{3s\,\omega_m}{\lambda_{Ac,fm}}} \tanh\left(\sqrt{\frac{3s\,\omega_m}{\lambda_{Ac,fm}}}\right)\right] \quad \text{(A-20)}$$

Or in short form:

$$\frac{\partial^2 \overline{p_{DLf}}}{\partial x_D^2} - s\,f_f(s)\overline{p_{DLf}} = 0 \quad \text{(A-21)}$$

where

$$f_f(s) = \frac{3\,\omega_f}{\lambda_{Ac,Ff}} + \frac{\lambda_{Ac,fm}}{s\,\lambda_{Ac,Ff}} \sqrt{\frac{3s\,\omega_m}{\lambda_{Ac,fm}}} \tanh\left(\sqrt{\frac{3s\,\omega_m}{\lambda_{Ac,fm}}}\right) \quad \text{(A-22)}$$

The general solution for Eq. A-21 is given by:

$$\overline{p_{DLf}} = A\cosh\left(\sqrt{s\,f_f(s)}\,x_D\right) + B\sinh\left(\sqrt{s\,f_f(s)}\,x_D\right) \quad \text{(A-23)}$$

The constants A and B are determined as:

$$B = 0 \quad \text{(A-24)}$$

$$A = \frac{\overline{p_{DLF}}}{\cosh\left(\sqrt{s\,f_f(s)}\right)} \quad \text{(A-25)}$$

Therefore, the final solution for Eq. A-21 is:

$$\overline{p_{DLf}} = \frac{\overline{p_{DLF}}}{\cosh\left(\sqrt{s\,f_f(s)}\right)} \cosh\left(\sqrt{s\,f_f(s)}\,x_D\right) \quad \text{(A-26)}$$

Macrofractures equation:

$$\frac{\partial^2 \overline{p_{DLF}}}{\partial y_D^2} = \omega_F\left[s\,\overline{p_{DLF}} - \overline{p_{DLF}}(y_D,0)\right] + \frac{\lambda_{Ac,Ff}}{3} \left.\frac{\partial \overline{p_{DLf}}}{\partial x_D}\right|_{x_D=1} \quad \text{(A-27)}$$

Initial and boundary conditions in Laplace domain are:

Initial condition: $\overline{p_{DLF}}(y_D,0) = 0$

Inner boundary: $\left.\frac{\partial \overline{p_{DLF}}}{\partial y_D}\right|_{y_D=0} = -\frac{2\pi}{s}$

Outer boundary: $\frac{\partial \overline{p_{DLF}}}{\partial y_D} = 0 \quad @\ y_D = y_{De} = y_e/\sqrt{A_{cw}}$

Using the initial condition, Eq. A-27 becomes:

$$\frac{\partial^2 \overline{p_{DLF}}}{\partial y_D^2} = \omega_F\, s\,\overline{p_{DLF}} + \frac{\lambda_{Ac,Ff}}{3} \left.\frac{\partial \overline{p_{DLf}}}{\partial x_D}\right|_{x_D=1} \quad \text{(A-28)}$$

Now differentiating Eq. A-26:

$$\left.\frac{\partial \overline{p_{DLf}}}{\partial x_D}\right|_{x_D=1} = \overline{p_{DLF}} \sqrt{s\,f_f(s)} \tanh\left(\sqrt{s\,f_f(s)}\right) \quad \text{. (A-29)}$$

Now Eq.A-28 becomes:

$$\frac{\partial^2 \overline{p_{DLF}}}{\partial y_D^2} - s\,\overline{p_{DLF}}\left[\omega_F + \frac{\lambda_{Ac,Ff}}{3s} \sqrt{s\,f_f(s)} \tanh\left(\sqrt{s\,f_f(s)}\right)\right] = 0 \quad \text{(A-30)}$$

Or in short form:

$$\frac{\partial^2 \overline{p_{DLF}}}{\partial y_D^2} - s\,f(s)\overline{p_{DLF}} = 0 \quad \text{(A-31)}$$

where f(s) is the definition for the fracture function for Model 1:

$$f(s) = \omega_F + \frac{\lambda_{Ac,Ff}}{3s} \sqrt{s\,f_f(s)} \tanh\left(\sqrt{s\,f_f(s)}\right)$$
$$f_f(s) = \frac{3\,\omega_f}{\lambda_{Ac,Ff}} + \frac{\lambda_{Ac,fm}}{s\,\lambda_{Ac,Ff}} \sqrt{\frac{3s\,\omega_m}{\lambda_{Ac,fm}}} \tanh\left(\sqrt{\frac{3s\,\omega_m}{\lambda_{Ac,fm}}}\right) \quad \text{(A-32)}$$

Using this fracture function in Eqs. 2 or 3 will give the triple-porosity fully transient response for constant rate or constant pressure cases, respectively.

Detailed derivations of the other three models are available in Al-Ahmadi (2010).

Simulation Study on Surfactant-Polymer Flood Performance in Fractured Carbonate Reservoir

By Nawaf I. SayedAkram, Saudi Aramco; Daulat Mamora,Texas A&M University.

This paper was prepared for presentation at the 2011 SPE Saudi Arabia Section Technical Symposium and Exhibition held in AlKhobar, Saudi Arabia, 15–18 May 2011.

Abstract

This paper presents a comprehensive simulation study on the impact of natural fractures on the performance of surfactant polymer flood in a field wide scale. The simulation model utilized for the study is a dual porosity dual permeability model representing 1/8 of a 20-acre 5-spot pattern. The model parameters studied include wettability alteration, interfacial-tension changes and mobility reduction effect. The results of this study clearly indicate the importance of reservoir description and fracture modeling for a successful surfactant-polymer flood. This may lead in huge difference in reserves booking from such EOR method.

Naturally fractured carbonate reservoirs are usually characterized by mixed wettablility and low matrix permeability which leads to low oil recovery and high remaining oil saturation. Enhanced oil recovery methods such as surfactant-polymer flood (SPF) enhance the recovery by increasing the spontaneous imbibitions either by lowering the interfacial tension or altering the wettability in the matrix. However, one of the main reasons for failed surfactant-polymer floods is under-estimating the importance of the reservoir and fluid characteristics especially the description of natural fractures and their effect on recovery.

Sensitivity runs were made in field size scale in order to compare oil recovery by capillary force, buoyancy force and viscous force. The simulation study indicates a relationship between water saturation and the start of altering wettability and/or interfacial tension to maximize oil recovery. Also, when a surfactant alters the rock wettability, an optimum IFT should be identified for faster and higher imbibitions. In addition, the study shows effect on recovery by permeability contrast between that

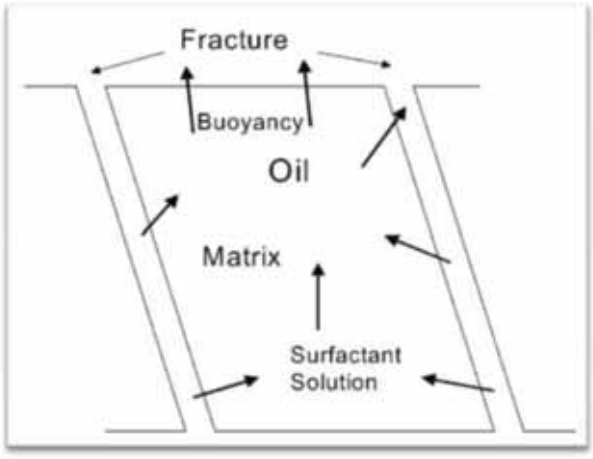

Fig. 1___Spontaneous imbibition through buoyancy force (Hirasaki and Zhang, 2004).

of the fracture and that of the matrix as well as fracture orientation with respect to injector-producer direction.

Introduction

About 40-60% of the original oil-in-place (OOIP) in reservoirs is left behind after secondary recovery. Over 60% of the remaining oil in the world can be found in carbonate reservoirs, which makes it a big area of interest for Enhance Oil Recovery (EOR) methods especially with the current oil price and increasing demand. Most of the carbonate reservoirs are fractured to a certain degree and either oil-wet or mixed-wet (Mohan, 2009).

The main characteristics of fractured reservoirs are the permeability enhancement provided by the fractures. In tight matrix blocks, fractures are the only means of fluid flow into a production well. However, the heterogeneity between fractures and matrix blocks can result in bypassed oil.

Chemical EOR

Chemical EOR is becoming more attractive with the current economics especially for water flooded reservoirs. Chemical EOR utilizes surfactant, polymers, alkaline agents or combination of these chemicals (Thomas, 2006). The use of the surfactant is either to:

- lower the interfacial tension IFT between the hydrocarbon and the injected fluid,
- create macro or micro-emulsions with oil and water that leads to improved sweep efficiency,
- change wettability to water wet through adsorption in the rock formation, or
- combination of the above.

A polymer is usually added to the injected water to enhance sweep efficiency by decreasing the mobility or increasing viscosity of the displacing fluid. Performance prediction of chemical EOR - such as surfactant-polymer flooding - in naturally fractured reservoirs is essential for pilot testing, field wide implementation and reservoir management. Generally, recovery prediction continues to be a challenging topic in fractured reservoirs. Not having a good simulation model that can capture all the interaction of the additives injected in the fractured reservoir can lead to a faulty estimation of field performance or wrong pilot design.

The main objective of this work is to study the effect of natural fractures on surfactant polymer flood (SPF) performance on a field scale using a dual-porosity dual-permeability (DPDP) simulation model. The parameters to be studied will include:

fracture permeability, spacing and orientation, matrix permeability and wettability, and the use of low interfacial tension versus capillary pressure for recovery. The main performance measurements used in this study are oil recovery with respect to the original oil-in-place (OOIP).

SOR Reduction

Interfacial tension (IFT) reduction plays a significant role in reducing the residual oil saturation (Sor). Taber (1969) found that, in order for a water flood to have effect on Sor reduction from the reservoir, interfacial tension must be lowered by a factor of 1,000 or more. IFT is generally hard to be measured in the field due to the high sensitivity to temperature, pressure and presence of

contaminants (Stegemier, 1974). The use of surfactant to reduce the IFT will diminish the capillary force which is the main driving force for spontaneous imbibitions in water wet conditions. However, spontaneous imbibitions will still occur by buoyancy force which becomes the dominant force of displacement even in oil wet conditions. Fig.1 illustrates the spontaneous imbibition caused by buoyancy in a fractured system (Hirasaki and Zhang, 2004).

Wettability alteration has been a proven method to enhance spontaneous imbibitions. In a mixed-wet or oil-wet rock, buoyancy driven flow will be resisted. In other words, reducing IFT to even ultra low will not recover the oil that adhere to the rock surface. The surfactant should be designed depending on the original wetting phase (Najafabadi et al., 2008). Fig.1.2 shows the effect of water flood based on wettability.

Schechter et al. ($N_B^{-1} = C\sigma\sqrt{\phi/k}\,/\,\Delta\rho g H$ ed capillary forces and gravity forces ition. The scale of contribution of each force is given by the inverse bond number, N_B^{-1} (Eq.1):

(1)

where C is a constant for capillary tube model, σ is interfacial tension, ϕ is the porosity, k is the permeability, Δρ is the density difference (m/L^3), g is the gravitational acceleration, and H is the height of the matrix block.

Schechter et al. (1994) found that the imbibition at high values of N_B^{-1} (>5) is dominated by capillary forces which increase by the current and counter-current of wetting phase and non-wetting phase, while at low values N_B^{-1} gravity force is the dominant one with vertical flow. At intermediate values of N_B^{-1} , recovery of the non-wetting phase was much faster than in each dominant force alone (Aldejain, 1999).

Modeling Fracture Reservoir

Simulation of chemical flooding in a fractured reservoir is either modeled as single porosity with discretized fractures or as continuum, such as multi-component dual porosity model with multiphase capability (Aldejain, 1999; Delshad et al. 2009). Both methods have their limitation. The discrete model is more detailed in representing fracture direction and flow behavior for each fracture property in a reservoir. However, in a highly fractured reservoir, discretization requires a huge computational demand which is considered one of its disadvantages. The dual porosity system, as originally developed by Warren and Root (1963), still has some limitation pertaining to fracture spacing, length, orientation and matrix flow contribution in extreme heterogeneous systems. However, dual porosity systems have evolved through the years and are still considered the best way and are widely used when modeling a naturally fractured reservoir (Tarahhom et al., 2009).

As a dual porosity model does not allow fluid to have matrix to matrix flow, dual permeability model should be used especially with relatively high matrix permeability. The dual permeability model will account for matrix-matrix flow as the pressure gradient increase in the matrix increases (Aldejain, 1999). With matrix-matrix flow included the gravity drainage is represented better than in a dual porosity model. However, it is not fully captured. Fig. 2 shows the fluid flow connectivity concept in the DPDP model.

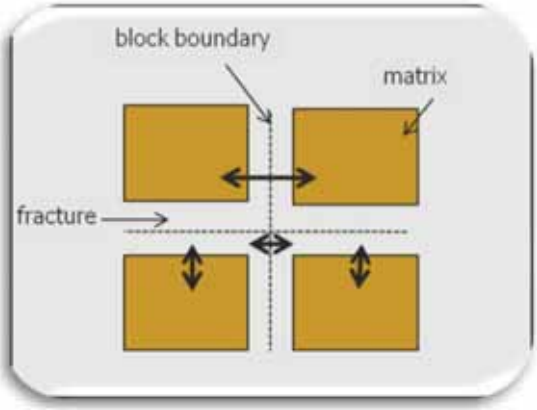

Fig. 2. Dual-porosity dual-permeability fluid communication.

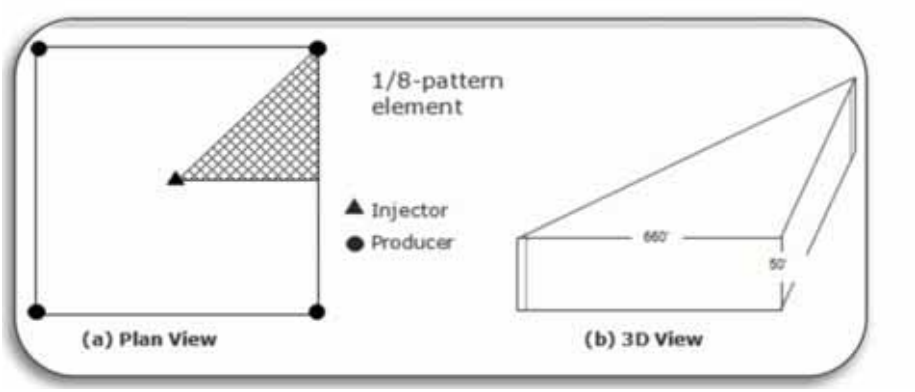

Fig. 3. Plan view and 3D view of the simulation model representing 1/8 of a 20-ac 5-spot pattern.

Table 1—Base case basic simulation data

grid block size	30x30x10	ft^3
number of grid blocks	16x31x5	
injector-producer distance	9334	ft
reservoir depth	5000	ft
reservoir pressure	2500	psi
Matrix properties:		
horizontal perm. (kh)	50	md
vertical perm. (kv)	5	md
initial oil saturation (S_{oi})	0.81	frac.
matrix porosity (ϕ)	0.2	frac.
connate water saturation (S_{wc})	0.19	frac.
Fracture properties:		
permeability (k_f)	1000	md
porosity (ϕ_f)	0.01	frac.
fracture spacing	10	ft
initial oil saturation (S_{oi})	0.99	frac.

Approach

To achieve the research objective a hypothetical naturally fractured reservoir model has been built. A commercial simulator, CMG Stars version 2009.1, has been utilized which has the capability to simulate chemical EOR processes. The study involved the following steps.

- Build a 1/8 model of an inverted 5-spot pattern to simulate a surfactant-polymer flood in a carbonate light oil reservoir (black-oil model).
- Include dual-permeability dual-porosity (DPDP) model to capture the effect of fracture system in the field.
- Add rock and fluid parameters based on published data that represent a common carbonate reservoir from permeability and porosity to wettability conditions and capillary pressure.
- Assume that surfactant used has impact on both wettability alteration and IFT reduction while the polymer changes viscosity of the injected fluid.
- Run sensitivity study on surfactant polymer flooding (SPF) performance with respect to the start of the process and the length of the injection through the life of the field.
- Run a sensitivity study on fracture spacing, permeability, flow direction, and matrix permeability.

Model Construction

The reservoir is assumed to be a fractured carbonate reservoir characterized by high fracture flow and low matrix flow. Because matrix to matrix flow was not neglected, dual-porosity dual-permeability (DPDP) model was used to capture this flow behavior. The simulation study

Table 2—Fluid properties used in simulation

	water	polymer	surfactant	oil
Phase	aqueous	aqueous	aqueous	oleic
Mass density, lb/ft3	62.97	62.97	62.97	58.2
Mol. Weight	18	100000	548	100
liquid compressibility, 1/psi	3.00E-06	3.00E-06	3.00E-06	1.00E-05
Viscosity, cp	0.6	70	0.6	3.2
Phase concentration, (wt %)	0.91	0.00075	0.09	0.00

was done using a commercial simulator, CMG STARS 2009. A 16 x 31 x 5 Cartesian grid model has been used to represent a 1/8 of a 20-acre 5-spot pattern. The distance between the injector and the producer is 633ft. The grid blocks are constructed so that the grid blocks sides are either parallel or normal to the injector-producer direction. Fig. 3 is a schematic diagram showing the 1/8 of 5-spot pattern in plan view and 3D view. A 1/8 symmetry element of the pattern is used (instead of the typical 1/4) to reduce the number of grid blocks and hence cut down on the simulation run time. The production rate was set at a maximum of 1000 bbl/day (total oil and water) while the injection rate is constrained based on a maximum injector bottom hole pressure of 2500 psi which is the initial reservoir pressure.

Injection Sequence

In an experimental core floods it is common to continuously inject chemically enhanced brine from initial oil saturation until ultimate recovery. However, in field application, the chemical injection period is much shorter due to the cost involved with respect to oil price. Therefore, to have a sensible sensitivity study on a field scale, injection period and sequence based on the published pilot trial on Big Muddy field (Saad and Sepehrnoori, 1989) was used. In this study the surfactant polymer flooding (SPF) will consist of:

- One year injection of surfactant-polymer
- Two years injection of polymer slug
- One year of polymer taper (lower concentration).

The base case will include one year of water flood before the chemical injection, and continuous water flood after the chemical injection period until the end of the assigned time of the simulation. The fluid properties of the injected fluid can be found in Table 2.

Wettability Modeling

The wettability of the matrix in the base case was assumed to be mixed-wet. The alteration in wettability affects the relative permeability curves and capillary pressure. As for the fracture system, a straight-line relative permeability and zero capillary pressure were assumed. These are common fracture properties and they were validated in the literature (Chen, 1995).

The modeling of the wettability alteration is based on an interpolation between the interfacial tension (IFT) and the capillary number which leads to calculating the relative permeability and capillary pressure at dimensionless time. There are two sets of relative permeability and capillary pressure curves that are input parameters; one set represents the rock conditions with no surfactant, and the other set represents the rock condition at maximum surfactant concentration. Fig. 4 and Fig. 5 show the relative permeability curves before and after surfactant effect. The initial relative permeability curves and capillary number behavior were selected based on the average curves of different trapping numbers presented by Delshad et al. (2009).

There are two sets of correlation that leads to interpolation between the relative permeability and capillary pressure curves before and after chemical injections based on the simulator. The first set of correlations is the IFT alterations based on the dissolved oil in the water caused by surfactant at each grid block. The second set of correlations is the capillary number

$$(N = \frac{v\mu}{\sigma})$$

which requires the interpolation of IFT first, in order to calculate the capillary number. Capillary number is presented in the simulator as the $\log_{10}(Nc)$ and called the trapping number (DTRAP). There are two trapping number for each interpolation set: one set for the wetting phase (DTRAPw) and the other for the non-wetting phase (DTRAPn). The relative permeability curves for matrix blocks for each phase are then calculated from the following equations:

$$k_{rl} = k_{rli} \cdot (1-\omega_l) + k_{rlf} \cdot \omega_l \quad (2)$$

and,

$$P_c = P_{ci} \cdot (1 - \omega_{pc}) + \omega_{pc} \cdot P_{cf} \quad (3)$$

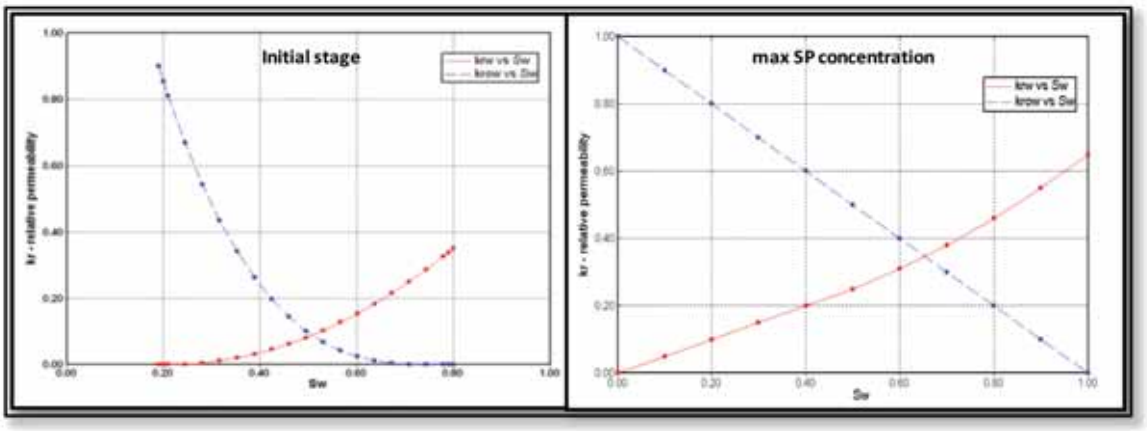

Fig. 4. Oil-water relative permeability curves at initial stage and at maximum surfactant concentration.

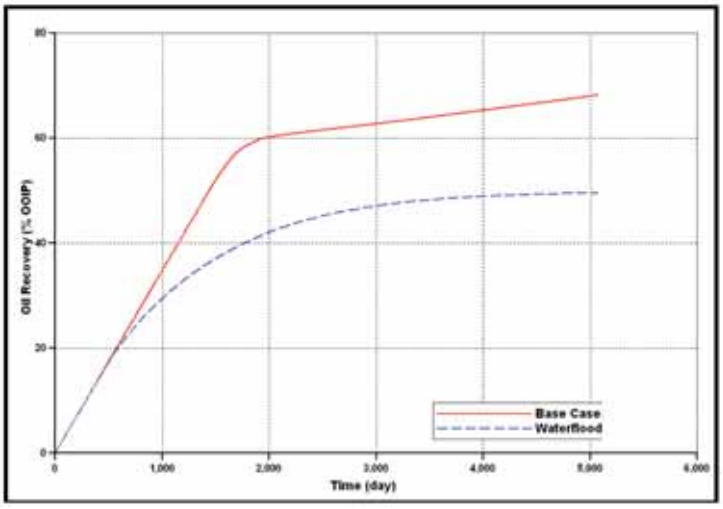

Fig. 5Oil recovery in base case model and water flood cases

where k_r is the relative permeability of phase /, i is the initial condition, f is for final condition or at maximum surfactant affect, P_c is the capillary pressure, and ω is the interpolation factor which is calculated from the interpolation equations of DTRAP number. ω_{pc} is the interpolation factor for the capillary pressure which is the average of the interpolation factor of each phase. Both interpolation factors are calculated as follows:

$$\omega_f = \frac{\log_{10}(Nc) - DTRAP_i}{DTRAP_i - DTRAP_f} \quad (4)$$

and,

$$\omega pc = (\omega_{oil} + \omega_{water})/2 \quad (5)$$

In base case model, the maximum amount of oil dissolved in water is set at 0.03 wt% which will result in IFT of 10 dyne/cm. The DTRAP numbers at initial and final condition for oil are -4 and -3, and for water are -5 and -1.5 respectively. These values are used to represent the change from mix-wet rock to water-wet rock at high surfactant concentration.

Adsorption modeling

The simulator has the capability to model additive adsorptions in the rock and add the adsorption term in the flow equations. In order to simulate this phenomenon, temperature effect, rock density, porosity, and fluid composition have to be known. Also the rate of increase of adsorption with fluid composition should be known as well as the maximum adsorption capacity. All these parameters are needed for the Langmuir isotherm correlation.

A hypothetical adsorption behavior was added in the model, based on previously built-in CMG model, for

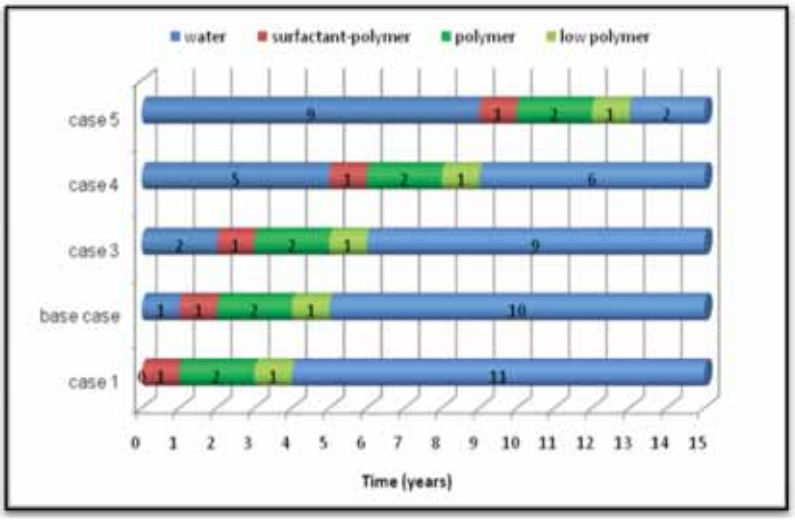

Fig.6Injection profiles for different injection cases.

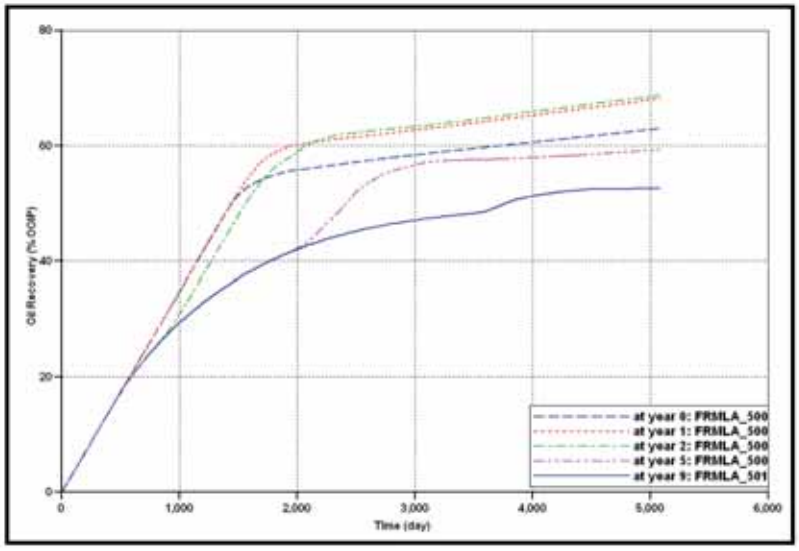

Fig. 7 Recovery factor for base case at different SP injection times.

the completeness of the surfactant polymer flooding process and flow equations. A maximum adsorption capacity of 0.1336 lb-mole/ft^3 surfactant and 0.28 lb-mole/ft^3 polymer was set for the matrix blocks.

Base case Results

To validate the use of surfactant polymer flooding (SPF) in fractured reservoir, the base case model was compared with water flooding (Fig. 5). Surfactant flooding (SF) and polymer flooding (PF) was also compared against the base case model to insure the effect of each chemical in the base case model. The results show high oil recovery in the base case model, around 15% incremental gain, compared to water flooding, SF, or PF. Results also show that polymer flooding (i.e. improving areal sweep), results in higher and faster recovery than surfactant flooding alone. This is an expected performance in a fractured reservoir where most of the surfactant injected will be channeling through the fractures which reduce its effectiveness. The combined surfactant-polymer process, as seen in the base case, shows high oil recovery due to the improved mobility that causes the surfactant to imbibe in more matrix blocks and change the wettability.

Starting SPF

Having only one year of surfactant flood makes it critical to decide at which oil saturation should chemical injection process start. Several injection scenarios have been simulated on the base case model. Fig. 6 shows the injection profile for each case.

The results of varying the start of the surfactant-poly-

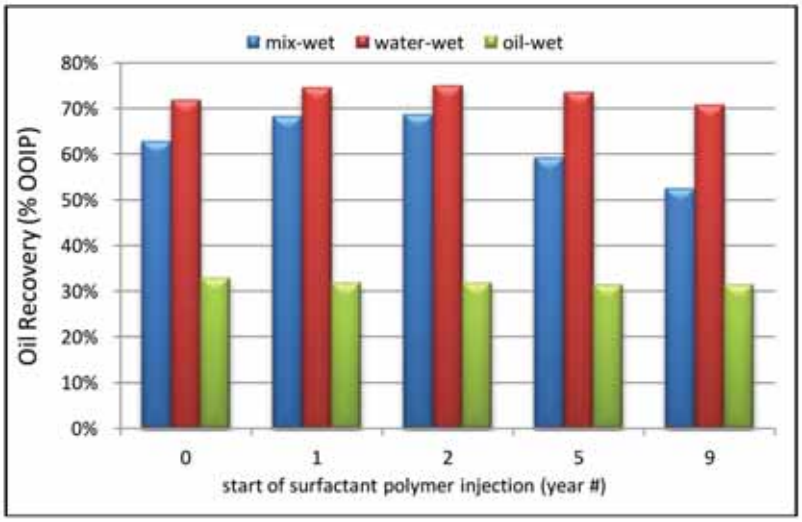

Fig. 8. Oil recovery at different SPF starting time for each wettability case

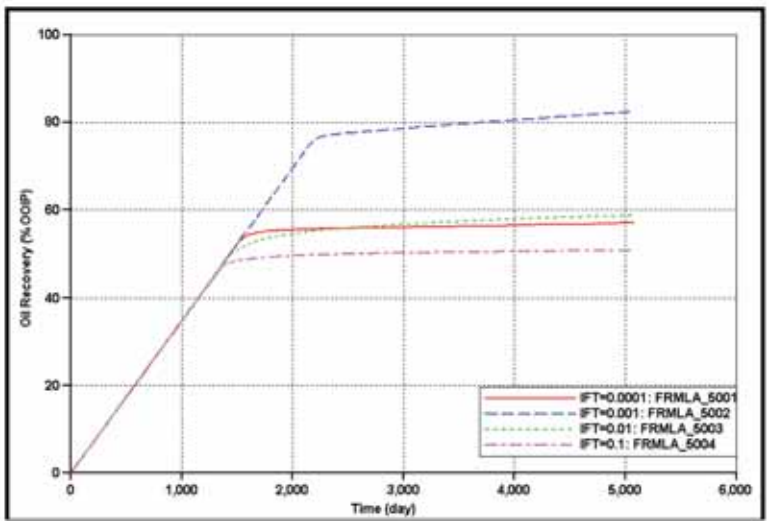

Fig. 9. Sensitivity of oil recovery to IFT in a continuous surfactant polymer flooding.

mer flood (SPF) showed inconsistent relationship with total recovery (Fig. 7). It seems that there is a critical water saturation that affects the recovery as seen in the decreasing recovery as the water saturation increase. On the other hand, starting the surfactant polymer process with no pre-water injection resulted in less oil recovery when compared to the base case where there was a pre-water flood. This could be related to the initial lowering of the capillary force (i.e. spontaneous imbibitions) by reducing the IFT before the effect of wettability alteration occurs. Starting injection of surfactant polymer as at high water saturation may result in a very low incremental recovery. It is worth mentioning that, when running the same study on single porosity model (no fractures), there was virtually no impact on recovery.

Base Case at Different Base Wettability

The same set of sensitivity run has been repeated twice after changing the initial wettability; one set of runs for water wet reservoir and the other for oil wet reservoir. The change has been done in the original relative permeability curves, capillary pressure curve, and capillary number. For the capillary pressure curve has increased to remove the negative capillary pressure, ranging from 10 to 0 psi. Oil-wet rock is characterized by the absence of a positive capillary pressure and the relative permeability curves intersect at less than 0.5 water saturation. Water flooding in that case is not effective. The capillary pressure in this study ranges from 0 to -10 psi.

After repeating the same set of sensitivity study on the different wettabililty cases, the most effected case is the

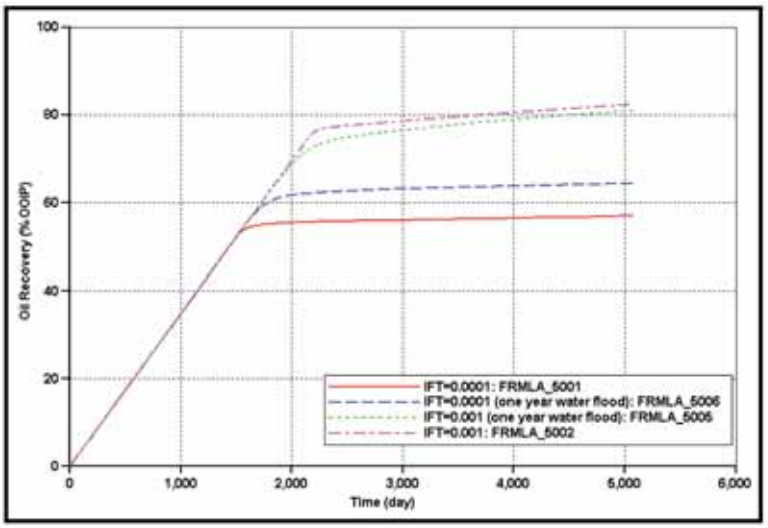

Fig. 10. Effect of pre-water injection on continuous SPF with different IFT reduction

mix-wet reservoir as shown in Fig. 8. The water-wet case showed similar trend but with much lower variation in recovery. The oil-wet case had the most recovery when SPF started at beginning of flood. However, the total recovery for all oil-wet case were low and with little variance. This clearly shows the importance of reservoir characterization and the contribution of fractures to the recovery that may lead in a big area of optimization

IFT Effect

A sensitivity study of oil recovery to interfacial tension, IFT, has been done on the base case model by keeping the concentration of the surfactant constant and changing the IFT value that corresponds to that concentration. Four simulation runs were made with the final IFT values of 0.1, 0.01, 0.001 and 0.0001 dyne/cm. The wettability alteration was kept constant in all runs. The injection of surfactant polymer was continuous from day 1 until the end run. No pre-water injection or polymer drive following the SPF. Fig. 9 shows the performance of continuous surfactant polymer flooding with different IFT effect. It was clear from the result that when surfactant is altering wettability in a fractured reservoir, an optimum IFT has to be achieved to maximize oil recovery. In the case with the lowest IFT, most of the injected fluid travels in a very high velocity through the fractures; until there is a barrier so more imbibitions will occur and increase the wettability alteration in the matrix.

The IFT sensitivity analysis shows that there is an optimum capillary number between fracture and matrix. This capillary number is altered by IFT reduction, wettability alteration, viscosity, or combinations of these factors. The results complement the work done by of Guzman and Aziz (1992) on injections rate in fractured reservoirs and its affect on capillary number. Also, this study shows that there is an optimum inverse bond number (NB)-1 that results is not only faster oil recovery but a much higher one. There is a need for further experimental and simulation work to support such conclusion.

Two additional runs were made to combine the effect of IFT with the effect of pre-water injection. A one year pre-water injection has been added to the lowest IFT cases (0.001 dyne/cm and 0.0001 dyne/cm). Fig. 10 shows the results of both cases along with original cases of no pre-water injection. In the lowest IFT case, the pre water injection was able to improve the oil recovery as seen in previous sensitivity analysis. However, in the optimum IFT case for this study (0.001 dyne/cm) the pre- injection lowered the oil recovery comparing to the performance of the continuous SPF without a pre-water injection. From these results, one can infer that there is an optimum inverse bond number that would yield maximum oil recovery similar to what was discussed in Schechter (2009). However, no attempt to calculate the bond number has been made.

Surfactant Polymer Optimization

The amount of surfactant-polymer used in SPF is a critical issue when it comes to cost of the chemical used per incremental oil recovered. Therefore, there is always a need to optimize the chemical injected and what is outcome in terms of ultimate recovery. A sensitivity study

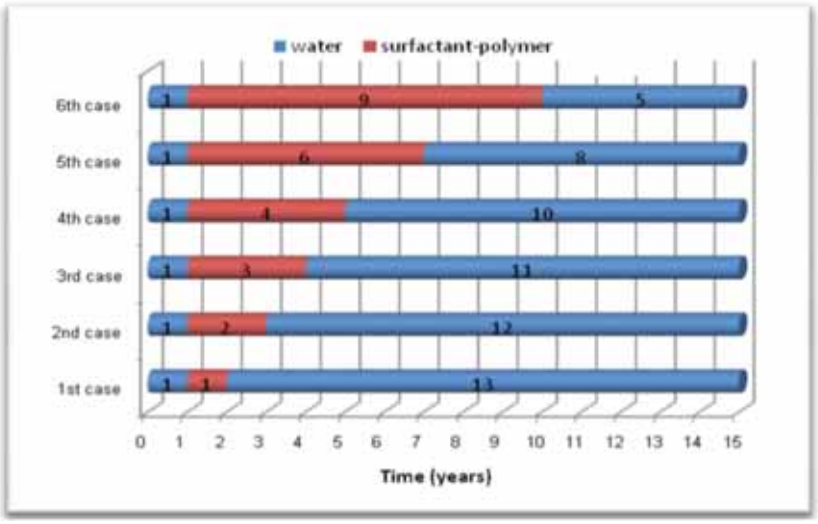

Fig. 11. Injection profile for each case in surfactant-polymer injection length study.

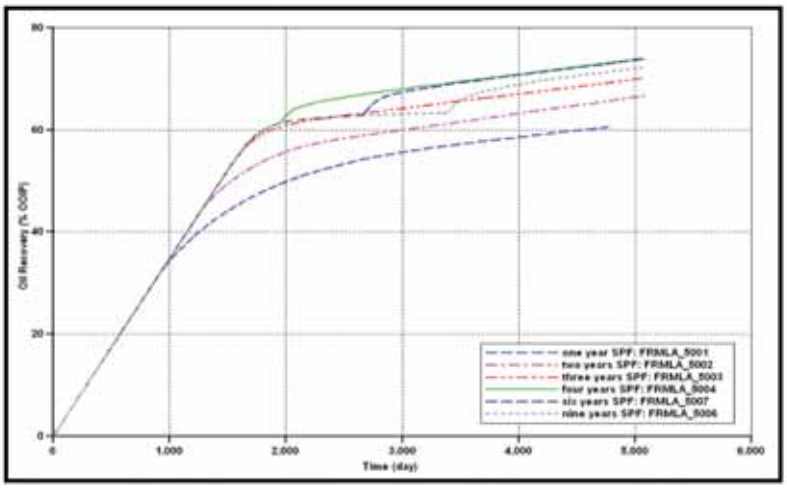

Fig. 12. Sensitivity of oil recovery to surfactant polymer flooding injection length.

has been done to compare only surfactant polymer flood (SPF) without polymer flood after SPF.

This is to have better comparison of each case in terms of chemical injected. All cases include a one year pre-water injection. The SPF injection period has been increased from 1 year to 2, 3, 4, 6 and 9 years. Fig. 11 shows the injection sequence of each case. The total PV injected was around 1.4 in all cases. Fig. 12 shows the oil recovery profiles for the sensitivity runs. The results indicate there is an optimum volume of surfactant polymer injected. Before that, the more surfactant is injected, the higher the oil recovery. Beyond the optimum length, the oil production rate starts to decline as well as the total oil recovery. It was noticed that in all cases the total production rate was not changing which indicates most of the injection if going directly to the producer. This behavior is not observed in a single porosity rock where any resistance or blockage in matrix will result in a drop in the total fluid produced. This is an essential knowledge in optimizing the use of surfactant polymer flooding in a fractured reservoir in order to maximize the recovery and reduce cost.

The drop in production can be related to several factors. One important factor is the fluid adsorption which reduces the relative permeability and may cause some blockage in the pores. There is a water-cut increase after reaching the maximum adsorption of surfactant. In other words, the injected fluid will continue to flow through the fractures with lower fluid imbibitions to matrix which explain the constant fluid production rate

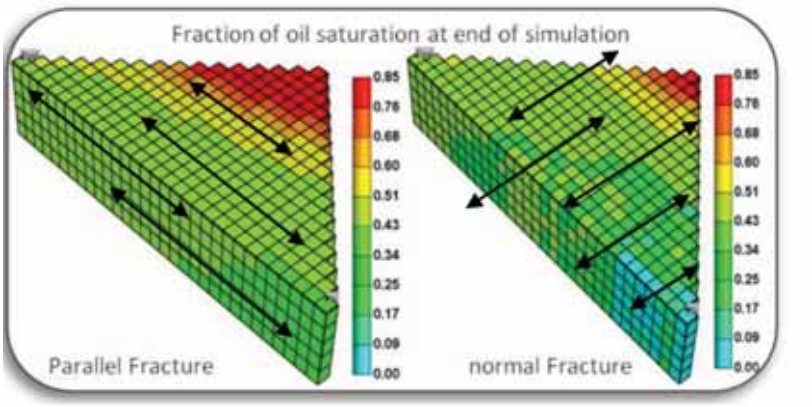

Fig. 13. Remaining oil saturation distibution at the end of SPF case for different fracture orientation.

when switching back to water flood which more fluid imbibed at a higher rate due to the reversibility character of the adsorption modeled in this study.

Another possible reason of the slight increase in oil rate is that the high IFT fluid injected will imbibe faster in the altered water-wet rock with higher capillary pressure which will cause faster oil recover. This phenomenon complements the study done by Gupta et al. (2009) which concluded that oil recovery increase in water-wet rock at higher IFT. The study was done in an imbibition cell experiment. In our case the mobility is adding more force not only in delaying the recovery but rather, decrease the recovery since the oil rate was dropping as more surfactant slug is injected.

Reservoir Sensitivity Studies

This section discusses performance of surfactant polymer flood at different reservoir parameter.

Permeability Contrast

Several simulation runs have been made with different fracture permeability and different matrix permeability. As expected, as the difference in permeability increases between fracture and matrix, the performance of surfactant-polymer flood will decrease. This is due to the increase in residence time of the injected chemicals which will increase its effect. However, the presence of polymer has reduced the impact of the permeability variation greatly.

Fracture Spacing

The base case run has been repeated with different fracture spacing (5 ft, 10 ft, and 20 ft). The spacing of the fracture in the DPDP model affects the width of the fracture as well as the matrix blocks size and thus, affects the communication between the matrix and fractures. The results show that as the fracture spacing decreases, the oil recovery increases. This is because the more fractures, the smaller the matrix block; this results in faster imbibitions between matrix blocks and fractures.

Fracture Orientation

Using DPDP model alone will not give enough representation of such a parameter. In the constructed grid block, there are only two cases of fracture flow direction (parallel or normal) with respect to the injector producer direction. In each case it was assumed 1000 made for fracture orientation and 50md for the opposite direction which is equal to matrix permeability. SPF injection sequence was similar to the base case model.

Fractures parallel to injector producer direction recover less than the case when fractures are at normal direction. The normal direction case along with the mobility control fluid has created more residence time and for the surfactant slug and better areal sweep which resulted in more imbibition and thus displacing more oil from the matrix. Fig. 13 shows the remaining oil saturation after SPF in both fracture cases. The remaining oil saturation shows a high areal sweep and low oil saturation in the normal fracture case compared to the parallel case.

Summary

A simulation study has been performed to evaluate the effect of natural fractures on the performance of surfactant-polymer floods. The study utilized a 16x31x5 Cartesian model that represents a 1/8 of a 20-ac 5-spot

pattern unit. Fractures were incorporated in the CMG STARS with a dual-porosity dual-permeability model. Simulation runs were made in which the following parameters were modified: injection scenarios, matrix wettability, IFT, and fracture and matrix properties.

Conclusions

The following main conclusions may be drawn from results of the simulation study and results of studies by researchers as gleaned from literature:

• Defining contribution of spontaneous imbibitions on the total recovery is an important parameter for a successful chemical EOR pilot.

• When spontaneous imbibition contribution to recovery is high in the reservoir, low IFT surfactant polymer should be injected after optimum water saturation has been reached by water flooding in order to utilize the capillary force and maximize oil recovery.

• Water saturation in a mixed-wet fractured reservoir has high impact on the success of SPF.

• Only in oil-wet reservoir with no positive capillary pressure, injecting enhanced brine at initial water saturation will result in higher oil recovery than if injected at higher water saturation. A pre-flush injection has other benefits such as reducing salinity or ion exchange – this should be considered as to its effect on whether a pre-water injection will yield faster oil recovery or not.

• In the study of continuous injection or surfactant-polymer flood, the result shows that in wettability altering surfactant, an optimum IFT should be combined in the surfactant effect. A change in the IFT effect from the optimum value will result in lower oil recovery.

• The smaller the permeability contrast between fractures and matrix, the higher the oil recovery. However, improved mobility will reduce this effect.

• When blockage is formed in the matrix blocks due to high chemical adsorption on the matrix, the injected fluid channels through the fractures, giving an increase in water cut without decreasing the total liquid rate.

• Injecting water after surfactant-polymer slug injection will enhance the imbibition of water from the fractures into the matrix and remove some of the precipitate because the matrix has been made more water-wet. These results need further evaluation which was outside the scope of this study.

• The higher the fracture density, the higher the imbibition rate which leads to a higher oil recovery.

• Performance of surfactant polymer flood can be affected positively or negatively by fracture orientation with respect to the injector-producer direction. The design of such EOR process should take into consideration this fracture parameter.

Recommendations

Based on results obtained in this study, the following recommendations for research are made.

1. A validation of a field scale simulation is required. Imbibition cell experiments may not adequately represent field conditions due to the lack of representation of viscous force. Research using a scaled quarter of 5-spot physical model containing a fractured porous medium is recommended.

2. Using the physical model mentioned in item 1 above, experimental research should be conducted to investigate the effect of injecting high IFT brine after wettability altering surfactant into the model.

Acknowledgments

Most of this work is based on the research conducted to fulfill the requirements for an MS degree in Petroleum Engineering by Nawaf I. SayedAkram at Texas A&M University. I would like to thank Dr. D. Schechter, Texas A&M for his valued opinions through this work. I would like also to thank Saudi Aramco for the full scholarship on my master's degree and granting the permission to publish this paper.

References

Aldejain, A. A. 1999. Implementation of a Dual Porosity Model in a Chemical Flooding Simulator, PhD dissertation, The University of Texas, Austin, Texas.

Chen, J., Miller, M.A. and Sepehrnoori, K. 1995. Investigations of Matrix-Fracture Transfer Flows in Dual Porosity Modeling of Naturally Fractured Reservoirs. Paper SPE 29562 presented at the Rocky Mountain Regional/ low-Permeability Reservoirs Symposium, Denver, Colorado, 20-22 March.

Delshad, M., Najafabadi, N. F., Anderson, G., Pope, G. A. and Sepehrnoori, K. 2009. Modeling Wettability Alteration By Surfactants in Naturally Fractured Reservoirs. *SPE Reservoir Evaluation & Engineering* 12 (3): 361-370.

Delshad, M., Najafabadi, N. F. and Sepehrnoori, K.

2009. Scale Up Methodology for Wettability Modification in Fractured Carbonates. Paper SPE 118915-MS presented at the SPE Reservoir Simulation Symposium, The Woodlands, Texas, 2-4 February.

Gupta, R., Mohan, K. and Mohanty, K. K. 2009. Surfactant Screening for Wettability Alteration in Oil-Wet Fractured Carbonates. Paper SPE presented at the SPE Annual Technical Conference and Exhibition, New Orleans, Louisiana, 4-7 October.

Guzman, R. E. and Aziz, K. 1992. Fine Grid Simulation of Two-Phase Flow in Fractured Porous Media. Paper SPE 24916-MS presented at the SPE Annual Technical Conference and Exhibition, Washington, D.C., 4-7 October.

Hirasaki, G. and Zhang, D. L. 2004. Surface Chemistry of Oil Recovery From Fractured, Oil-Wet, Carbonate Formations. *SPE Journal* 9 (2): 151-162.

Mohan, K. 2009. Alkaline Surfactant Flooding for Tight Carbonate Reservoirs. Paper SPE 129516-STU-P presented at the SPE Annual Technical Conference and Exhibition, New Orleans, Louisiana, USA, 4-7 October.

Najafabadi, N. F., Delshad, M., Sepehrnoori, K., Nguyen, Q. P. and Zhang, J. 2008. Chemical Flooding of Fractured Carbonates Using Wettability Modifiers. Paper SPE 113369-MS presented at the SPE/DOE Symposium on Improved Oil Recovery, Tulsa, Oklahoma, 19-23 April.

Saad, N. and Sepehrnoori, K. 1989. Simulation of Big Muddy Surfactant Pilot. *SPE Reservoir Engineering* 4 (1): 24-34.

Schechter, D. S., Zhou, D. and Jr., F. M. O. 1991. Capillary Imbibition and Gravity Segregation in Low IFT Systems. Paper SPE 22594-MS presented at the SPE Annual Technical Conference and Exhibition, Dallas, Texas, 6-9 October.

Stegemeier, G. L. 1974. Relationship of Trapped Oil Saturation to Petrophysical Properties of Porous Media. Paper SPE 4754-MS presented at the SPE Improved Oil Recovery Symposium, Tulsa, Oklahoma, 22-24 April.

Taber, J. J. 1969. Dynamic and Static Forces Required To Remove a Discontinuous Oil Phase from Porous Media Containing Both Oil and Water. *Soc. Pet. Eng. J.* 9 (1): 3 - 12.

Tarahhom, F., Sepehrnoori, K. and Marcondes, F. 2009. A Novel Approach to Integrate Dual Porosity Model and Full Permeability Tensor Representation in Fractures. Paper SPE 119001-MS presented at the SPE Reservoir Simulation Symposium, The Woodlands, Texas, 2-4 April.

Warren, J. E. and Root, P. J. 1963. The Behavior of Naturally Fractured Reservoirs. *Soc. Pet. Eng. J.* 3 (3): 245 - 255.

The 20th World Petroleum Congress

4-8 December 2011, Doha, Qatar

www.20wpc.com

20TH WORLD PETROLEUM CONGRESS
4-8 December 2011
Doha - Qatar

Photo: Maersk Oil

Register online at www.20wpc.com

Host Sponsor

Qatar Petroleum

National Sponsors

QAFCO · QAPCO · QATARGAS · RasGas

Platinum Sponsors

Chevron · ConocoPhillips · Dolphin Energy · ecoPetrol · ExxonMobil · Maersk Oil · ORYX GTL · Occidental Petroleum Corporation · Sasol · Saudi Aramco · Shell · Total

Gold Sponsors

bp · Abu Dhabi National Oil Company · nexen · PDVSA · Petrobras · Qatalum · VC · Sonangol · Wintershall

Official Partners

Official Law Firm and Carbon Offset Partner: Baker & McKenzie

Official Auditor and Business Advisor: Deloitte.

Official Publication: First World Petroleum

Official Airline: Qatar Airways

Official International Business Newspaper: The Wall Street Journal Europe

Official Daily Newsletter: upstream

Silver Sponsors

ITOCHU Corporation · LNG Japan · Marubeni Corporation · Mitsui & Co., Ltd. · pwc · Qatar Electricity & Water Co. · Repsol · Schlumberger · Statoil

A Novel 4-D Reservoir Simulation Workflow for Optimizing Inflow Control Device Designs in a Giant Carbonate Reservoir

By Oloruntoba Ogunsanwo, SPE, Schlumberger, Byung Lee, Hidayat Wahyu, SPE, Saudi ARAMCO, Edmund Leung, Varma Gottumukkala, Feng Ruan, SPE, Schlumberger

This paper was prepared for presentation at the 2011 SPE Saudi Arabia Section Technical Symposium and Exhibition held in AlKhobar, Saudi Arabia, 15–18 May 2011.

Abstract

A new 4-D inflow control device optimisation workflow has been developed using a sector model on the west flank of Field A, offshore Saudi Arabia. The approach involves the application of time-lapse monitoring of reservoir saturation profiles for injectors and producers as well as 4-D water flood front movement in the reservoir to understand dynamic reservoir challenges. These are zones of future water breakthrough, dynamic injection/production interaction, impact of reservoir drive mechanism on well injectivity or productivity, initial and future reservoir conditions.

With this understanding, an initial rate optimization process is performed with open hole injectors and producers. Thereafter, the completion is optimized to achieve uniform influx profile, flow control and zonal isolation where required along the horizontal section. Four different completion strategies were evaluated by alternating between Inflow Control Device (Nozzle based) completion and open hole in injectors and producers.

The sector model used in this study is subject to further calibrations as more geological, petrophysical and production data become available; the study outcome based on the novel workflow demonstrated the challenges involved in determining a completion strategy with ICDs in injectors and producers. The results illustrated an incremental cumulative oil gain of 5% with a one year delay in water breakthrough for a 20 year prediction. Moreover, further improvement in recovery can be attained with ICD completions above that achieved with rate optimization process alone.

The study demonstrates the positive impact that ICD completions can be beneficial in challenging reservoirs with mobility ratios considerably greater than one.

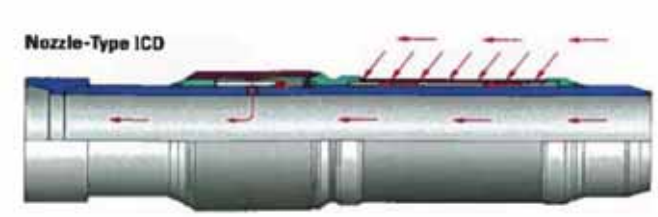

Figure 1: Typical Nozzle Based ICD with wire wrapped screen

The industry should consider this novel 4-D well – reservoir integrated modeling approach to assist in determining a completion strategy in evaluating ICD completion designs prior to deploying them in a field wide campaign.

1. Introduction

In order to achieve maximum reservoir contact in a carbonate field with large hydrocarbon deposits, long horizontal wells are necessary to improve the productivity and injectivity of producers and injectors respectively. However, the presence of a tight layer of tar deposit with very high viscosity underlying the producing reservoir layers has prevented communication with the bottom water aquifer. In addition to heterogeneities in reservoir rock properties (permeability, porosity etc.), the viscosity of the oil also varies with depth. Therefore, pattern or peripheral waterflood injection is necessary for pressure maintenance while producing from this field. Even if reservoir rock properties were to be homogenous, challenges such as heel-to-toe effect will still be encountered for these long horizontal production/injection wells of 3000 – 6500 ft Open Hole (OH) sections. The effect will cause more production from the heel section and will usually lead to early water or gas breakthrough. In view of these challenges, the questions that need to be accounted for during the planning stage of water flooding scheme are summarised below.

- Will there be a relatively uniform injection profile if Open Hole (OH) completions are adopted for the horizontal injectors ?
- Will few reservoir zones dominate production in the OH horizontal producers ?
- Will efficient reservoir sweep be attained with a minimum number of injectors and producers ?
- How can water channeling from injectors through high perm streaks be retarded by delaying water breakthrough or minimizing water cut in producers ?
- Can ICD completion strategy be adopted and if YES, how much more improvement in the field recovery will it offer over OH completions ?

2. Principle and design of Inflow Control Devices (ICD)

There are various types of Inflow Control Device (ICD); however, only the design and principle of nozzle based configurations will be discussed in this paper. Interested readers can refer to (Alkhelaiwi et al, 2007; Ellis et al, 2009; Ouyang 2009) for other types of ICD. A typical nozzle based ICD joint is a piece of blank pipe having wire wrapped sand screen for sand control or debris barrier for carbonate formation mounted on one end and fitted with an ICD housing which protects the ceramic nozzles on the other end, Fig. 1. This section also utilises centralizers. There are four to six nozzle ports in each of the ICD joints depending on application. The nozzle are in various sizes and are usually fitted on the rig, based on a final ICD tally design considering actual LWD well log data, other well and reservoir data. Each ICD joint is about 12m or 40 ft in length. The unique manufacturing process employed for the wire wrapped screen ensures a shrink fit between the screen jacket and the base pipe. This provides the screen with the same mechanical strength as the base pipe and making it possible to rotate the ICD completion string while running in hole if required. With nozzle based ICDs, the design and optimization can be achieved by determining the number of ICDs, their nozzle sizes or configurations and packer placement. This flexibility, provides a large number of possible nozzle size combinations to achieve production control and optimization in horizontal wells. This is a clear distinction between nozzle based devices compared to helical/tube ICD systems which do not offer this flexibility.

ICDs are designed to optimize production from horizontal completions by equalizing the reservoir inflow along the entire length of the well bore. As shown in Fig.1, fluid flow from the reservoir flows across the screen into the annulus between the screen and the base pipe and then flows through the nozzle into the inside of the base pipe. The fluid flow from the reservoir into wellbore annulus is governed by Darcy Eq 1 while fluid flow across the nozzles into inside of the base pipe is based on Bernoulli Eq 2 of an incompressible fluid.

$$\Delta P_F = \mu \frac{Lv}{k} = \frac{\mu L}{kA} q = c_F q \qquad (1)$$

Where

ΔP_F = Drawdown pressure = $P_{Reservoir}$ - $P_{well\ flow\ (annulus)}$
μ = fluid viscosity
k = Absolute permeability
L = Length of reservoir section
A = Cross-sectional area
q = Volumetric flowrate of the flowing liquid
c_F = □L/ kA = 1/PI (PI: Productivity Index)

When fluid flow across the nozzle, the potential energy is transformed into kinetic energy and thus a controlled pressure drop between wellbore annulus and inside of the base pipe is generated to achieve the desired uniform inflow profile along the wellbore, equation 2. The pressure drop is proportional to square of the rate (velocity) and density, but independent of viscosity. Whereas, helical and tube ICD types which are both dependent on rate and fluid viscosity can possibly provide more or less pressure drop than required or initially designed since fluid properties change with increase in well water cut.

$$\Delta p_N = C_u \frac{\rho v^2}{2C_v^2} = C_u \frac{\rho Q^2}{2C_v^2 A^2} \qquad (2)$$

Where

ΔP_N = pressure drop in nozzles per joint (psi)
ρ = fluid density at reservoir conditions (ib/ft^3)
Q = volumetric rate of the flowing fluid per joint, [bbls/d] @ reservoir conditions
A = inflow area of nozzles per joint, [ft^2]
v = the fluid velocity (ft/s)
Cu = unit conversion constant
Cv = the flow coefficient

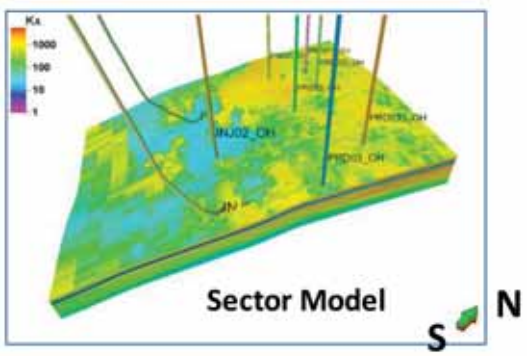

Figure 2: Map view of the Field A Reservoir showing the sector model

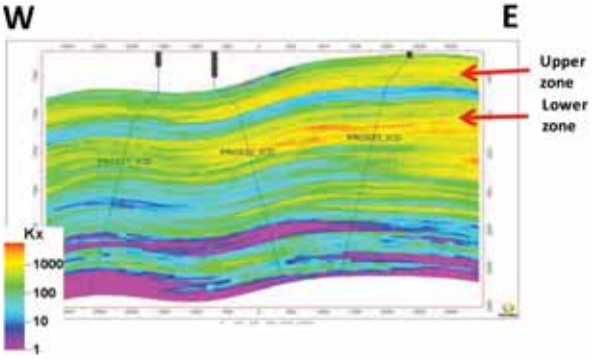

Figure 3: Vertical cross section showing upper and lower reservoir units separated by tight low perm zone

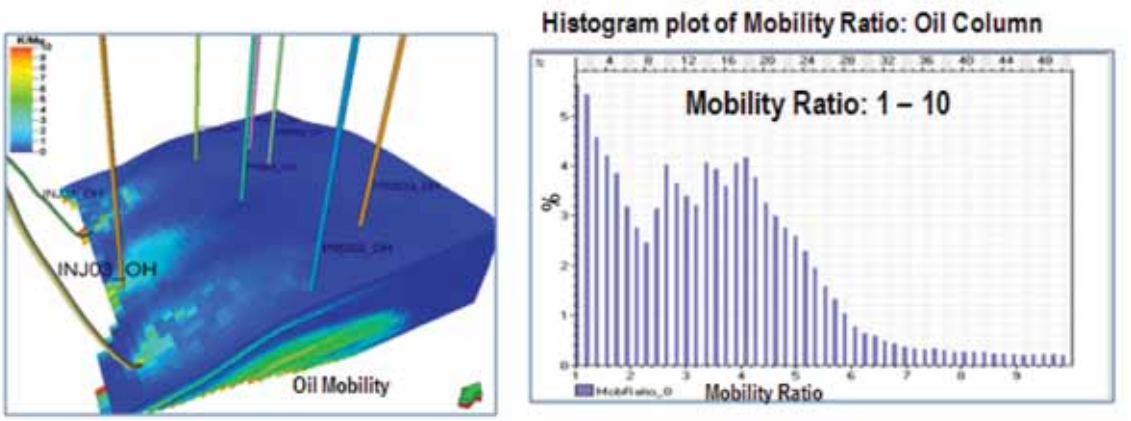

Figure 4: 3-D mobility ratio distribution and Histogram for the Oil Column zone above the Tarmat

Potential benefits of ICDs are not limited to:

• Correct heel to toe effect in long horizontal wellbore as accelerated produces from the heel section in a conventional completion (perforated liner).
• Achieve uniform reservoir sweep and improve recovery
• Delay water or gas breakthrough and reduce well water cut in reservoirs with higher water mobility than oil and wellbore proximity to fluid contacts
• Prevent crossflow during production
• Improve wellbore clean-up since fluid is drained uniformly along the wellbore.
• Offer sand or debris control

3. Field Overview

The field comprises of carbonate reservoirs modeled as single porosity and permeability with no fracture network. It is located in the shallow waters of the Western Arabian Gulf, Saudi Arabia. The sector model used is a subset of Field A, Fig. 2. It has a down-dip structure towards the south. Two good reservoir zones are observed from south to north separated by a very very low permeability layer, Fig. 3. In the upper reservoir zone, there is a continuous and relatively high permeability zone at the bottom. However, in the lower reservoir zone, the relatively high permeability zone is located at the top of the section. A bottom water aquifer is interpreted to be connected to the reservoir from the south. However, the presence of a very high viscous Tarmat zone, (20–40 ft thickness and viscosity ranges above 3000 cP) underneath the oil column disconnects the aquifer from the reservoir; thus, leaving the reservoir to a depletion drive mechanism. Consequently, for efficient field recovery, a peripheral water injection scheme has been considered prior to starting the next phase of field production to improve reservoir sweep and pressure maintenance. The reservoir fracture gradient is 0.75 psi per foot TVD. Different flow units with different saturation regions from the special core analysis data have been identified in the two zones. They extend from north to south.

It is an undersaturated reservoir with crude oil gravity of 26 0API. The initial reservoir pressure is an order of magnitude greater than bubble point. The oil column and water viscosities at initial reservoir conditions are 4.22 cP and 0.4 cP respectively. Water in the reservoir has a much higher mobility than oil. Mobility ratio at water breakthrough is considerably greater than one. Therefore, water channeling through the oil will be a major challenge for the water flooding scheme.

4. Challenges

The reservoir challenges observed in Field A have been categorized below based on reservoir heterogeneities and structural complexities.

• Rapid reservoir pressure decline due to the presence of a tarmat zone preventing the producing reservoir layers from

communicating with the bottom aquifer water
• Reservoir uncertainty associated with the areal distribution of the Tarmat zone across the Field
  - Reservoir characterization
  - The placement of some of the injectors inside the Tarmat zone
• Areal and vertical variation of the permeability profile distribution across the field, Fig. 3. There are high permeability streaks at the bottom section of the upper reservoir zone. This is aided by gravity segregation,

which will lead to early water breakthrough in the producers. The reservoir heterogeneity will yield uneven water injection and oil production profile; thereby, reducing oil recovery.
• When the mobility ratio is greater than one at water breakthrough considering that oil viscosity is an order of magnitude higher than water viscosity, Fig. 4. This is further magnified as different flow units with different saturation regions have been identified.
• Long Open Hole section for the producers and injectors, about 3000 and 6000 ftMD respectively.
• Establishing optimum injection and production rates.
• Completion selection and optimization.

5. Objectives and Scope

Owing to the highlighted reservoir challenges, the study has been conducted to understand the optimum completion strategy for the injectors and producers that will improve recovery and reservoir sweep, delay water breakthrough and decrease water cut. A novel workflow process was developed and used to study the project objectives below.

• With the aid of 4-D dynamic modeling, identify factors that significantly impacts recovery.
• Establish optimum injection and production rates
• Perform various sensitivities on ICD completion design
• Determine optimum completion strategy that will improve recovery. Evaluate the different nozzle based ICD completion strategy and compare each with the open hole base case.
- ICD in Injector and ICD in Producer
- ICD in Injector and Open Hole (OH) in Producer
- OH in Injector and ICD in Producer
- Base case: OH in Injector and OH in Producer

The study is based on a sector model of Field A in Saudi Arabia. There are six horizontal producers and three horizontal injectors. The injectors are aligned in the first row, followed by second and third rows of the producers. This geological model was built in seismic to simulation software, PetrelTM. The rate optimization process was simulated using Patterned Flooding Management Optimizer, PFM, using a streamline simulator, FrontSimTM. Multisegment well option and advanced ICD completion were modeled and simulated using a grid based numerical simulator, ECLIPSETM. Using Pattern Flood Management (PFM) optimizer in FrontSim, optimum injection rates for the peripheral water flooding scheme and production rates will be assessed. These optimized rates will be the basis for evaluating the potential benefits of an optimized nozzle based ICD completion design over standard open hole wells.

6. Workflow Background

6.1 Traditional well centric Workflow

In traditional wellbore centric approach, the optimum completion design is achieved by distributing ICDs based on near wellbore permeability profile and performing sensitivities on number of ICDs, ICD nozzle sizes, number of packers and its placement. The main objective is to achieve influx balancing along the horizontal open hole (OH) section, minimize or eliminate heel-to-toe effect and reduce well water cut. The optimum ICD completion design will be selected based on incremental field cumulative oil gain over OH horizontal wells and a minimum pressure drop across the ICD completion.

However, in reservoirs with mobility ratios considerably greater than one, gravity drainage dominated and having a water injection scheme, stimulating relatively low permeable zones with ICDs can be a source of future water entry leading to high water cut in producers and ultimately lower oil recovery than conventional completions. This methodology may even lead to a wrong completion strategy if adopted in field wide reservoir studies with wells intended for ICD completions.

6.2 Novel 4-D well – reservoir integrated dynamic modeling workflow

The approach that will be discussed in this novel 4-D well – reservoir integrated workflow, Fig. 5, is that distributing ICDs using wellbore permeability as performed in traditional well centric approach is insufficient because it fails to consider the effects of reservoir heterogeneities and dynamics on well performance as listed below. Moreover, these factors change with time as well as their impact on well performance.

• Effects of reservoir connectivity and interference with neighboring wells to account for future water breakthrough
• Water flood front movement in the reservoir
• Injection/production interaction dynamics
Completion selection and optimization.
• The impact of reservoir drive mechanism on well productivity or injectivity
• Initial and future reservoir conditions.

This approach is based on performing 4-D dynamic modeling using a history matched reservoir model. Thereafter, using Time-Lapse signature (4-D) of PLT/

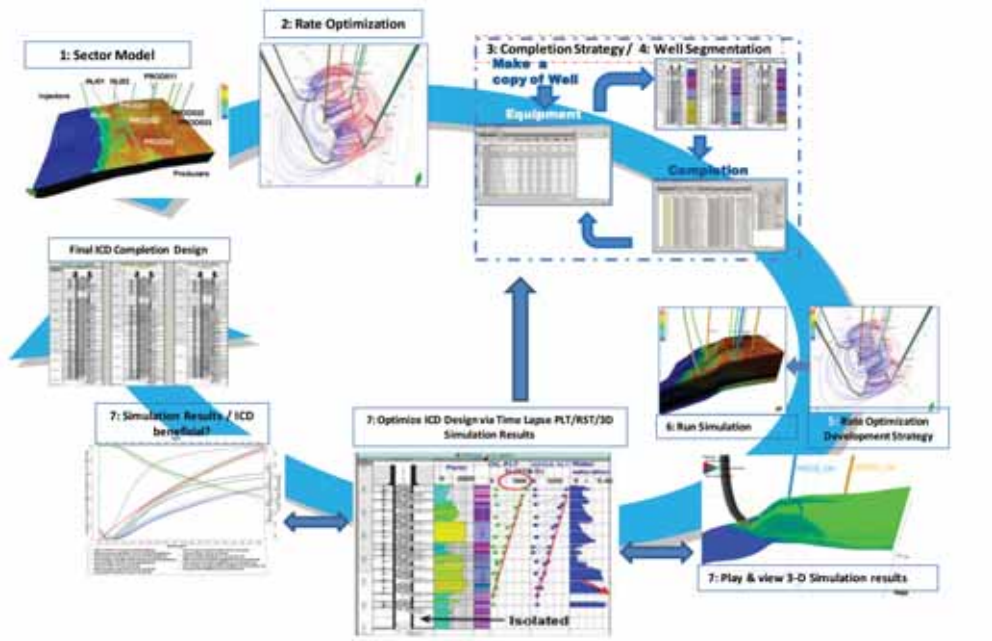

Figure 5: Novel 4-D well-reservoir integrated dynamic workflow

FSI and reservoir saturation profile near the wellbore for injectors and producers and 4-D water flood front monitoring, the reservoir engineer will understand how these reservoir drivers change over time. With this insight, one can then re-distribute ICD completions along the horizontal section to achieve either influx balancing, control or zonal isolation as required. One can decide whether a zone requires influx balancing or flow restriction at the beginning of well production or injection. For instance, if there will be early future water breakthrough or high water saturation from a zone due to the producer trajectory dipping downward in the reservoir layer and its interaction with neighboring injectors, such that the zone requires only flow restriction or isolation. Therefore, the number of ICDs and nozzle size sensitivities will be designed to counter the negative impact of these reservoir drivers. The workflow will be elucidated in the simulation results section.

7. Novel 4-D Well Reservoir Integrated Workflow

7.1 Summary of Novel 4-D Well – Reservoir Integrated Dynamic Modeling Workflow

The individual steps for designing ICD completion in the novel 4-D workflow, Fig. 5, are outlined below.

1. The workflow starts by creating a sector model from full field model (FFM) that has been history matched.

2. Rates optimization process for the open hole injectors and producers was performed using a PFM optimizer in a streamline simulator to determine optimum injection and production rates.

3. Since the geological model was built in Seismic to Simulation modelling application, the completion strategy for the horizontal injectors and producers were designed by populating ICD completion (Nozzle based ICD joint, add-on / slip-on packers, reamer shoe at end of completion string) along the wellbore. The ICD design methodology that is being proposed in this paper will be further elucidated in the detail section.

4. An advanced multi-segment well model was incorporated into ICD completion for the injectors and producers using a homogenous flow model, which considers all phases flowing with the same velocity.

5. The results of the rate optimization sensitivities from the PFM optimizer was inputted into the development strategy of the simulation cases considered in the grid based numerical simulator. This simulator was selected because of its capability to simulate injection and production performance of horizontal wells with ICD completions.

6. Various cases using different ICD completion designs and sensitivities were defined and simulated.

7. Optimum ICD completion design for both injectors and producers were achieved by combining the two approaches below. The first approach is the application of time-lapse (4-D) monitoring of synthetic PLT/FSI profile and near wellbore reservoir saturation in the injectors and producers. With the selected grid based numerical simulator, these well profiles can be generated during the prediction run. Alternatively, the investigation of the water flood front movement (synthetic 4-D monitoring) both areally and vertically can also be assessed. Combining both approaches, one will be able to understand the sweep pattern dominating drive mechanisms, interaction between well performance and reservoir behaviour, reservoir heterogeneities and therefore the impact on recovery. The effectiveness of the described workflow relies on a history matched sector model as well as field scale monitoring of strategic injectors and producers with PLT/FSI profiles.

7.2 Details of the novel 4-D workflow

7.2.1 Rates Optimization and Development Strategy

Reservoir heterogeneity can yield uneven water injection and oil production profiles. Dynamic streamline simulation is used to reveal the impact of vertical and areal sweep efficiency of injectors in this heterogeneous reservoir sector model. An optimization approach was developed to obtain open hole injection guide rates for this sector model using FrontSim streamline simulator Pattern Flood Management (PFM) module. It should be noted that as production data become available, the reservoir properties in the sector model can be further improved through history matching and then the open hole optimized injection guide rate can be revised. Such open hole optimized guide rates can not only impact on far field water flood sweeping fronts, but also in the near wellbore ICD completion design planning phase for new and existing wells. Thus, far field sweep pattern design obtained from streamline simulation is integrated with ICD nozzle completion design in this workflow.

PFM provides an automatic injection rate by using a spatial injector - producer pair rate allocation to determine injector efficiency. PFM features the voidage replacement mode (VRP) designed to control either local injector pattern set pressure or full field pressure by including all injectors. It also features the injection efficiency mode designed to speed up balanced producer recovery associated with a selected set of injectors.

Sensitivity Criteria	Traditional Workflow 1	Traditional Workflow 2	Reservoir Centric 1	Reservoir Centric 2	Reservoir Centric 3 - Optimum
Time-Lapse PLT / near Wellbore Reservoir Saturation	NO	NO	YES	YES	YES
FrontSim Optimization	NO	NO	NO	NO	YES
Injection Rates [MBBLS/D]	25	25	20	20	15 - 20
Producer Rates [MBBLS/D]	7	7	7	7	7 – 8.5
Injection BHP [psi]	6000	6000	5000	5000	5000

Table 1: Rates Optimization and ICD completion Sensitivities Criteria

The VRP control option of PFM was used to set up multiple scenario runs using the Petrel optimizer with an aim to understand sensitivities of injector and producer operating constraints. The results were fed into the development strategy of the grid based numerical simulator. In order to use the optimized development strategy plan from the optimizer for ICD design in the grid based numerical simulator, the same simulation case was run in ECLIPSE and the production and pressure responses were compared. The results from both simulators agreed.

7.2.2 Completion strategy, well segmentation and development strategy

In the completion strategy, one is expected to distribute along the OH section of the injectors and producers using various ICD design sensitivities. The completion design is performed by considering in isolation, the concept of traditional and 4-D workflow methodologies. Each ICD design was simulated considering the completion strategy stated in the project study objectives.

The injectors and producers were modeled using multi-segment well modeling, MSW, by dividing the wellbore into a series of 1 – dimensional segments. This will enable accurate modeling of multiphase flow in the wellbore, effects of multilateral topology of the well path on the fluid behavior, complex crossflow effects, and flow across ICDs. Homogeneous flow model where all the phases flow with the same velocity was adopted with the MSW option (ECLIPSE technical Manual 2010).

For the purpose of comparing results from both workflows, some ICD design sensitivities were performed based on traditional workflow concept while others were conducted on the basis of the 4-D workflow. This paper presents the final two and three sensitivities of traditional and 4-D well– reservoir integrated workflows respectively by comparing OH/OH vs. ICD/ICD completion strategy for both injectors and producers, Table 1. Other disparities in the development strategy are in injection rates, injection BHP constraints and the use of rate optimization process results.

Sensitivity criteria considered in addition to Table 1 were

- Number of ICDs in injectors and producers
- ICD nozzle size
- Number of packers
- Packer spacing

8. Summary of Simulation Results

This section discusses the simulation results of the project study based on six horizontal producers and three horizontal injectors. The simulation runs were conducted for a 20 year period. The results emphasize the benefits of using the new approach to identifying optimized ICD design. They also promote a departure from the traditional method of using only permeability profile to identify optimum design because this can often lead to poor ICD design and completion strategy. It demonstrates the importance of considering other dynamic reservoir responses through 4-D dynamic modeling to understand their effects on well performance and thereafter ICD design to counter or promote the behavior. This study has proposed a novel workflow to designing an optimum ICD completion design. However, the results obtained from traditional workflow are compared against the optimum ICD completion design to further illustrate the new 4-D workflow.

The simulation cases ran for each set of development strategy, considers the scenarios below; however, only the ICD completion strategy 3 will be reported.

- Base Case: OH Injectors and OH producers
- ICD Strategy 1: ICD Producers and OH Injectors
- ICD Strategy 2: OH Producers and ICD Injectors
- ICD Strategy 3: ICD Producers and ICD Injectors

8.1 Criteria for Optimum ICD Completion Design

The Optimum ICD design can be selected by comparing additional recovery and field wide flowing bottom hole pressure of various ICD design sensitivities performed for each ICD completion strategy against an OH Case. The criteria are but not limited to:

- Extent of incremental field cumulative oil production of ICD strategy over the OH case.
- Compare field pressure of the three optimum ICD Completion strategies against the OH base case.
- Compare field pressure of various sensitivities for each ICD completion strategy separately against the OH base case.
- Reduction in well/field water cut for ICD over OH case.
- Delay in water breakthrough time between an ICD and OH case.
- Qualitatively assess reservoir sweep of individual ICD strategy on well basis over OH.

8.2 Results of PFM and ICD Design Sensitivities

The initial optimization results reveal that a simple increase of injection rates can lead to a reduction of

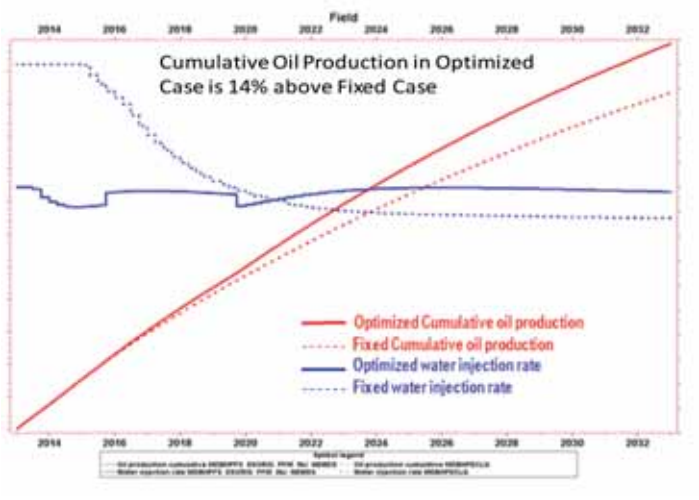

Figure 6a: Comparing Field Cumulative Oil Production Total and Water Injection Rate for optimized and non-optimized (fixed)

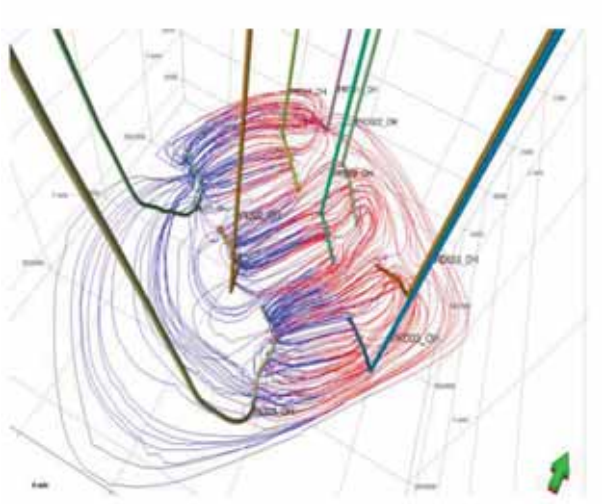

Figure 6b: Streamline simulation pattern of the PFM optimized open hole case

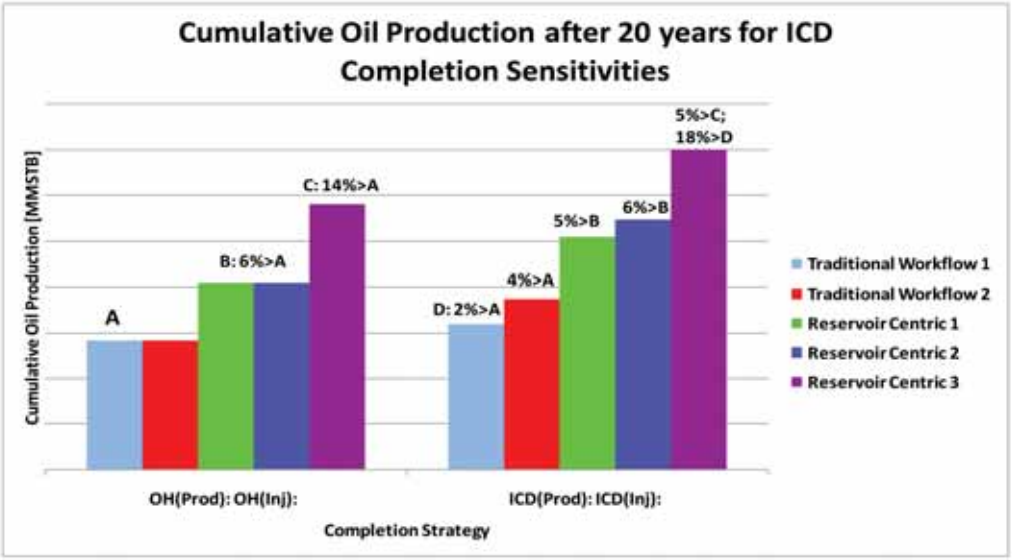

Figure 8: Results of Rates Optimization and ICD completion Sensitivities Criteria

overall cumulative oil production. Very high injector rates will result in early water breakthrough for the first line of producers (Prod-01/02/03); thereby, reducing recovery from these producers. This phenomenon can be attributed to high mobility ratio of water to oil. The same results also reveal that very low injection rates would not be able to provide the intended pressure support to all the six producers. Results indicated that PFM rates can reduce field injection water recycling to producers and maintain similar or higher cumulative oil production compared to a non PFM case reservoir sector model. Fig. 6a.

Based on this understanding, the PFM rate optimization process was revised into a two stage approach. The first stage was to maximize sweep for the first line of producers while the second stage is aimed at improving sweep and recovery for the second line of producers. PFM voidage replacement mode was chosen to ensure field pressure is above bubble point, and also to ensure injector rates are constrained below fracture gradient of 0.75 psi/ft to avoid wellbore fracturing.

Using the streamlines bundle emanating from an injector, voidage in the injector's region is continuously

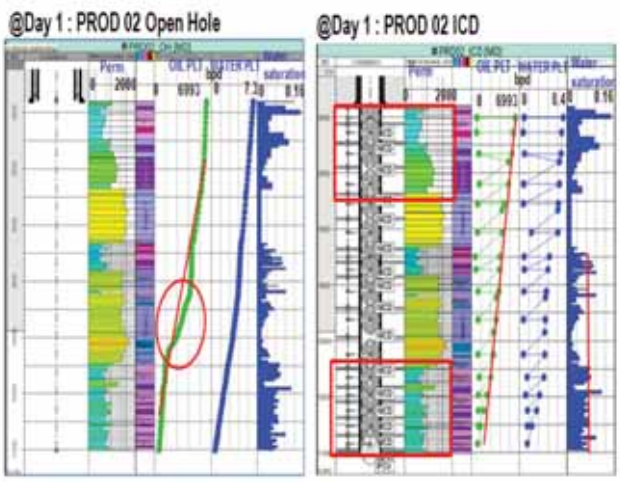

Figure 9a: Synthetic PLT and RST profile @ day 1 (beginning of production) for PROD-02

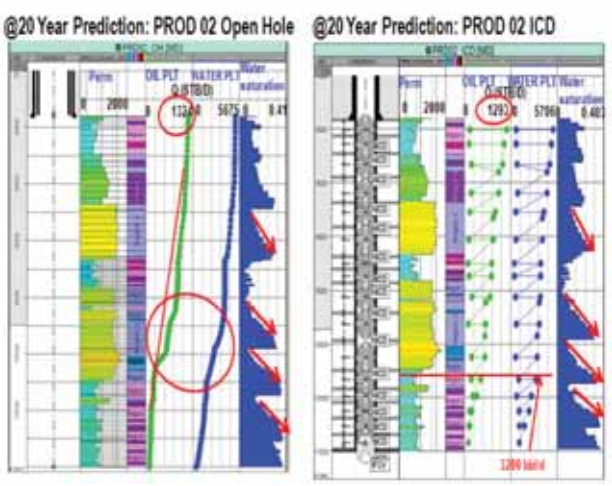

Figure 9b: Synthetic PLT and RST profile @ 20 year prediction) for PROD-02

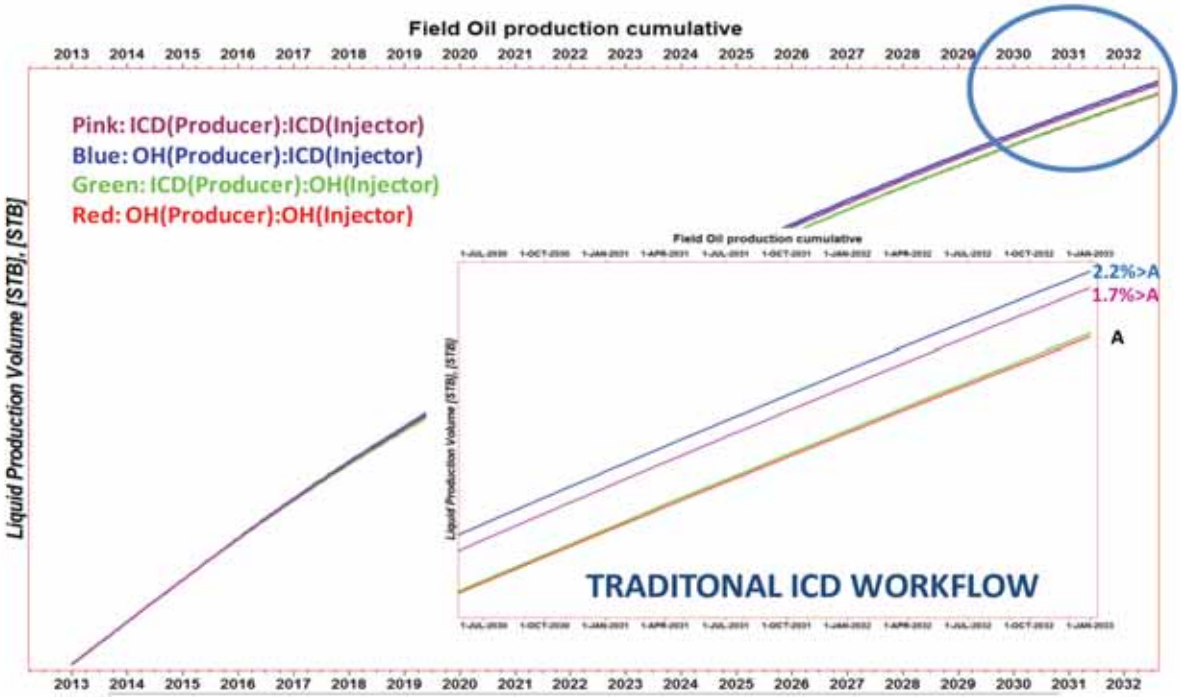

Figure 10: Field Oil Cumulative Oil Production based on Traditional Well Centric Approach

tracked, Fig. 6b. Its injection rate is then modified to achieve the user specified voidage replacement ratio. Sensitivities were done on injection BHP constraints between 5000 and 6000 psi, injection rates of 15 – 25 MBBLS/D and well production rates (7000 and 8500 STB/D) @ BHP constraint of 1500 psi. The optimized injection rates were found to be between 15 – 20 MBBLS/D. The six producers should be put on production at 7000 STB/D; however, production rates for PROD-011, 022 & 033 should be increased to 8500 STB/D after 5- 7 years of production.

A summary of rate optimization results and ICD completion design sensitivities on cumulative oil production is shown in Fig. 8 and Table 1. The results illustrate an improvement in recovery even with a reduction in injection rates. It also demonstrates that recovery can be further improved by increasing production rates to

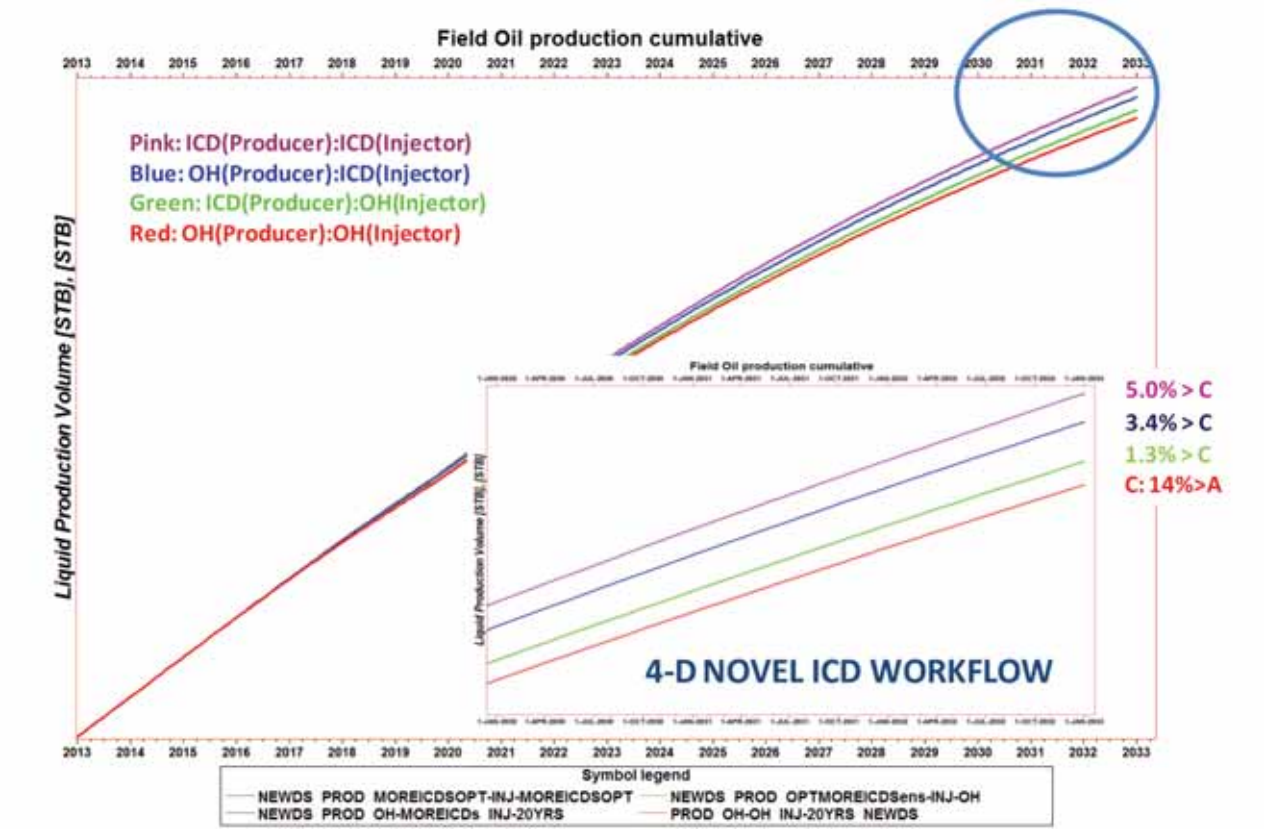

Figure 11: Field Cumulative Oil Production based on novel 4-D integrated well – reservoir workflow

8500 STB/D after 5 -7 years for PROD-011, 022 and 033.

The rates optimization process further recommended injection and production rates that will achieve optimum field cumulative oil production with minimum pressure loss across the ICDs. The results also illustrates that designing ICD completions based on traditional workflow concept will yield lower cumulative oil production than ICD completion based on the new 4-D well-reservoir integrated dynamic modeling workflow. Field recovery can be achieved by optimizing injector and producer rates alone but with the introduction of ICD completions, recovery can be further improved.

8.3 Traditional Well Centric Approach Results

ICD design in traditional well centric approach is performed by increasing number of ICDs and/ or choosing a higher nozzle size, reducing packer spacing etc. in low permeability zone with reverse of these parameters in high permeability zone along the horizontal section as shown by the rectangular boxes, Fig. 9a(@ day 1:Prod 02 ICD. This type of ICD design produces uniform cumulative oil PLT profile at the start of production. However, on evaluating the PLT profile and near wellbore reservoir saturation of the producers using Time-Lapse technique, it will be observed that this approach failed to consider factors affecting fluid flow behavior and their impacts on well production performance as explained in the 4-D workflow above. The concept of Time-Lapse technique mentioned in this paper involves investigating well injection and production profiles at different future time steps where factors affecting fluid flow behavior away from the wellbore are expected to be fully acting. For instance, Fig. 9b, (@ 20 year prediction: Prod 02 ICD, the cumulative water PLT profile showed that more than 50% of water production in this well (Prod-02) would be produced from the toe section in the future. This is simply because five ICD joints are placed in this 750 ft interval with each ICD joint in a sub-compartment of about 150 ft. This section is being over produced. As a result, producers in completion strategy of ICD completion in both injectors and producers were producing

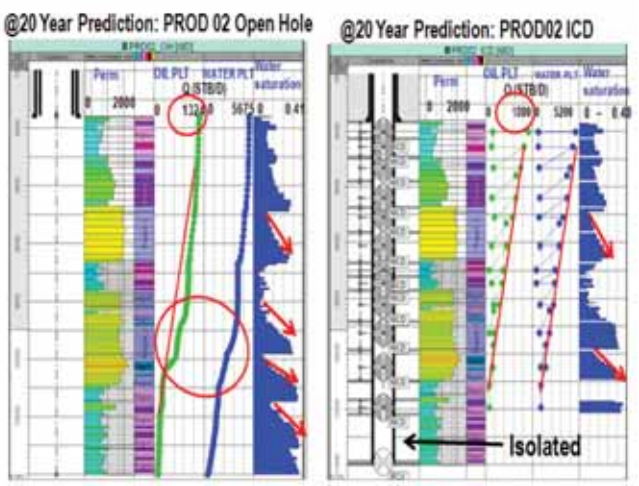

Figure 12a: Synthetic PLT and RST profile @ 20 year prediction (Time-Lapse approach) for PROD-02 using 4-D integrated well-reservoir workflow.

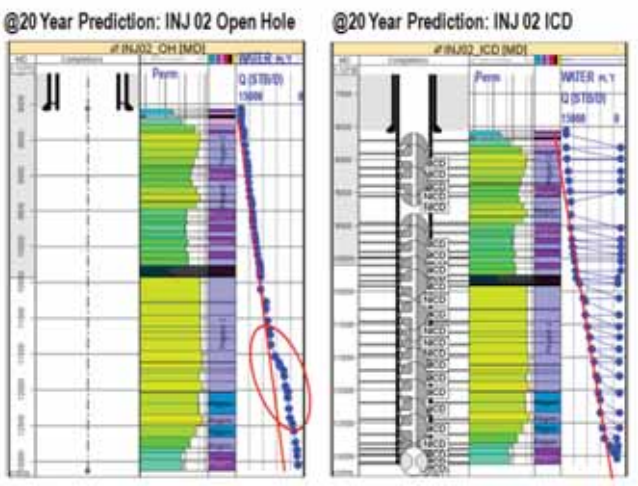

Figure 12b: Synthetic PLT and RST profile @ 20 year prediction (Time-Lapse approach) for INJ-02 using 4-D integrated well-reservoir workflow.

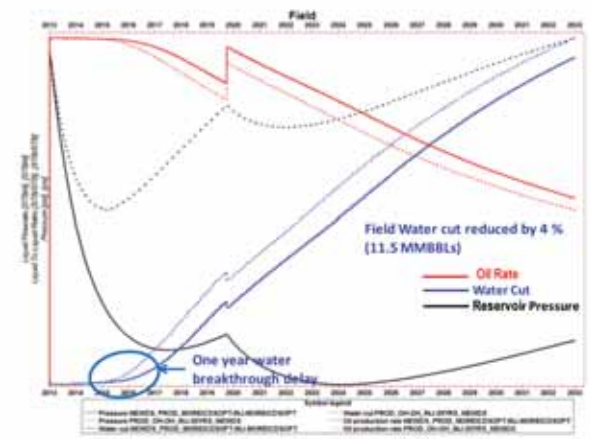

Figure 13: Field Pressure and Production Rates for the six producers ICD / ICD vs. OH base case based on novel 4-D integrated well – reservoir workflow

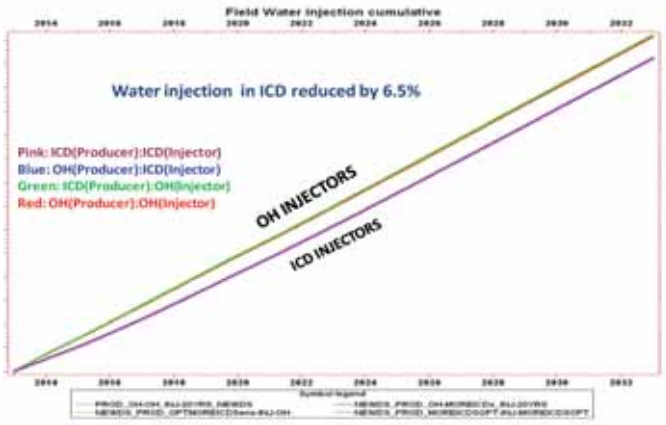

Figure 14: Field Cumulative Water Injection for the three Injectors based on novel 4-D integrated well – reservoir workflow

higher water cut than producers in completion strategy of ICD completion in Injectors and OH producers, Fig. 9b. Cumulative oil production obtained from applying traditional well centric concepts showed ICD completion in Injectors and OH producers as the best completion strategy, Fig. 10. This is a flawed approach because it does not consider the impact of reservoir dynamics. Please note that only one well plot is displayed for illustration purpose but similar effects are seen in the other producers.

8.4 Results of Novel Well – Reservoir Integrated Dynamic Modeling Workflow Results

The results of the well-reservoir integrated dynamic modeling approach indicated the optimum completion strategy as ICD completion in injectors and producers, Fig. 11. The results were achieved by carefully using Time Lapse technique (4-D) for PLT profiles and reservoir saturation in addition to wellbore permeability profile to understand future water entry zone i.e. heel to toe and the impact of gravity on sweep patterns and well performance, Fig. 12a. This explains why fewer numbers of ICDs have been placed in the low permeability section near the toe of the producers since this section will experience high water saturation in the future and will be the source of future water entry into the well if over produced with a high number of ICDs and/or larger nozzle sizes. Fig. 12b illustrates the injec-

tion profile for one of the three injectors. The approach also considers a 4-D water flood front movement to understand the impact of gravity on the water flood front away from the wellbore i.e. in the reservoir. In other words, identify which of the reservoir layer flood fronts is traveling fastest. These were studied from simulating the three injectors and six producers as open hole for 20 years. Having understood potential future well performance if left as open hole, ICD completion was then designed considering the above sensitivity criteria in each of the injectors and producers to either restrict or improve injection or production profile or provide zonal isolation from the two reservoir units – upper and lower.

The synopsis of the results for optimized ICD design in both injectors and producers are summarised below.

• Achieve an additional cumulative oil production of 3.2% and 5% above what the optimized open hole base case would have produced after 10 years and 20 years respectively from the six producers, Fig. 11.
• Reservoir pressure in the ICD scenario is maintained up to 3254 psi as compared to 3994 psi in the optimized base case OH-OH, Fig. 13
• Reduce water cut by 4 % and achieved a one-year delay in water breakthrough, Fig. 13
• Lower cumulative water injection by 6.5%, Fig. 14. This water injection reduction phenomenon is attributed solely to the performance of ICDs in injectors alone.

9. Conclusions

The conclusions made in this study are based on reservoir simulation sector model which is still subject to further calibrations as further geological, petrophysical and production data become available in the future.

• A novel 4-D workflow for ICD optimization has been developed which utilises PLT profile, near wellbore reservoir saturations, permeability profile, monitoring of water flood front movement, present & future reservoir conditions and challenges.
• The application of the 4-D well-reservoir integrated dynamic workflow, the optimum completion strategy can be determined for ICD Completions in Producers and Injectors.
The potential GAINS of ICD completions in both Injectors and Producers for 10 / 20 year period are:
• Improves cumulative oil production by 3.2% and 5% above what the optimized open hole base case would have produced after 10 years and 20 years respectively from the six producers.
• Reduce cumulative water injection by 6.5% from the three injectors.
• Reduces field water cut for the six producers in sector model by 4 %
• Delay water breakthrough for one year by retarding the water flood front in the bottom high permeability unit in upper reservoir zone
• Reservoir pressure using ICDs is maintained up to 3254 psi which is above the bubble point
• Optimum injection rates for the three injection wells in the sector model are between 15 – 20 MBBLS/D. Higher injection rates will yield lower cumulative oil production.
• Optimum production rates for the six producers in the sector model are between 7 – 8.5 MBOPD. However, the production rates for second line of producers (PROD-011, PROD-022 AND PROD-033) should be increased to 8.5 MBOPD after 5 – 7 years while the first line of producers can be maintained at or reduced below 7 MBOPD throughout since water cut increases in these wells. This conclusion is limited to the wells studied.
• Multiple data acquisition and integration are required. Time-Lapse monitoring of the reservoir performance through implementation of periodically acquired PLT/ FSI and reservoir saturation near wellbore to understand water flood front movement and water breakthrough zones in the reservoir.
• Factors that impact recovery and ICD completion design in Field A Sector Model have been identified as:

- Gravity effect aiding water breakthrough in the producers through bottom high permeability unit in upper reservoir zone
- Effect of high mobility ratio on water flood front movement.
- Effects of reservoir connectivity and interference with neighboring wells to account for future water breakthrough.

10. Acknowledgements

The author will like to thank SAUDI ARAMCO and Schlumberger for permission to publish this study and also acknowledge Byung Lee, ARAMCO PESD Supervisor for his support during the project.

11. Nomenclature

FCV Flow Control Valve
FFM Full Field Model
FS FrontSim
FSI Flow Scan Imager profile
ICD Inflow Control Device

LWD Logging while Drilling
MSW ECLIPSE Multi-Segment Well Model
OH Open Hole
PESD Aramco Petroleum Engineering Support Division
PFM FrontSim Patterned Flood Module Optimizer
PLT Production Logging Tool Profile
PVT Pressure, Volume and Temperature
PWI Power Water Injector
RST Reservoir Saturation Profile
VRP Voidage Replacement Ratio Control mode

12. References

1. Dake, L. P., 1998: Fundamentals of Reservoir Engineering, Elsevier Science B.V., pp 337 - 367.

2. Ellis, T., Erkal A., Goh, G., Jokela T., Kvernstuen, S., Leung, E., Moen, T., Porturas, F., Skillingstad, T., Vorkinn, P.B., Raffn, A.G., "Inflow Control Devices – Raising Profiles", Oilfield Review Winter 2009/2010, p30-37.

3. Holmes, J. A., Barkve, T. and Lund, O., 1998. "Application of a Multi-segment Well Model to Simulate Flow in Advanced Wells." SPE 50646, presented at the SPE European Petroleum Conference, The Hauge, The Netherlands, 20-22 October.

4. Leung, E., Nukhaev, M., Gottumukkala, M., Samosir, H., Abd El-Fattah, M., Ogunsanwo, O., Gonzalez, A., 2010 "Horizontal Well Placement and Completion Optimisation in Carbonate Reservoirs" SPE 140048, presented at the SPE Caspian Carbonates Technology Conference, Atyrau, Kazakhstan, November 2010.

5. Neylon, K. J., Reiso, E., Holmes, J. A. and Neese, O. B. 2009. "Modeling Well Inflow Control with Flow in Both Annulus and Tubing." SPE 118909, presented at the SPE Reservoir Simulation Symposium, The Woodlands, Texas, USA, 2-4 February.

6. Ouyang, L.B., "Practical Consideration of Inflow Control Device Application for Reducing Water Production", SPE 124154, SPE Technical Conference and Exhibition, New Orleans, Louisiana, U.S.A., October 2009.

7. Raffn, A.G., Hundsnes S., Kvernstuen, S., Moen, T. 2007 "ICD Screen Technology Used To Optimize Waterflooding in Injector Well" SPE 106018, presented at the Production and Operations Symposium, Oklahoma, U.S.A., 31 March – 3 April.

8. Rahimah, A.K., Azrul, N.M., Goh, K.F., Asyikin, A.N., Leung, E., Johan, M. 2010. "Horizontal Well Optimization with Inflow Control devices (ICDs) Application in Heterogeneous and Dipping Gas-Capped Oil Reservoirs" SPE 133336, presented at the SPE Annual Technical Conference and Exhibition held in Florence, Italy, 19-22 September.

9. Shahri, A., M., Kilany, K., Hembling, D., Lauritzen, J., E., Gottumukkala, V., Ogunyemi, O., Becerra, O.: 2009: Best "Cleanup Practices for an Offshore Sandstone Reservoir with ICD completions in Horizontal wells" SPE 120651.

10. Schlumberger, 2010. FRONTSIM 2010.1 Technical Description.

11. Schlumberger, 2010. ECLIPSE 2010.1 Technical Description.

Sensitivity Analysis of Interfacial Tension on Saturation and Relative Permeability Model Predictions

By Wael Abdallah, SPE, Weishu Zhao, SPE, and Ahmed Gmira, SPE, Schlumberger, Ardiansyah Negara, SPE, King Abdullah University of Science and Technology, and Jan Buiting, SPE, Saudi Aramco.

This paper was prepared for presentation at the 2011 SPE Saudi Arabia Section Technical Symposium and Exhibition held in AlKhobar, Saudi Arabia, 15–18 May 2011.

Abstract

Interfacial tension (IFT) measurements of Dodecane/brine systems at different concentrations and Dodecane/deionized water subject to different Dodecane purification cycles were taken over extended durations at room temperature and pressure to investigate the impact of aging. When a fresh droplet was formed, a sharp drop in IFT was observed assumed to be a result of intrinsic impurity adsorption at the interface. The subsequent measurements exhibited a prolonged equilibration period consistent with diffusion from the bulk phase to the interface. Our results indicate that minute amounts of impurities present in experimental chemical fluids "used as received" have a drastic impact on the properties of the interface. Initial and equilibrium IFT are shown to be dramatically different, therefore it is important to be cautious of utilizing IFT values in numerical models. The study demonstrates the impact these variations in IFT have on relative permeability relationships by adopting a simple pore network model simulation.

Introduction

Understanding the reservoir and what can be done to maximize oil recovery continues to be an active area of research; quite simply we typically only produce about 30-40% of original oil in place (OOIP) (Swenson et al., 2011; Shen et al., 2006). The fundamentals dominating hydrocarbon recovery don't change but the reservoir models used to evaluate such recovery scenarios can be improved by better understanding the fundamental interaction mechanism of fluid/brine/rock systems and its chemistry. Core flooding and centrifugal methods are commonly used to determine recovery factor, relative permeability, capillary pressure, and the overall efficiency of the flooding process. These techniques are applied for all types of improved or enhanced oil recovery techniques – water, engineered or "Smart" water; chemical or miscible gas injection. Generally this is performed through preserved cores cut from the target formation or increasingly through numerically simulated cores mimicing the rock and reservoir conditions. As with all

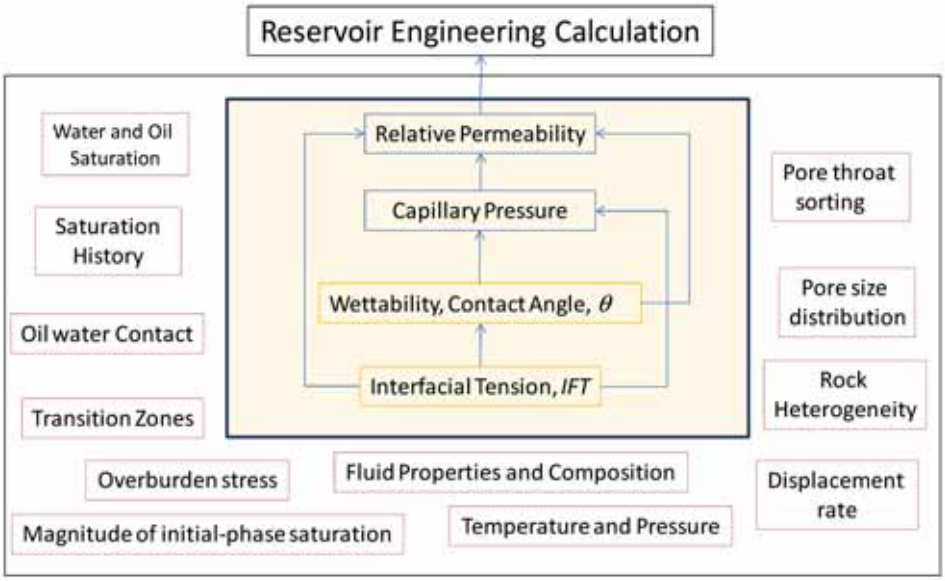

Figure 1: Parameters affecting reservoir models (Anderson, 1987; Bennion et al., 1993)

laboratory techniques, the value of the results depends entirely on how representative the acquired core plugs and fluid samples are. The extended durations required to perform representative dynamic core floods , coupled with limited preserved core samples also, limit the range of flooding experiments that can be achieved. Numerical techniques of course, (Koplik et. al., 1989; Venturoli and Boek, 2006; Kovscek et. al., 1993), allow one to simulate as many flooding scenarios as required. Clearly results are critically dependent on the quality of porous media representation, the fluids and wetting status modeled therein. Before one accepts the outputs of a numerical technique, one has to comprehend the impact of a wide range of parameters as demonstrated in Figure 1.

Two key parameters that have attracted interest in the past are the roles of interfacial tension between the two immiscible liquids and surface rock wettability. These two parameters among others are key to mathematically predicting relative permeability that can be fed into reservoir simulation models; most commonly used to compare and evaluate EOR methods prior to field deployment. With fluids interaction, a reduction in IFT decreases capillary pressure and increases capillary number, which increases the mobilization of trapped oil through the rock pore structure. Interaction with the rock pore structure, wettability describes how immiscible fluids adhere to a rock surface influencing a variety of parameters pertaining to oil flow. The fluid distribution in predominantly oil-wet rocks is significantly different to that in water-wet rocks. In the former, oil occupies more fractions of the tiny pores and wets the surface of large pores. This fluid distribution increases residual oil saturation, possibly decreases relative permeability to oil, and can lead to early water breakthrough under flooding.

Wettability can be measured by different techniques such as contact angle (θ), Amott (I_w/I_o), Amott-Harvey (IAH), USBM (IUSBM) and NMR (Abdallah et al., 2007). All these methods are loosely correlated and many factors as demonstrated in Figure 1 may affect the correlation between these measurements.

Most of the experimental work performed in literature to measure interfacial tension between two immisible fluids assumes equilibrium status is achieved in terms of seconds or few minutes (Michaels and Hauser, 1951; Jasper et al., 1970; Janczuk, 1993). If the interface is allowed to equilibrate for longer time, IFT will drop considerably which could represent better the true reservoir condition. Interfacial tension is subject to a highly dynamic process governed by diffusion, adsorption and desorption mechanisms occurring at the interface (Ikeda et al., 1991). The introduction of fresh fluid creates an instantaneous interface between the two immiscible fluids that is strongly affected by the presence of impurities. In the case of crude oil, it contains thousands of components including polar and non-polar species that alter the capillary forces at interfaces and consequently the interfacial tension and wettability.

The purpose of this study is to investigate the sensitivity of relative permeability predictions to observed decreases in fluid interfacial tension with time using a pore network model (PNM) approach (Janczuk, 1993;

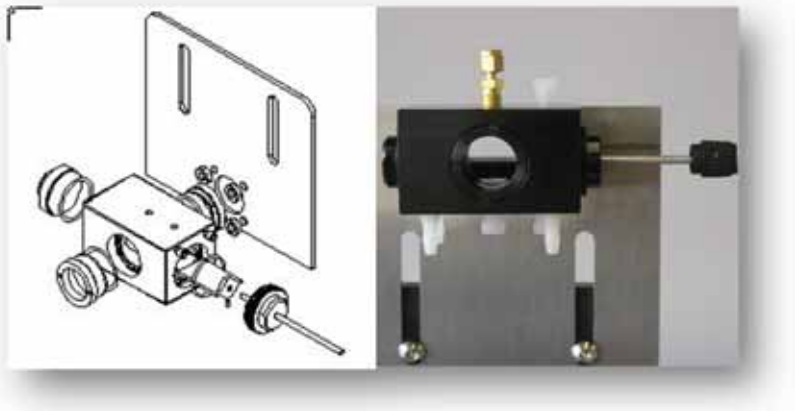

Figure 2: FTA Interfacial Tension Cell

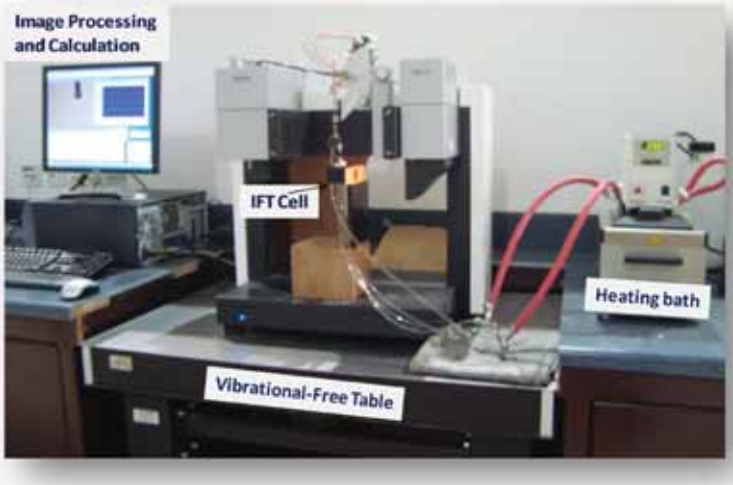

Figure 3: IFT Experimental Setup

Valvatne and Blunt, 2004). Pore network modeling has advantage in wettability studies over many other direct methods in that it is possible to define local wettability states at the pore scale by contact angle. With the given fluid's physical properties and pore network structure, fluid distribution and interface configuration in a model are controlled by specifying contact angle distribution after any wettability alteration caused by the displacing fluid. The fraction of oil invaded pores in which contact angle alteration takes place can be specified, typically in terms of a volume based percentage of pores ordered from largest to smallest. This would mimic the behavior of oil filling an originally water filled porous medium to a given saturation state, and then altering wettability of contacted surfaces.

The interfacial tension inputs were based upon an extensive experimental IFT study, which highlighted the dynamic nature of these measurements. PNM relative permeability and residual oil calculations demonstrated the high degree of sensitivity to IFT input values, especially for water-to-neutral wet rocks.

These findings have direct implications on static and dynamic reservoir modeling and relative permeability prediction. Furthermore, these results can be applied to modeling sweep efficiency and recovery under varying scenarios of temperature and salinity values.

Interfacial Tension Measurements

Experimental Setup

A First Ten Angstrom (FTA) interfacial tension sealed cell was used to measure pendant drop interfacial tension for all studied systems. The cell capacity is 22 ml with a 25 mm view port window to allow light passage (Figure 2). The cell is mounted on adjustable jacket in front of optical system from KRŰSS (DSA100) and the overall setup sits on top of a vibration free table for accurate measurements of interfacial tension as shown in Figure 3. The IFT cell is sealed with Viton o-rings and rated to 100 psi and operates up to 200 °C by circulating a heated fluid through two internal loops within the cell. A liquid drop is formed using a stainless steel needle with tip diameter of 0.71 mm. A Dell desktop computer was used to acquire the digital image of the pendant oil

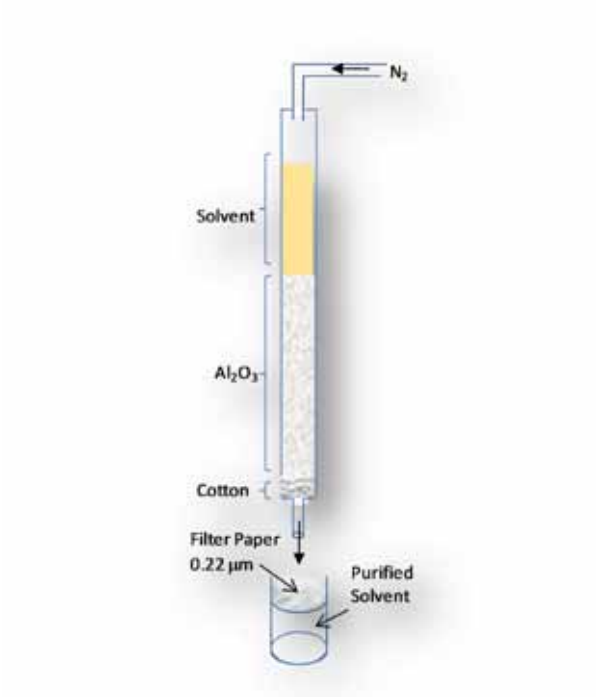

Figure 4: Solvent Purification Setup using basic alumina oxide

or brine drop and perform the subsequent drop image analysis, digitization, and computation; DSA1 v1.9 drop shape analysis from KRŰSS was used. The interfacial tension was calculated using Young-Laplace equation. The IFT cell body and its various parts were cleaned using acetone followed by deionized water when model alkanes and brines were used in addition to toluene when crude oil was used, then fully dried by air.

Dodecane (reagent plus >99% purity) from Sigma-Aldrich, deonized water purified by Milipore system to <30 ppb TDS, acetone (GC 99% purity) from Riedle-de Haen and basic activated alumina oxide Brochman I from Sigma-Aldrich were used in our study. Alumina oxide was used to purify Dodecane from Amphiphilic impurities. Dodecane was passed through a column filled with alumina oxide and pushed through the packed alumina using low flow rate dry nitrogen gas as illustrated in Figure 4.

Pore Network Modeling

A pore network model is an idealized pore space, generally incorporating a pore physical pore-scale events. Disordered and geometrically complex pore space can be conceptually simplified as pore bodies and throats and then mapped onto a lattice of nodes and bonds for consolidated porous rocks. assumed to simplify the pore elements and analytical equations are used to simulate complex multiphase flow and transport processes in the medium. Significant advances have been made in recent years in predictive pore network modeling (Zhao et al., 2010; Idowu and Blunt, 2010; Bakke and Øren, 1997), where geologically realistic networks are constructed from 3D voxel-based images that may be generated by X-ray microtomatography or by 3D reconstruction (stochastic or process based) informed by 2D thin sections as shown in Figure 5

The general approach to pore network modeling for single phase fluid flow is to impose a macroscopic pressure difference across the pore network. For laminar flow of Newtonian fluids, Poiseuille's law is usually applied at the bonds. The pressure field in the pore network is determined from the solution of a system of algebraic equations obtained by applying mass conservation at the nodes. The fluid flow rate in each bond can then be calculated and the macroscopic properties such as permeability can be easily obtained from Darcy's law. For more complicated two phase flow a simulator developed in Imperial College (Valvatne and Blunt, 2004) is used in this study. The model takes advantage of the angular-shaped elements used in pore networks such that the fluid distribution and interface configuration can be explicitly accounted for in the pore throats. Flow of two fluids (oil and water) can be simultaneously simulated in network elements with exact descriptions of the underlying physics. One of the advantages of this kind of model is that the wettability impact on fluid displacement can be conveniently studied. Capillary pressure can be directly calculated from the local geometry, contact angle and interfacial tension. These key input parameters determine the fluid distribution in the element.

The model is designed to simulate displacement cycles: the pore network is initially saturated with water when the medium is assumed strongly water wet. The sequence of primary drainage, spontaneous and forced imbibitions and secondary drainage can be modeled. The process of one fluid displacing another is governed by the macroscopic pressure difference imposed across the pore network and the local capillary pressure at each element. The simulation resembles a core flooding experiment: oil is forced into water saturated network through the inlet pores until all all mobile water has been displaced. Water subsequently imbibes into the system when the oil phase is gradually depressurized until water again saturates the system or the remaining oil is trapped. The model adopts a quasi-static approach that rests on the assumption that the flow is dominantly capillary an the viscous and gravitational forces are ignored. Each simulation step assumes that the system is in an equilibrium state and the invasion percolation rule is followed, ie, non-wetting phase always invades the adjacent element

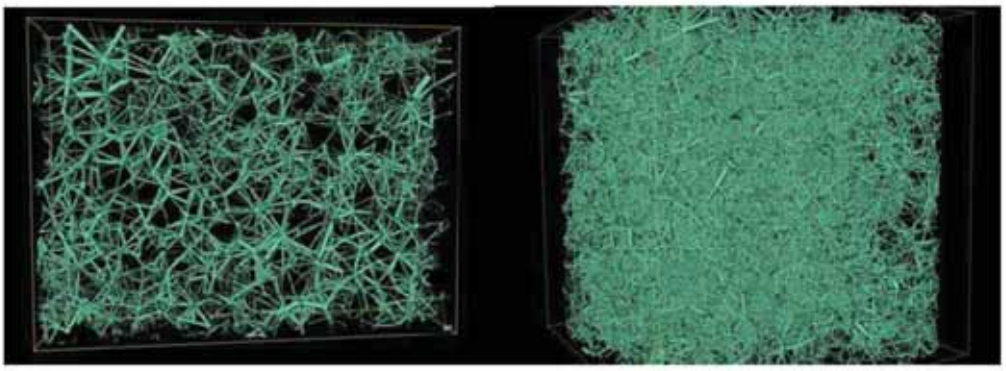

Figure 5: Pore network generated from the m-CT image (The pores are not shown to scale)

Rock Type	Carbonate	Sandstone
Porosity	28%	20%
Number of pores	14,421	110,810
Number of throats	41,031	247,084
Mean coordination number	5.8	4.4
Formation factor	9.0	20.8
Water viscosity (cp)	0.735	0.735
Oil viscosity (cp)	0.542	0.542
Water density (kg/m^3)	997	997
Oil density (kg/m^3)	703	703

Table 1: Statistical parameters of the pore network and fluid properties

with lowest capillary resistance while wetting phase always invades the adjacent element with highest capillary resistance. The final distribution and interface configuration in network elements is updated at each step without keeping track of the exact advancement of the interfaces. Two fluids are considered incompressible and flow indepedently at steady state until the interfaces are locked in position for the step. Fluid snap-off is also modeled. More details about the algorithm development in the simulator can be found in (Valvatne, 3004). The pore network models used in this study are extracted from a carbonated and a standstone sample. The core plugs are imaged and analysed in Australia National University (ANU) using high resolution X-ray microtomatography (micro CT). Statistical parameters of the pore network and flud properties are listed in Table 1.

Results and Discussion

Interfacial Tension Measurements

The establishment of interfacial tension at a newly created interface is a dynamic process. This means it required time to establish equilibrium when a fresh interface is formed between two immiscible fluids. The fluids used in experiments are not pure. Model solvents, such as alkanes received from chemical companies, contain impurities, which will affect an interface.Crude oil consists of thousands of components, including polar fractions such as asphaltenes and carboxylic acids. Brines contain several electrolytes and in waterflooding experiments surfactants are usually added in the water phase. Therefore, to reach equilibrium, sufficient time must be given to allow diffusion within both phases and adsorption/desorption at the interface to take place (Goebel and Lunkenheimer, 1997; Kuz, 1993). Literature reported values of IFT are measured within time scales of a few seconds to a few minutes after the interface is formed and in most cases appears to be insufficient to reach equilibrium (Alotaibi and Nasr-El-Din, 2009).

Figure 6a shows the dynamic behavior of IFT as a function of time (14 hours) for dodecane and deionized water and for the dodecane/brine systems at 25°C and atmospheric pressure. The brines are made of deionized/degassed water and NaCl salt with the following concentration 40 kppm (close to sea water salinity), 78 kppm, and 238 kppm (close to certain types of formation brines). The initial IFT value of Dodecane/deinozed water system is 52.5±0.1 mN/m measured within a few seconds after forming a pendant drop of water in Dodecane. This result is similar to reported literature values of 52.8 mN/m (Huanglee, 2000 and Alotaibi and Nasr-El-Din, 2009).

The initial IFT values for Dodecane / brine systems for the above listed salinities are 53.9±0.1, 54.9±0.1 and 61.1±0.1 mN/m, respectively, exhibiting a linear increase with salinity as demonstrated in Figure 7. The slope ($\Delta\gamma/\Delta m$) is about 1.53, which is similar to

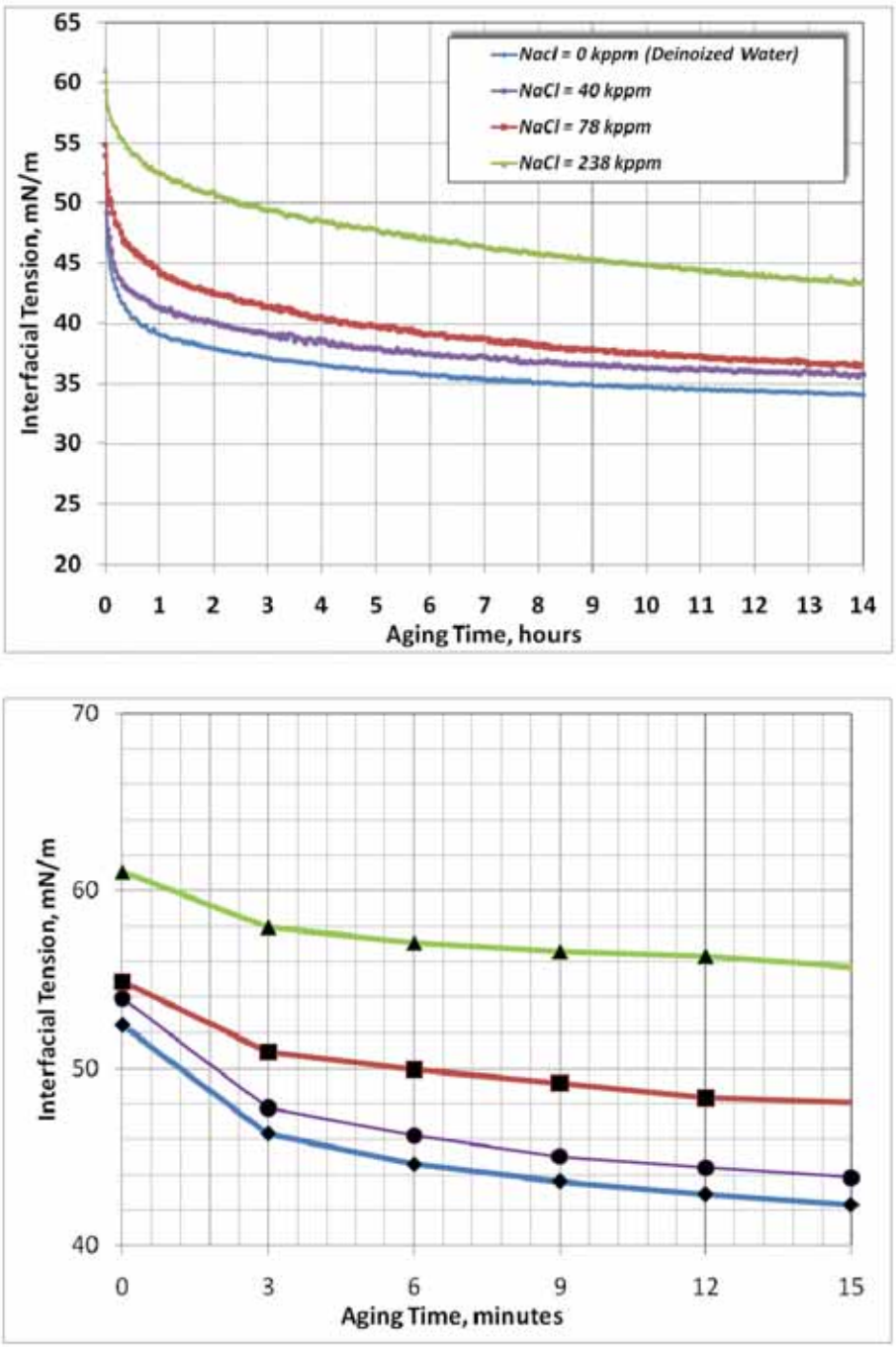

Figure 6: Interfacial tensions of dodecane/brine systems with different salinities at 25°C and atmospheric pressure (A) 14 hours aging (B) 15 minutes magnification

what has been reported in literature for alkane/NaCl brine systems (Ikeda et al., 1991; Johansson and Eriksson, 1974; Aveyard and Saleem, 1976). Ikeda et al. (Ikeda et al., 1991) measured IFT for Hexane/NaCl brine as a function of pressure and temperature for different NaCl brine concentration and up to a molality of 1M, in both systems; he reported a slope of 1.54 ($\Delta\gamma/\Delta m$).

Looking at the impact of aging, it is apparent that even up to 14 hours the IFT still did not reach a clear equilibrium. It is clear from these experiments that the changes in IFT over time compared to the initial values are considerable, i.e. in the order of 33%. Note also in figure 7, that the increase in interfacial tension with salinity for measurements taken after 14 hours aging is consistent with but slightly larger than initial IFT results with a slope ($\Delta\gamma/\Delta m$) of 1.65.

The repeatable phenomenon observed here is a rapid drop in IFT within the first seconds from forming the interface, followed by a slow decay (Figure 6). We believe this is primarily due to the quick adsorption at

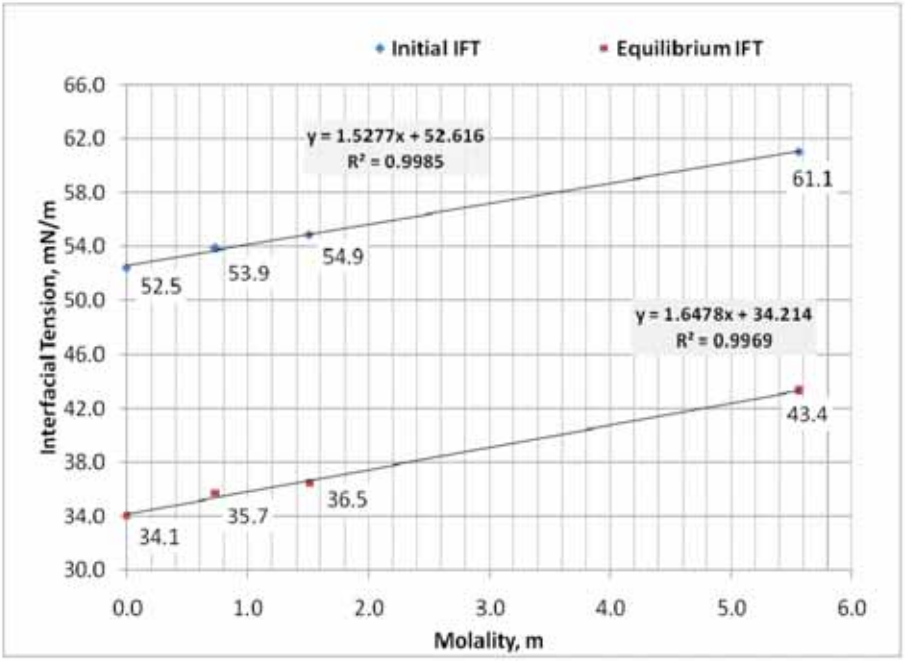

Figure 7: Initial and pseudo-equilibrium IFT of dodecane/brine systems with different molalities at 25°C and Patm

the interface of the active impurities present in the dodecane and electrolytes of the brine, followed by a subsequent diffusion effect in the bulk of both phases. This is a much slower process, which could explain the long equilibration time. The phenomenon has been reported several times in the literature (Netzel et al., 1964; Kuz, 1993), and remains under further investigation within this author group.

Impact of Dodecane Purification

Figure 8 shows the interfacial tension of dodecane/deinozed water at different purification cycles. The term "purification cycles" refer to the number of cycles the Dodecane is passed through the basic alumina oxide column as illustrated in Figure 4. The IFT value for all runs 0, 1 and 4 cycles once the drop is formed is 52.5±0.1, 54.4±0.1 and 57.6±0.1 mN/m, respectively. The IFT after 14 hours aging timeis 34.1±0.1, 38.0±0.1 and 50.5±0.1 mN/n, respectively.

Evaluating these results, there are a number of of interesting observations:

- The interfacial tension tends to equilibrate faster with higher purification cycles, and the initial sharp decrease of IFT at the first minutes from forming the drop is less observed.
- The interfacial tension value increases with higher purification and differs from that reported in literature for such system (Huanglee, 2000).

The IFT increase for n-alkane/water interfaces is however in line with common findings on the effect of surface active trace impurities on the surfactant solutions' surface tension (Aveyard and Saleem, 1976). As a rule, removing these trace impurities from the chemicals will result in a increase in the corresponding interfacial tension. These measurements were repeated a second time and results were reproducible. The question remains as to how far this purification impacts the IFT measurement and at what point the actual IFT for the fluids under study is reached.

Effect of IFT dynamics on fluid flow simulation

IFT is a key input parameter in pore network modeling of multiphase flow. As shown previously, IFT value may not be trusted if equilibrium was not established during the measurement. Using such inputs may lead to inaccurate simulation results. In this study, we qualitatively test this effect using two pore network models (Table 1). It is assumed for this evaluation that for a model with a fixed solid/fluids system, the capillary pressure in each model element (pore or throat) should only depend on local geometry. From Young-Laplace equation, different contact angles correspond to different IFT values used in the model.

For example, in a system with equilibrium IFT of 30 mN/m with contact angle at 30°, an IFT input of 50 mN/m will imply a 58.7° contact angle in order to maintain the same capillary pressure. This relationship

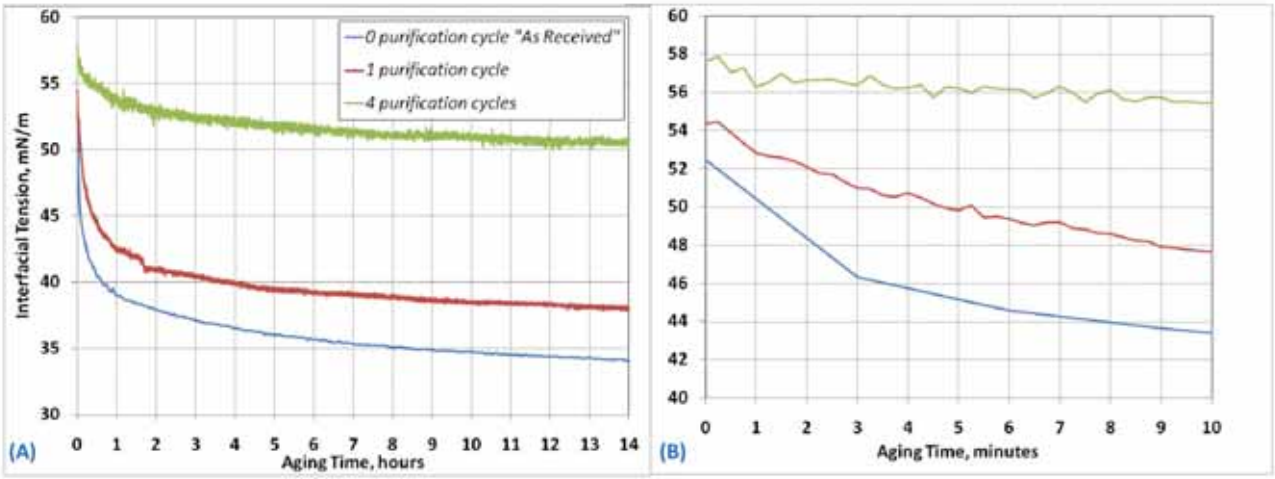

Figure 8: Initial and pseudo-equilibrium IFT of dodecane / brine systems with different molalities at 25°C and Patm

is shown in Figure 9. Since contact angle controls interface configuration and thus fluid distribution in model elements, different flow scenarios can be expected. Example results of relative permeability curves using two pore networks are shown in Figure 10 and 11. Both figures show the effect on simulation results caused by feeding erroneous IFT value in the model, which results in a problematic interpretation of fluid distribution and flow scenario. With only MICP data available, one can imagine that using non-equilibrium IFT value may lead to wrong contact angle calculation, which have significant impacts on relative permeabilities and residual oil saturations.

Although the aim of this study is not to model the effect of IFT reduction on sweeping efficiency, it appears from both Figures 10 and 11 that reducing IFT from 50 to 30 mN/m shifts the normalized relative permeability curves to the left, suggesting reduced sweep efficiency and the impact of modifying contact angle to normalized relative permeability curves is overriding any recovery factor improvement by IFT reduction. This may be consistent with the accepted notion that a mixed wet system is more optimal from a water flood standpoint than either water or oil wet [Jadhunandan and Morrow, 1995; Kennedy et. al., 1955; Lorenz et. al., 1974].

In addition, the results of this simulation highlight the potential impact of this 20mN/m change in IFT from 50 to 30mN/m – in a transition zone where perhaps there is 40% water saturation, the oil relative permeability is altered by a factor of 2 to 3. This can have marked consequences on development decisions when attempting to efficiently recover oil with a water flood. It also greatly impacts the remaining saturations in these swept intervals.

Conclusions

Interfacial tensions take a long time to equilibrate after interfaces are created. Diffusion, adsorption, and desorption of impurities may cause interfacial tension to change with time and the nature of these impurities will affect further such equilibrium. When an interface is formed, the initial differences in concentration between the interface and the bulk phases act as the driving force of the system. Minute amounts of impurities present in experimental chemical fluids "used as received" have a drastic impact on the properties of the interface. Results of pore network simulations imply that caution should be taken when IFT values are adopted in numerical models.

This all converges to addressing the question of field sampled fluid interfacial tensions. Crude oil contains many polar components that if not sampled or handled correctly will alter the results of IFT measurements. Presumably within the formation the fluids have reached a suitable "equilibrium", and it is not obvious from our studies that the conventional methods for IFT measurement are replicating the downhole environment rigorously. The impact of inaccurate IFT; similar to fluid properties or SCAL measurements; is clear when at-

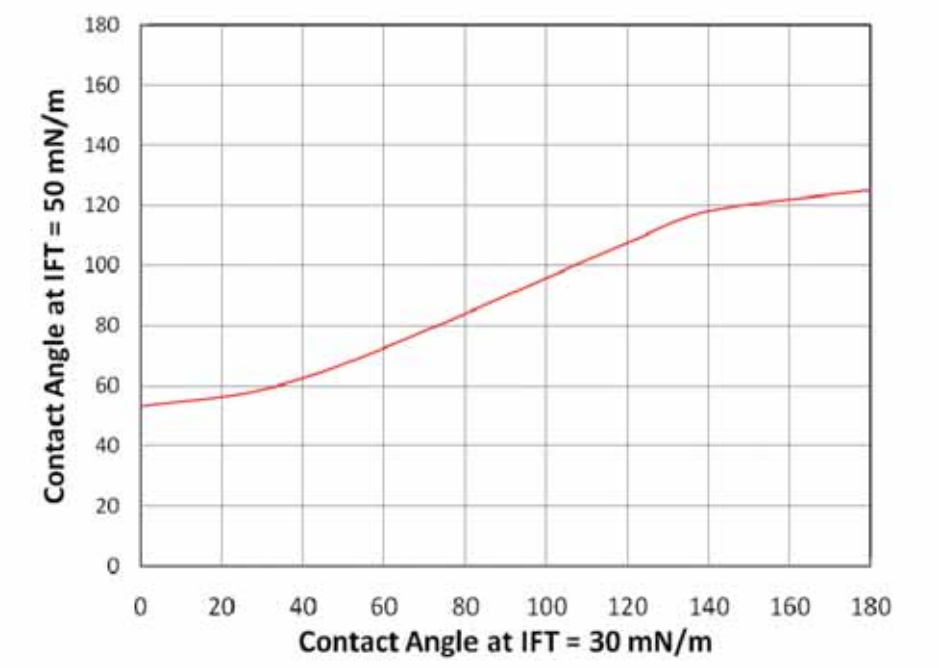

Figure 9: Relationship between contact angles at different IFTs with a fixed capillary pressure

tempting to build a field development plan based upon reservoir simulations, and therefore demands attention.

Acknowledgement

The authors would like to acknowledge Steve Dyer for his insightful discussion on the importance of such subject to reservoir upscaling.

References

Abdallah, W., Buckley, J.S., Carnegie, A., Edwards, J., Herold, B., Fordham, E., Graue, A., Habashy, T., Zeleznev, N., Signer, C., Hussien, H., Montaron, B., and Ziauddin, M., 2007. Fundamentals of Wettability, *Oilfield Review* 19(2): 44-61

Alotaibi, M.B., and Nasr-El-Din, H.A., 2009. Effect of Brine Salinity on Reservoir Fluids Interfacial Tension. SPE-121569, Presented at the 2009 EUROPEC/EAGE Annual Conference and Exhibition held in Amsterdam, The Netherland, June 8-11.

Anderson, W.G., 1987. Wettability Literature Survey – Part 5: The Effects of Wettability on Relative Permeability, *J Petro Techno*, 39: 1453-1468

Aveyard, R., and Saleem, S.M. 1976. Interfacial Tension at Alkane-Aqueous Electrolyte Interfaces, *J Chem. Soc. Fara. Trans. I,* 72: 1609-1617

Bakke, S. and Øren, P-E., 1997. 3-D Pore-Scale Modeling of Sandstones and Flow Simulation in the Pore Networks, SPE-35479. Presented at the European 3-D reservoir modeling conference held in Stavanger, Norway, April 16-17.

Bennion, D.B., Sarioglu, G., Chan, M.Y.S., Hirata, T., Courtnage, D., and Wansleeben, J., 1993. Steady-State Bitumen-Water Relative Permeability Measurements at Elevated Temperatures in Unconsolidated Porous Media. SPE-25803, Presentaed at the International Thermal Operations Symposium held in Bakerfield, CA, U.S.A., February 8-10.

Goebel, A., and Lunkenheimer, K., 1997. Interfacial Tension of the Water/n-Alkane Interface, *Langmuir*, 13: 369-372

Huanglee, L., 2000. The gap between the measured and calculated liquid-liquid interfacial tensions derived from contact angles, *J. Ad. Sci. Techno.*, 14(2): 167-185

Idowu, N.A. and Blunt, M.J., 2010. Pore-Scale Modeling of Rate Effects in Waterflooding. *Transp Porois Med.*, 83: 151-169

Ikeda, N., Aratono, M., and Motomura, K., 1991. Thermodynamics Study on the Adsorption of Sodium

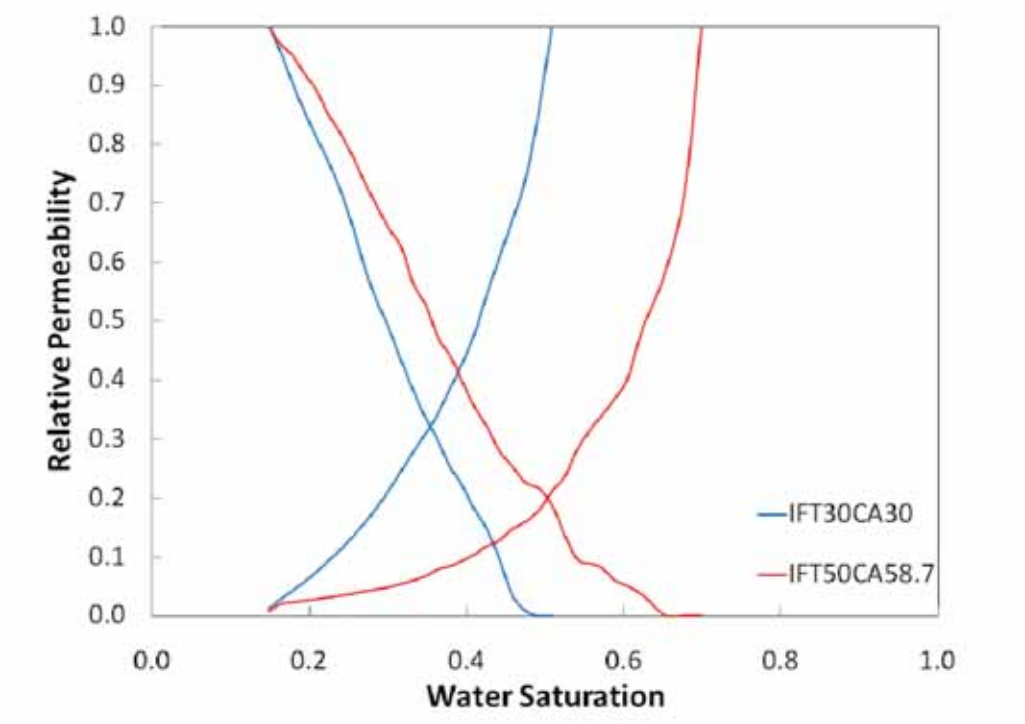

Figure 10: Normalized relative permeability curves for model 1.

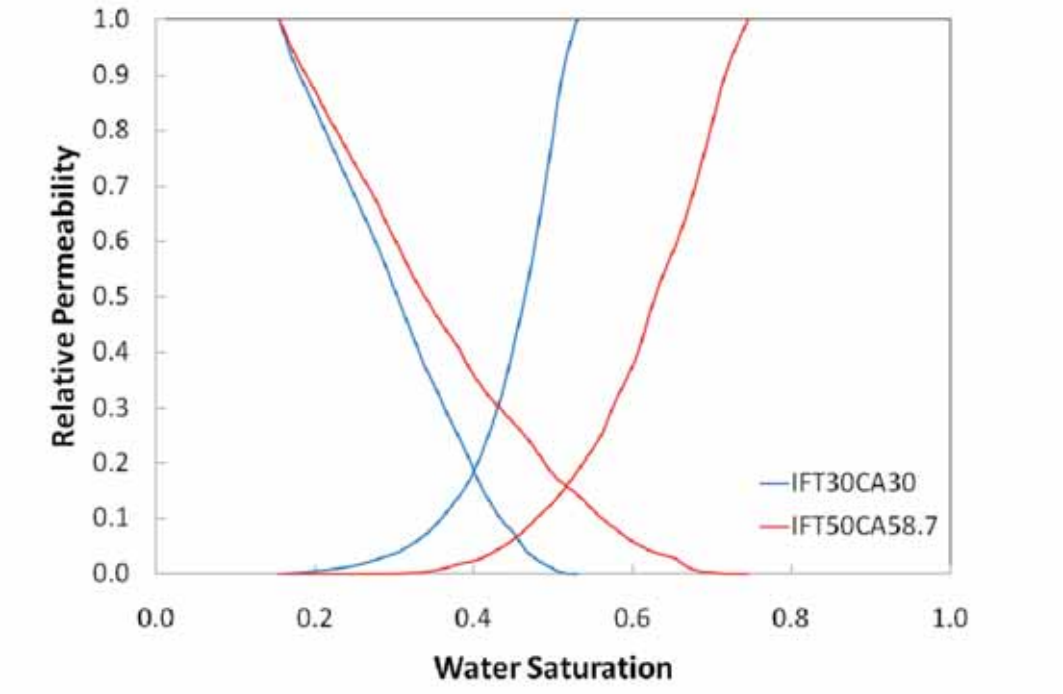

Figure 11: Normalized relative permeability curves for model 2.

Chloride at the Water/Hexane Interface, *J. Colloids. Inter. Sci.*, 149(1): 208-215

Jadhunandan, P.P., and Morrow, N.R., 1995. Effect of Wettability on Waterflood Recovery for Crude-Oil/Brine/Rock systems, SPE-22597, Presented at the 1991SPE Annual Technical Conference and Exhibition held in Dallas, U.S.A., Oct. 6-9.

Janczuk, B. Wójcik, W. and Zdziennicka, A., 1993. Determination of the Components of the Surface Tension of Some Liquids from Interfacial Liquid-Liquid Tension Measurements, *J. Colloids Inter. Sci.*, 157(2): 384-393

Jasper, J.J., Nakonecznyj, M., Swingley, C.S., and Livingston, H.K., 1970. Interfacial Tensions against Water of Some C10- C15 Hydrocarbons with Aromatic or Cycloaliphatic Rings, *J. Phy. Chem.*, 74(7): 1535-1539

Johansson, K., and Eriksson, J.C., 1974. γ and dγ/dT measurements on aqueous solutions of 1,1-electrolytes, *J. Colloids Inter. Sci.*, 49(3): 469-480

Kennedy, H.T., Burja, E.O., and Boykin, R.S., 1955. An investigation of the effects of wettability on the recovery of oil by waterflooding, *J. Phys. Chem.*, 59:867-869

Koplik, J., Banavar, J.R., and Willemsen, J.F., 1989. Molecular dynamics of fluid flow at solid surfaces, *Physics of Fluids A.*, 1: 781-794

Kovscek, A.R., Wong, H., and Radke, C.J., 1993. A pore-level scenario for the development of mixed wettability in oil reservoirs, *AIChE Journal*, 39: 1072-1085.

Kuz, V.A., 1993. The aging of a Liquid Drop, *Langmuir*, 9: 3724-3727

Lorenz, P.B., Donaldson, E.C., and Thomas, R.D., 1974. Use of centrifugal measurements of wettability to predict oil recovery, U.S. Bureau of Mines, Bartlesville Energy Technology Center, Report 7873.

Michaels, A.S., and Hauser, E.A., 1951. Interfacial tension at elevated pressure and temperature. II Interfacial Properties of Hydrocarbon-Water Systems, *J. Phy. Chem.*, 55(3): 408-421

Netzel, D.A., Hoch, G., and Marx, T.I., 1964. Adsorption studies of surfactants at the liquid-vapor interface: Apparatus and method for rapidly determining the dynamic surface tension, *J. Colloid Sci.*, 19(9): 774-785

Swenson, P.D., Horvath-Szabo, G., Abdallah, W., and Eskin, D., 2011. A Novel Centrifugal Method for Wettability Characterization of Granulates, *Ind. Eng.Chem. Res.*, Accepted for publication in February 15.

Shen, P., Zhi, B., Li, X.B., Wu, Y.S., 2006. The Influence of Interfacial Tesnion on Water/Oil Two-Phase Relative Permeability, SPE-95405 Presented at the SPE/DOE Symposium on Improved Oil Recovery held in Tulsa, Oklahoma, U.S.A, April 22-26.

Valvatne, P. and Blunt, M., 2004. Predictive pore-scale modeling of two phase flow in mixed wet media. *Water Resour. Res.*, 407406.

Valvatne, P., 2004. Predictive pore-scale modeling of multiphase flow. PhD Dissertation, Earth Science and Engineering, Imperial College, UK.

Venturoli, M., and Boek, E.S., 2006. Two-dimensional lattice-Boltzmann simulations of single phase flow in a pseudo two-dimensional micromodel, *Physica A.*, 362: 23-29.

Zhao, X; Blunt, M.J.; and Yao, J., 2010. Pore-Scale modeling: Effects of wettability on waterflooding oil recovery, *J. Petro. Sci. Eng.*, 71: 169-178

Saudi Arabia oil & gas

Saudi Arabia Oil & Gas (Print) ISSN 2045-6670

www.saudiarabiaoilandgas.com

Saudi Arabia Oil & Gas (Online) ISSN 2045-6689

For advertising, contact:

UNITED KINGDOM
Adam Mehar
268 Bath Road, Slough, Berkshire,
United Kingdom
Main 44 1753 708872
Fax 44 1753 725460
Mobile 44 777 2096692
adam.mehar@saudiarabiaoilandgas.com

UNITED ARAB EMIRATES
Abdul Hameed
abdul.hameed@eprasheed.com
Tel: (971) 5056 8515

SAUDI ARABIA
Akram ul Haq
PO Box 3260, Jeddah 21471
akram.ul.haq@saudiarabiaoilandgas.com
Tel: (966) 557 276 426

DAILY NEWSLETTER

2011 SPE-SAS/DGS Annual Technical Symposium and Exhibition

Sunday May 15, 2011

Major Highlights

- **Pre-Event Program**
- **ATS&E Opening Ceremony**
- **Exhibition Opening**

From the Chairman:

The 2011 Annual Technical Symposium and Exhibition (2011 ATS&E) was launched on May 14, 2011. The event took place in AlKhobar, Saudi Arabia over the period: May 15 - 18. The event was organised by the Saudi Arabian section of the Society of Petroleum Engineers (SPE SAS) and the Dhahran Geoscience Society (DGS).

This annual event is the largest annual gathering for engineers and geoscientists in the region. It evolved to be a major gathering for knowledge transfer, experience exchange and networking in the Gulf region. The annual growth journey of the ATS&E continues strongly in 2011. The Symposium received a lot of international attention where the Program Committee received abstracts from more than 30 countries. With a total number of 412 received abstracts, the 2011 ATS&E broke every record throughout its history.

This year's theme "Tackling Upstream Challenges: Fueling the World Safely, Reliably and Cost-Effectively", called for new technologies in all operations related to exploration and production of oil and gas.

IIf you could not actively participate in the Symposium, the purpose of this newsletter was to keep you updated on some of the key activities taking place in the Seef Center, AlKhobar, Saudi Arabia.

I would like to thank the technical committee for choosing the best papers to be presented in this event.

Last but not least, a big thank you to the organizing committee for their tremendous efforts making this event a success, thank you for your hard work & dedication over the last 11 months.

Dr. Ghaithan A. Al-Muntasheri
Chairman, 2011 SPE/DGS Annual Technical Symposium & Exhibition
Email: ghaithan.muntasheri@aramco.com

Pre-Event Program

This year, the ATS&E hosted 4 technical courses and a workshop. Thanks to our sponsors and training partners. This pre-event program was held in the Gulf Le MeridienHotel, AlKhobar on Saturday and Sunday, 14-15 May. The courses and the workshop were fully booked. As a matter of fact, they were booked within very few days right after we announced them

back in March. A total of 133 seats were occupied. The topics were carefully selected to reflect on the current needs for petroleum engineers and geoscientists.















DAILY NEWSLETTER

2011 SPE-SAS/DGS Annual Technical Symposium and Exhibition

Monday May 16, 2011

Today, the ATS&E started Tackling Upstream Challenges through its technical program. A total of 24 technical presentations were given today. Not only that, there were 6 invited speakers from different regions in the world. They were from: Saudi Aramco, Baker Hughes, Halliburton, Weatherford, Delft University of Technology; The Netherlands and Stanford University; USA.

The 8 sessions were heavily attended. There were 260 delegates attending each pair of ongoing session. Hot and pressing issues in the upstream oil & gas industry were discussed. These were covered in the 8 sessions: Reservoir Geology & Geophysics, New Emerging Technologies in the Upstream Oil & Gas, Drilling Operations, Unconventional Resources, Integrated Reservoir Management, Health, Safety & Environment, Advances in Improved Oil Recovery/Enhanced Oil Recovery and Advances in Reservoir Characterization.

The Invited Speakers were:

Mr. Dave Clark Director, Dhahran Research and Technology Center, Baker Hughes, Saudi Arabia

Mr. Robert H. Gales Vice President, Unconventional Resources Projects, Weatherford

Dr. Nabeel Al Afaleq Manager, Northern Area Reservoir Management Department, Saudi Aramco

Mr. Darren Franklin Country Manager, Health, Safety, Environment & Operational Excellence Halliburton

Dr. Pacelli L. Zitha Delft University of Technology, The Netherlands

Dr. Amos Nur Director, Rock Physics & Borehole Geophysics, Stanford University, USA

Luncheon was generously sponsored by Baker Hughes.

The presenter was **Hans Christian Freitag** , *Baker Hughes*
His presentation title was: *Technology, Development & Implementation, successes, pitfalls and opportunities.*

During lunch raffles were drawn for four gifts: iPad, Mobile Phone, a Laptop and a Printer

Gift were provided by our sponsor Al-Maktaba

DAILY NEWSLETTER

2011 SPE-SAS/DGS Annual Technical Symposium and Exhibition

Tuesday May 17, 2011

Tuesday May 17 Highlights:

Tuesday was an exceptional day by all means. The program was in its peak of experience exchange and knowledge sharing. It involved 4 technical sessions. These were:

1. Production Operations (1)
2. Advanced Rock Physics
3. Reservoir Simulation
4. Drilling Operations (2)

It involved two invited speakers from Saudi Aramco. These are Mr. Khalid O. Al Subai and Mr. Omar Al Husaini

Mr. Khalid O. Al Subai gave a presentation titled: State of the Art Processes and Technologies for Modeling Giant Fields.

DAILY NEWSLETTER

2011 SPE-SAS/DGS Annual Technical Symposium and Exhibition

Wednesday May 18, 2011

Wednesday May 18 Highlights:

Technical Sessions:

The program on Wednesday was rich. The morning session had 4. These are:

- Well Completion
- Production Operations (2)
- Drilling Operations (3)
- Reservoir Engineering and Management.

They involved 2 invited speakers from: Saudi Aramco and Petroleum Development Oman. The speakers were:

- Mr. Naji al-Umair of Saudi Aramco
- Dr. Riyadh Moosa of Petroleum Development Oman






Exits from the Hydrocarbon Highway

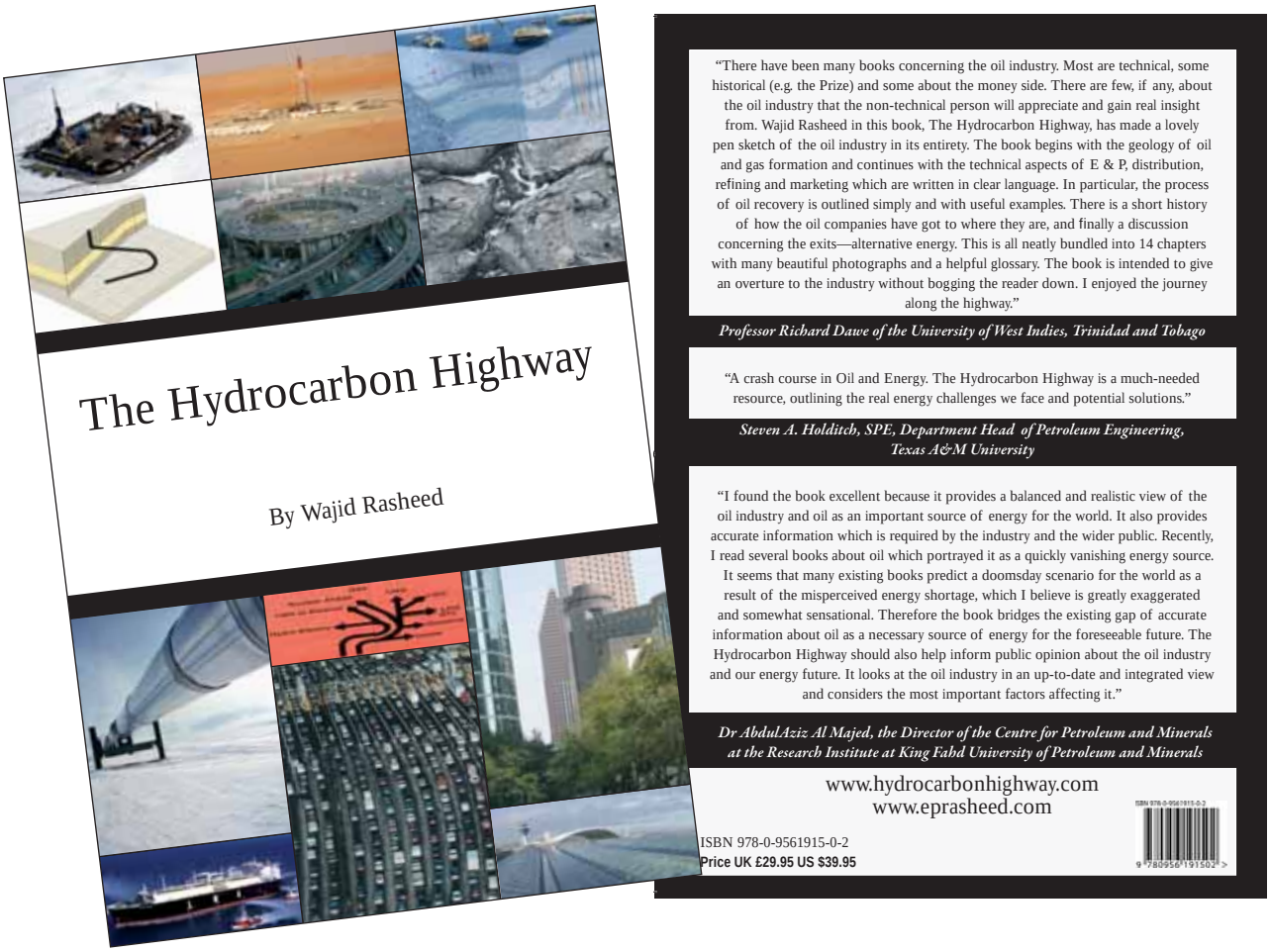

'Sometimes the best exit is the way we came in.'

Wajid Rasheed

Picture this: primeval man struggling to move a big kill or a great log. Carcasses of meat were no doubt hard to drag, but logs could be rolled and the invention of the wheel was not far off. Fast forward to the 21st century and witness the evolution of the wheel which is now entirely mechanised, powered by the internal combustion engine and fueled by petroleum. While petroleum is not a 'perfect' fuel (it is finite and pollutes), the high density energy that is packed into every litre and the convenience with which it can be moved make it hard to beat. That is why it is not going away. Together, this triple combo – wheel, engine and petroleum – ranks

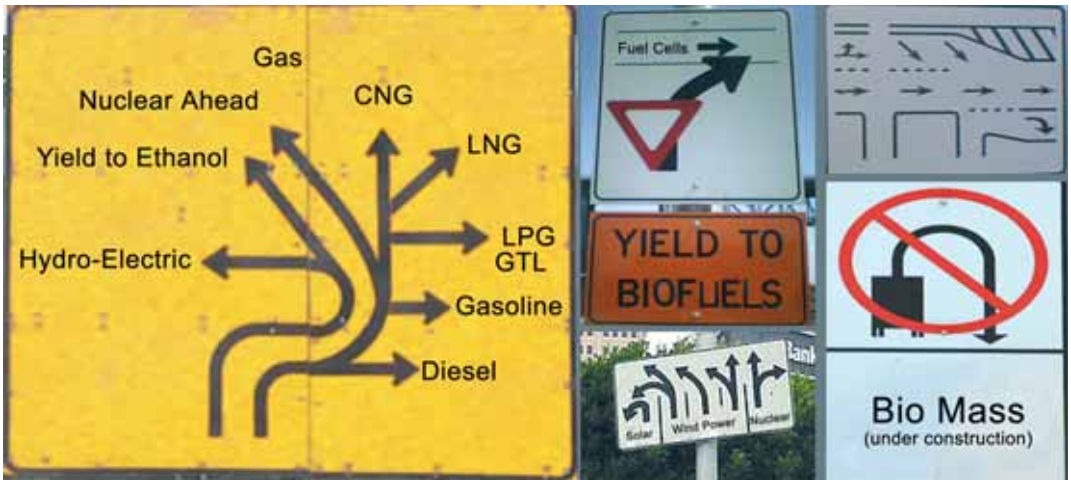

Our Energy Future Images 1- Plenty of Signs Beckon But Where Do They Lead?

among mankind's greatest inventions and has rolled-out mankind's greatest infrastructure endeavour, the Hydrocarbon Highway.

Our route along the Hydrocarbon Highway has shown that peak oil is not a physical shortage; there is plenty of untapped and unmapped oil. Moreover, technology is continually improving recovery.Consequently, peak oil is more of a psychological shortage. Our route has taken us behind the 'Oil Curtain' revealing the causes and effects of oil nationalism. We have seen how valuable oil leases are acquired, developed and how 'Extreme EP' and intelligent wells are the future of production. Not least, we have considered renewable energy sources against the backdrop of carbon emissions and climate change. Before we reach our final destination, 'beyond petroleum', we have to define those scenarios and 'exits' to the highway where oil and gas can be practically replaced.

Plenty of signs jostle for our attention and some seem easy to take – do nothing, business as usual. Others require complex questions to be considered: should more gas infrastructure be developed?; where should we build nuclear plants?; where should we dispose of nuclear waste?; what will compensate for shortfalls in renewable power?; how should we store electricity effectively?; and, are biofuels causing food poverty? Tackling such difficult questions provides some insight into why there is so much dependence on hydrocarbons. We need to identify exits that are genuine and not those that just detour back to the hydrocarbon highway. This means fully thinking through where energy is supplied from and its end-use consumption (see Our Energy Future Images 1, above).

In order to move beyond petroleum, we need to understand that there are no easy exits to hydrocarbon dependence; there is no silver bullet. Many so-called exits are still early prototypes 'under construction' requiring extensive research and development, political will, investment and time. It will take at least a generation before they become widely used. Still, each exit is applicable in certain scenarios only. Not all countries wish to build or handle spent nuclear waste. Cold temperate climates do not lend themselves to solar power and wind power may not always be consistent. Not all countries can grow biofuels. The pivotal point is that no single energy source fits all needs.

All energy sources suffer from limitations related to fit-for-purpose technicalities, start-up costs, output efficiency or societal trade-offs (see Our Energy Future Images 2). Any practical future energy scenario must include each and every one of these energy sources. Consequently, the answer lies in researching all options. That means experimenting and developing all applications until we find what works. The bottom line is that the Hydrocarbon Highway just got longer.

Gas Is the 'New' Oil

From all perspectives, gas emerges as one of the best potential exits from the Hydrocarbon Highway. If gas is a hydrocarbon though, how can it be an exit? Isn't it just the same as oil being a finite fossil fuel? Gas is the best choice that we have as a bridge to the truly 'renewable energy' scenario as it can be man-made or naturally produced and has low carbon emissions when burnt. The role of gas becomes clear in the energy models from the present period to the year 2030 which show that gas re-directs and eases off considerable demand for a broad number of oil applications[1]. The foundations for a 'gas' future have already been built using a broad set of advanced gas[2] technologies. Exemplifying this are Liquefied

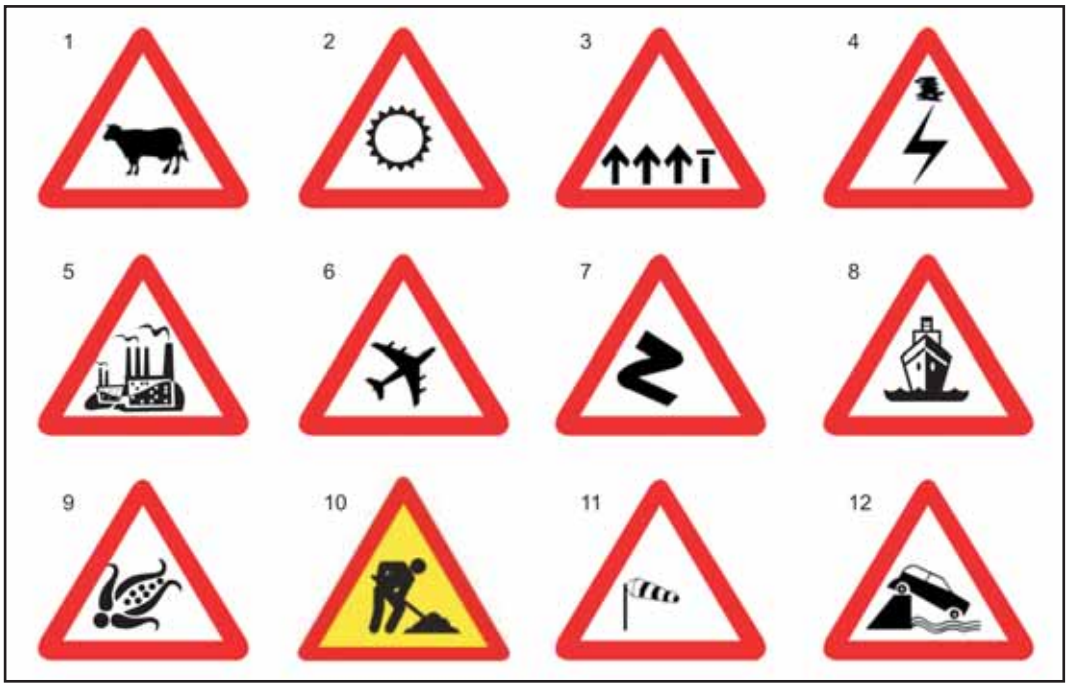

Our Energy Future Images 2 - All Energy Sources Have Limitations Therefore We Need All Options

Natural Gas (LNG) which mobilises and commercialises stranded reserves. Additional examples are Compressed Natural Gas (CNG) and Liquefied Petroleum Gas (LPG) which provides fuel for the transport and power-generation sectors through to Gas to Liquids (GTL) technology which offers high quality gasoline fuel but at a high cost. Capping it all is renewable methane or man-made 'bio-gas' which is biologically produced. Gas is not a panacea though; it has limitations too.

So how much of a choice does gas or any other energy source really provide? That depends on whether the fuel can actually replace oil and how well it fits into future energy scenarios. In a major oil application such as aviation fuel, for example, gas in any form cannot replace oil due to engine design. Further complications exist as gas is not as easily transported as oil. It needs a specialised infrastructure to be developed which may be cost-effective at a high oil price but not at a low one (see Figure 1).

The reason for considering all possible energy sources, and evaluating their strengths and weaknesses objectively, is to create a logic-based demand and supply equation for oil – one that qualifies, future energy sources so that replacements can be identified.

By asking whether oil can be replaced and whether the resulting carbon emissions are lower than those of oil, we can see just how far each energy source can really take us. Once they pass this qualification stage, they can then be fitted into future energy trends allowing us to glimpse the future.

Summary: The Masses

Most of today's hydrocarbon dependence can theoretically be 'phased-out' over the long term with renewable resources theoretically 'phased in' by 2050. This cannot happen in the short or medium term because replacements for oil do not offer straight oil swaps in mass; they are only usable in minute niches contributing to less than 5% of total oil energy demand worldwide. In contrast, 90% of oil and natural gas consumption is concentrated in trillions of transactions[3]. This vast consumption is most visibly spread worldwide among fleets of cars, planes, trains and specialised machinery and equipment.

In order to appreciate the vast scale involved, imagine reconfiguring every gasoline station in your home town or city, in the state itself, the country, the continent and the world. Then think about the network of distribution and storage behind the retail outlets. That would represent half the equation – supply side only. The consumption side consisting of the engines that power the world's fleet of cars, trucks and buses would need to be reconfigured too. Imagine doing the same for aviation, maritime and rail transport. There is demand in other components that would need to be considered too. Imagine reconfiguring existing power generation and industrial processes. The mass automotive and aviation products and mass processes such as power-generation

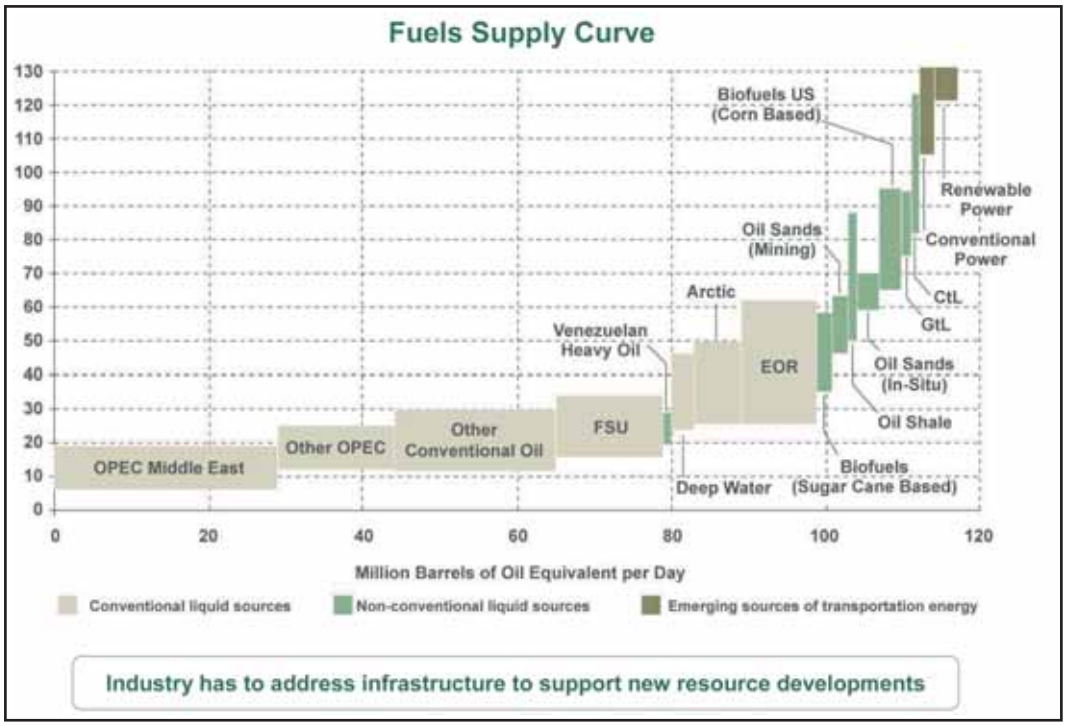

Figure 1 - Higher oil price expands biofuels, unconventional oil, EOR and opens new frontiers (Source Booz Allen Haminton/IEA/Petrobras—Assumed average vs. marginal costs; 10% return for conventional and 13% return for unconventional technologies; no subsides for biofuels; no carbon offset costs; after severance and production taxes.

plants and petrochemical feedstock are configured for oil and natural gas usage; they are extremely difficult to change. In the short run, not much changes because of the demand inelasticity; however, in the medium term, a growing number of gas-based technologies, as well as growing volumes of ethanol and biodiesel can replace oil in mass products and mass processes*. Not only does this strengthen investment in the infrastructure and usage of gas, ethanol and biodiesel but this also acts as a safety valve to dampen the demand for oil, redirect the excess demand from oil to gas and ultimately to the development of renewable resources.

This allows the next generation of new mass products and mass processes to be designed using gas, GTL, biodiesel, ethanol or co-generation while allowing the existing infrastructure to be reconfigured. In the long run, this acts as an exit as greater oil and gas demand elasticity is achieved overall [4].

Energy Consumption Models

Principally developed by governments, energy companies and universities, energy models seek to map out trends in future energy consumption. Many variants exist, but essentially models are geared to low, medium and high levels of population, economic and demand growth. Salient trends are identified and drawn up as scenarios allowing organisations to better handle potential future risk and opportunity. Corporate models are generally kept confidential due to their commercial nature, while certain state and academic models are publicly available[5].

US EIA/IEO Reference Case to 2030

For our purposes, the US Energy Information Administration (EIA) or International Energy Outlook (IEO) reference case was selected as a global model for future energy consumption*. Considered by the US EIA to be the 'business as usual' future scenario, the IEO2008 reference case estimates world energy demand and supply to the period ending 2030. It attributes principal energy supply from oil, gas, coal, nuclear and hydroelectric sources and separates the consumption of energy into the categories of transport, industrial, residential and commercial usage. Total global energy demand is estimated to increase by 50% from 462 quadrillion Btu to 695 quadrillion Btu in 2030 (see Figure 2). This is mostly driven by sustained consumer demand in the Organisation for Economic Co-operation and Development (OECD) and industrial growth in Brazil, Russia, India and China (the 'BRIC's) (see Figure 3). World Gross Domestic Product (GDP) and primary energy consumption also grows more rapidly in the first half than in the second half of the projections, reflecting a gradual slowdown of economic growth in non-OECD Asia. The model envisages sustained high

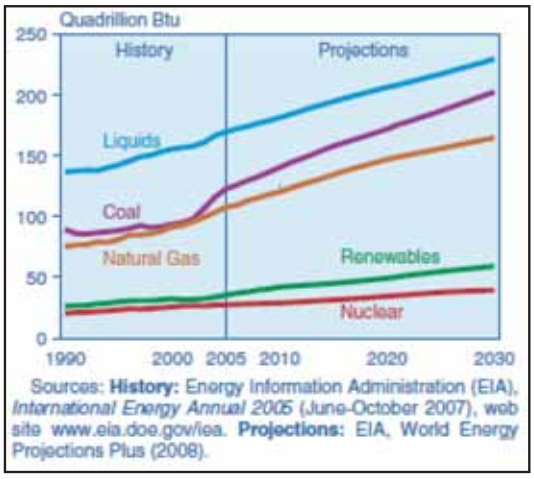

Figure 2 - World Energy Demand and Supply Use By Fuel Type 1990-2030 (Source US EIA)

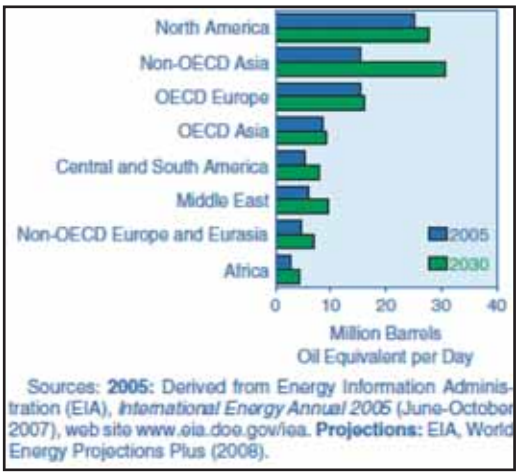

Figure 3 - World Liquids Consumption by Region 2005-2030 (Source US EIA)

per capita energy consumption in western countries and growth in consumption in certain non-OECD countries such as Asia, China and India. This reflects the trend that western populations continue to grow and consume a disproportionate amount of energy as compared with the rest of the world[6,7].

Values for the principal sources of energy demand and supply have been plotted for convenience (see Figure 2 World Energy Demand). In the case of oil demand growth, this is predicted to increase from 83.6 million barrels per day (MMbbl/d) in 2005 to 95.7 MMbbl/d in 2015 and 112.5 MMbbl/d in 2030. At first sight, when one looks at these figures, it is hard to imagine 16 MMbbl/d coming onto the market. When one considers the new frontiers of extreme E & P and mature fields, however, the figure seems plausible[8].

To meet world liquids demand in the IEO2008 reference case, total liquids supply in 2030 is projected to be 28.2 MMbbl/d higher than the 2005 level of 83.6 MMbbl/d. The reference case assumes that the Organisation of the Petroleum Exporting Countries (OPEC) maintain its market share of world liquids supply, and that OPEC member countries invest in additional production capacity for conventional oil leading to approximately 40% of total global liquids production throughout the projection. Increasing volumes of conventional liquids (crude oil and lease condensate, natural gas plant liquids and refinery gain) from OPEC contribute 12.4 MMbbl/d to the total increase in world liquids production, and conventional liquids supplies from non-OPEC countries add another 8.6 MMbbl/d (see Figure 4 World Liquids Production) . Unconventional resources (including oil sands, extra heavy oil, biofuels, coal-to-liquids and GTLs [see Figure 5 World Production of Unconventional Liquids]) from both OPEC and non-OPEC sources are expected to become increasingly competitive as indicated in the reference case.

The following serves as a breakdown of the categories of demand and supply.

Transportation

To the year 2030, transportation emerges as the strongest component of future oil and gas demand contributing 74% of all increased future oil demand (see Figure 6 Consumption by Sector). To 2015, demand is concentrated most heavily in Western countries such as the US and UK which have high numbers of vehicles per capita and respectively the largest worldwide fleets and numbers of private, commercial and industrial vehicles. After 2015, transport demand in the BRICs and eastern countries is of a magnitude higher with the Indian and Chinese numbers of vehicles per capita showing only strong growth in demand for transportation fuel (see Figures 7, 8 and 9)[9]. Energy consumption in transportation increases from 93.2 quadrillion Btu in the present period to 135.4 quadrillion btu in 2030. In barrel terms, the increase results in the following consumptions: North America (28 MMbbl/d); China and India combined (31 MMbbl/d); and, Europe (15 MMbl/d). In this model, oil is one of the most important fuels for transportation because there are few alternatives that can compete widely with liquid fuels. With world oil prices remaining relatively high through 2030, the increasing cost-competitiveness of non-liquid fuels reduces many stationary uses of liquids (that is, for electric power generation and for end uses in the industrial and building sectors). These replacements based on alternative energy sources, increase the transportation share of liquids con-

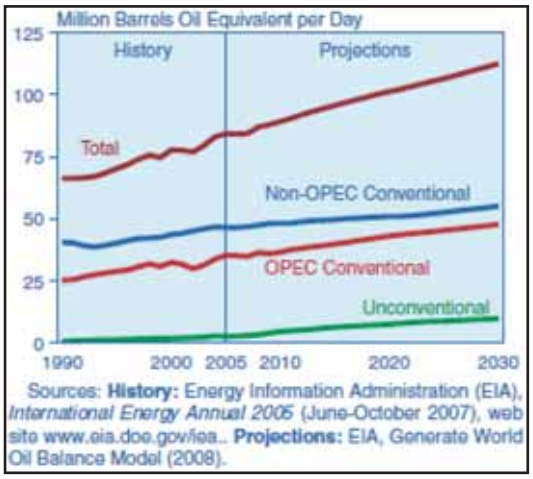

Figure 4 - World Liquids Production 1990-2030 (Source US EIA)

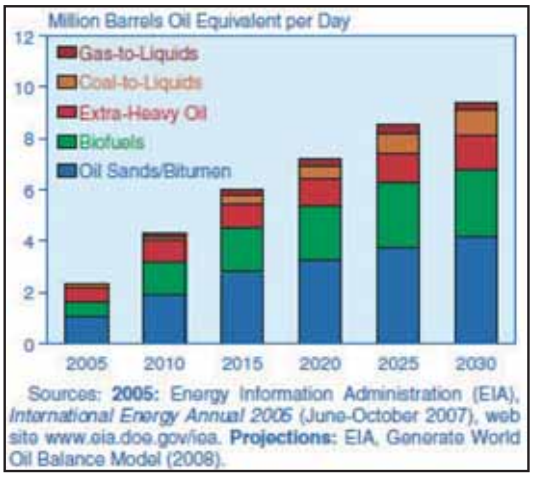

Figure 5 - World Production of Unconventional Liquids 2005-2030 (Source US EIA)

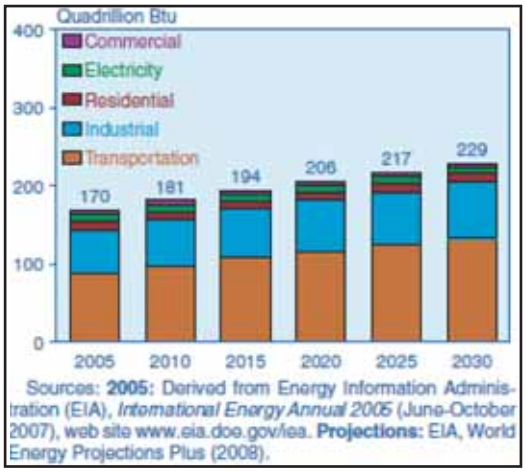

Figure 6 - World Liquids Consumption by Sector 2005-2030 (Source US EIA)

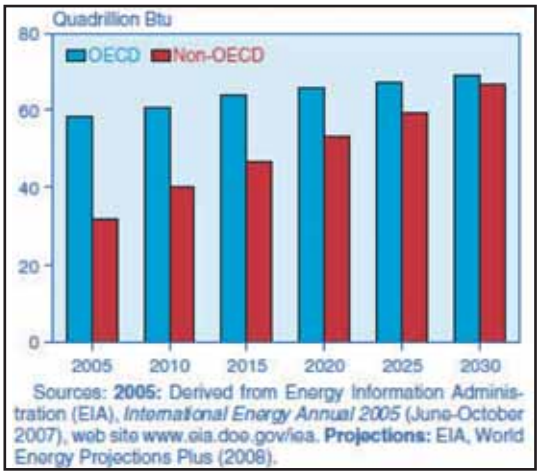

Figure 7 - Transportation Liquids Consumption 2005-2030 (Source US EIA)

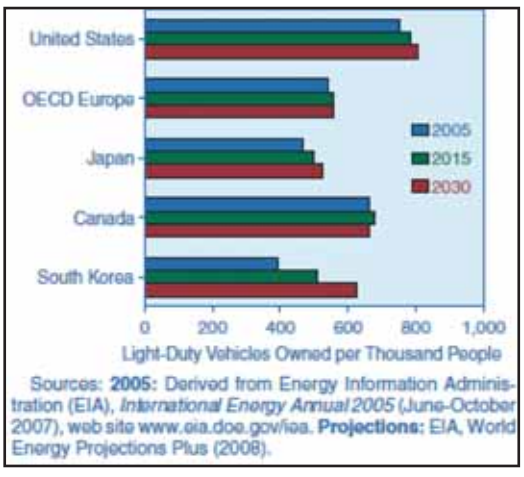

Figure 8 - Motor Vehicle Ownership in OECD Countries 2005, 2015 and 2030 (Source US EIA)

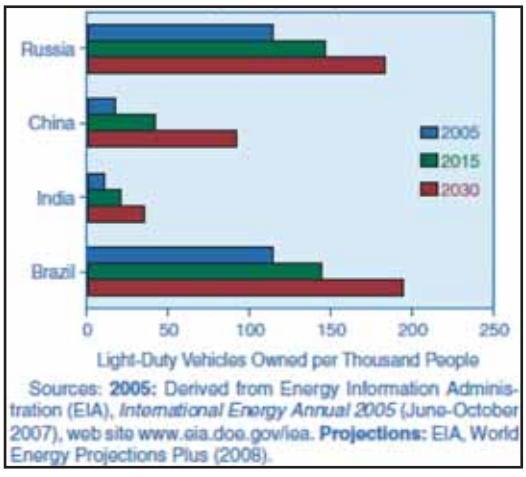

Figure 9 - Motor Vehicle Ownership in Non-OECD Countries 2005, 2015 and 2030 (Source US EIA)

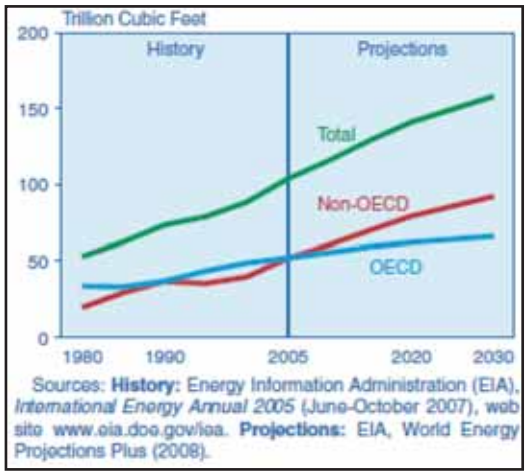

Figure 10 - World Natural Gas Consumption 1980-2030 (Source US EIA)

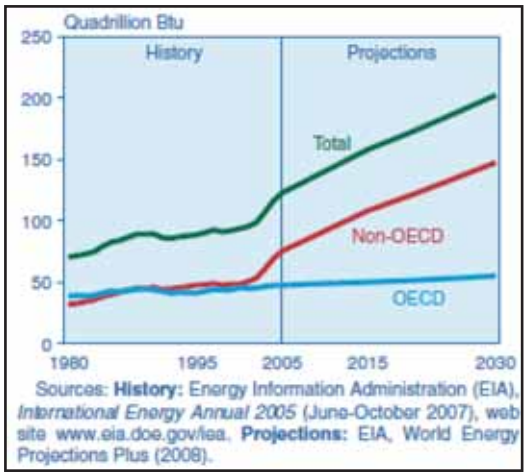

Figure 11 - World Coal Consumption (Source US EIA)

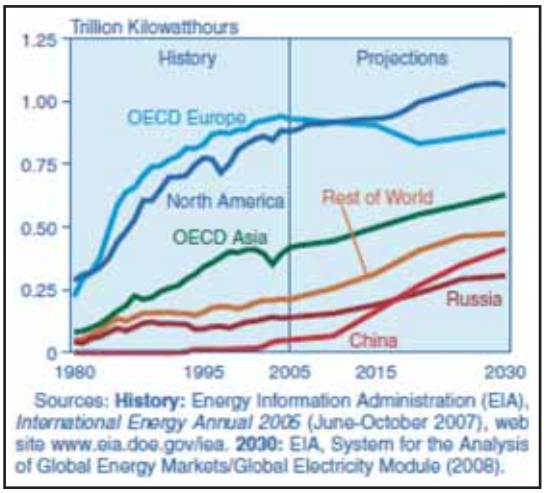

Figure 12 - Nuclear Power Generation 1980-2030 (Source US EIA)

sumption. Gas consumption for transportation purposes increases from 1 quadrillion Btu from 2005 to 1.6 quadrillion Btu in 2030.

Industrial

The second largest demand component is created by industry which increases from 57 quadrillion Btu in 2007 to 72% quadrillion Btu in 2030 (see Figure 6 World Liquids Consumption by Sector). Industrial demand is concentrated in the eastern hemisphere in countries such as China and India. This reflects the cost-driven migration of industrial and manufacturing processes to China and India from western hemisphere countries. The industrial sector including manufacturing, agriculture, mining, and construction accounts for a 39% share of hydrocarbon demand comprising mainly petrochemical feedstock[10]. Industrial consumption of gas increases from 45.2 quadrillion Btu in 2005 to 70.2 quadrillion Btu in 2030.

Commercial

The commercial sector – often referred to as the services sector or the institutional sector – consists of businesses, institutions, and organisations that provide intan-gible services, as opposed to those in manufacturing or agriculture. Demand for commercial energy increases from the present 5.1 quadrillion Btu to 5.3 quadrillion Btu in 2030. Demand for commercial energy grows more acutely in OECD countries rather than India and China. This is interesting as it appears that the latent demand in India and China do not materialise as strongly as widely reported by other energy models with growth only averaging 2.2% per annum[10]. Commercial consumption of gas increases from 7.3 quadrillion Btu to 9.6 quadrillion Btu.

Residential

Residential demand for energy increases from the current 10.4 quadrillion Btu to 11.1 quadrillion Btu in

Energy Source	MMBtu/bbl	Energy Source	MMBtu/bbl
Crude Oil	5.800	Natural Gasoline	4.620
Natural Gas Plant Liquids	3.735	Pentanes Plus	4.620
Asphalt	6.636	Petrochemical Feedstocks:	
Aviation Gasoline	5.048	Naphtha < 401° F	5.248
Butane	4.326	Other oils >= 401° F	5.825
Butane-Propane (60/40) Mixture	4.130	Still Gas	6.000
Distillate Fuel Oil	5.825	Petroleum Coke	6.024
Ethane	3.082	Plant Condensate	5.418
Ethane-Propane (70/30) Mixture	3.308	Propane	3.836
Isobutane	3.974	Residual Fuel Oil	6.287
Jet Fuel, Kerosene-type	5.670	Road Oil	6.636
Jet Fuel, Naphtha-type	5.355	Special Naphthas	5.248
Kerosene	5.670	Still Gas	6.000
Lubricants	6.065	Unfinished Oils	5.825
Motor Gasoline - Conventional	5.253	Unfractionated Stream	5.418
Motor Gasoline - Oxygenated or Reformulated	5.150	Waxes	5.537
Motor Gasoline - Fuel Ethanol	3.539	Miscellaneous	5.796
Source: U.S. Department of Energy, Energy Information Administration (2001)			

Table 1 - Approximate Heat Content of Petroleum Products Million Btu (MMBtu) per Barrel

2030. Demand for energy consumption grows most in non-OECD countries in the residential sector at an average of 2.7%. Residential gas consumption increases from 19.1 quadrillion Btu to 25.2 quadrillion Btu[11].

Gas

Consumption of natural gas worldwide almost doubles from 104 trillion cubic feet (tcf) in 2005 to 158 tcf in 2030 as per the IEO2008 reference case (see Figure 10). Although natural gas is expected to be an important fuel source in the electric power and industrial sectors, the annual growth rate for natural gas consumption is slightly lower than the projected growth rate for coal consumption. Higher world oil prices in the IEO2008 increase the demand for and price of natural gas, making coal a more economical fuel source in the projections. Industry accounts for the largest component of natural gas demand worldwide, generating 52% of the total growth in natural gas use in IEO projections. Natural gas also provides the power generation sector with increasing supply and accounts for 39% of the increase in global natural gas demand to 2030[12].

Coal

In the IEO2008 reference case, world coal consumption increases by 65 percent over the projection period, from 122.5 quadrillion Btu in 2005 to 202.2 quadrillion Btu in 2030 (see Figure 11). The increase in coal consumption averages 2.6 percent per year from 2005 to 2015, then slows to an average of 1.7 percent per year from 2015 to 2030[13].

Nuclear Power

Electricity generation from nuclear power is projected to increase from about 2.6 trillion kilowatthours in 2005 to 3.8 trillion kilowatthours in 2030, (see Figure 12). This is based on rising fossil fuel prices, concerns regarding energy security and greenhouse gas emissions which tend to support new and existing nuclear power generation[14].

Renewables

Renewables including hydroelectric power (and other generating capacities fueled by renewable energy resources) are projected to increase by 352 billion kilowatt hours from 2007 to 728 billion kilowatt hours in 2030, at an average annual rate of 3.2%[15].

Hydrocarbon Demand Supply Equation

The IEO reference case is a very useful map to under-

stand the direction of future energy. It still requires systematic treatment and evaluation of specific renewable energy sources as well as oil-price dynamics which are non-linear. Its approach, however, is a very good basis from which to consider global energy markets, oil and gas segments and how mass transactions fit in the overall picture. The oil and gas demand supply equation serves this purpose by outlining the six major oil and gas applications and the twenty-one uses (mass products/mass processes) that result in mass transactions. This serves to pinpoint exit scenarios where oil and gas demand can be phased using an energy resource that is renewable. The value of the exercise lies in qualifying what is technically replaceable given an economic framework, i.e. high oil prices or government subsidies rather than calculating the economic or market value of each replacement.

What emerges from the analysis is an extremely broad and complex set of oil and gas applications and ultimate uses or transactions. These range from transportation, to power generation, heating, petrochemicals, lubricants and surfacing. It was necessary to detail each specific end usage in order to determine whether oil and gas were replaceable commodities.

This is a key step in achieving higher elasticity of demand by satisfying end usage with replacement options. We assume that the production of petroleum will peak and then plateau, but that the broad range of petroleum applications that we see today will narrow down to a few that cannot be substituted by gas or other renewables.

Today, the only oil application that cannot be substituted given the necessary economic framework, i.e. high oil prices or government subsidies, is aviation fuel which generates 5.7 million Btu per barrel compared to ethanol which generates 3.5 million Btu. Aviation fuel then takes up approximately 0.61 times the volume of jet kero or it has 0.61 of the Btu[17].

Firstly, there are six major categories of petroleum applications which are split into a further 21 sub-categories all of which have been kept as broad as possible, i.e. derivatives are split into Alkanes, Alkenes and Arenes which cover demand for derivatives such as plastics and pharmaceuticals.

Secondly, successfully substituting oil and gas depends on several unpredictable factors. These include global economic stability in order to maintain oil prices above certain levels. Each alternative energy source has a corresponding oil price threshold at which it becomes profitable – or not – to pursue R & D. That threshold is not simple to calculate; for example, in the case of bioethanol, it may be considered that an oil price of US $40 to US $60 per barrel makes ethanol production viable, but this does not take into consideration government intervention in the form of subsidies or incentives that are hidden away from ethanol or biofuel production. It is worth remembering that all biofuels are subject to seasonal conditions required for harvest. Unpredictable events such as inclement weather, hurricanes or market speculation can distort the acceptance curve of renewables, accelerating or delaying the overall uptake[18].

Thirdly, on a macro level there are no consensual figures on global consumption versus production data from major authorities. Much credit should go to BP for putting the statistical review together. Regarding country and global data, the issue is that ultimately all collating organisations must rely on country export data as they have no way of verifying that data. The statistics therefore incorporate OPEC/OGJ (Oil and Gas Journal)/ non-OPEC data and so on. The approach has been to use regional or local data sources wherever possible.

Further discrepancies between consumption and production data exist from the same source; for example, the BP statistical review 2008 places global oil production at 81.53 MMbbl/d and consumption at 85.22 MMbbl/d. According to the BP statistical review, there is a deficit of oil and a surplus of gas. The standard and fundamentally sound explanation for this discrepancy is explained by fuel additives, refinery gains, measurement and rounding up differences, inventories, etc. The discrepancy may also be partially explained due to illicit production not reported at the well-head, GTL production of liquids, gasification and liquids from coal[19]. Another challenge with the data is conversion between physical volumes and oil equivalent volumes. The US EIA includes volume adjustments to the production side so that production and consumption balance. The implicit assumption is that stocks don't change.

Beyond Petroleum

As we look through the demand/supply equation it is apparent that it will take many years to provide other choices beyond petroleum. Indeed, oil may not be completely replaced; rather, other choices will be offered that have their own set of costs, trade-offs and limitations. Natural gas has emerged as an energy bridge to nascent renewables. Liquefaction commercialises stranded reserves, while biologically produced methane offers renewability. Capping it all, GTL offers high quality gasoline. Others such as oil-fired power generation can be replaced by gas, nuclear, hydroelectric, or other re-

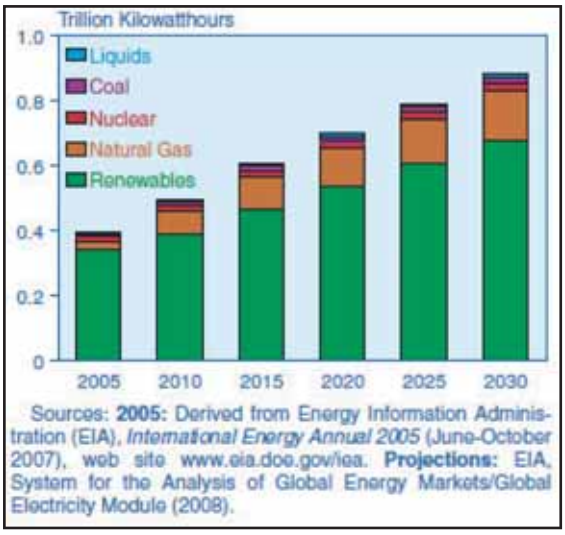

Figure 13 - Electricity Generation in Brazil by Fuel (Source US EIA)

newables. Co-generation and biomass production processes that create methane or ethanol also offer effective renewable solutions. Last but not least, bio-diesels can be created from vegetable seed oil via trans-esterification to provide replacements for diesel usage[20].

The US EIA sees real resource limits to vegetable seed oil conversion to diesel, however, gasification of biomass and then conversion to diesel should have much more promise in terms of available volumes.

The early trend here, and that which accompanies other oil and gas applications, is that until a new broadly applicable fuel is found, oil and gas will remain the preferred source for global energy, against a backdrop of a myriad of developing energy sources. This diverse scenario – the energy inclusive model – exists in Brazil, India and Pakistan, albeit in a nascent form (see Figure 13 Electricity Generation in Brazil by Fuel and 14 overleaf Brazilian Fuel Options at the Pump). These countries are already using advanced gas technologies and ethanol. Most countries worldwide are at different points of energy development, with emphasis on hydro-electric, nuclear or other renewables varying from country to country[21].

2008 World Demand (Consumption)

1. Gas 2921.9 Bm^3. This figure is based on storage facilities, liquefaction, the disparities with production are due to definition, measurement or conversion, proposed additional sources, flaring and GTL[22].

2. Oil 85.22 MMbbl/d. The difference in consumption and production is due to inventories, additives such as ethanol, stock changes, substitutes, measurement/conversion, proposed additional sources, illicit production and GTL[23].

2007 World Supply (Production)

1. Gas: 2940 Bm^3 which excludes GTL, Coal to Gas)[24].

2. Oil 81.53 MMbbl/d which includes NGL and GTL production[25].

For detail on the individual demand or supply components, refer to the Notes at the end of the book. The major categories are: transportation, heating, petrochemicals, lubricants, surfacing and power generation. Now let us look at the demand components and what choices we have for oil replacement.

Transportation (Aviation, Automotive, Marine and Rail)

Replacements in high-demand areas of aviation, automotive and marine usage are limited. Choices exist, but they are tempered by engine type, fuel tank size*, upgrading retail outlets and upgrading existing automotive and marine fleets. From the outset, the thermodynamic cycle and engine type – Otto or Diesel – dictates application suitability. Otto cycle engines use gasoline which can be replaced by ethanol. Diesel cycle engines use diesel which can be replaced by biodiesel. Both are ideal for spark-ignition and compression-ignition engines.

Ethanol, the much vaunted 'flex-fuel', offers only a partial exit scenario by substituting gasoline in the Otto cycle applications only. It is also fair to note that Brazil's adoption of ethanol (and LPG) technologies took at least 30 years to achieve, with car manufacturers and oil companies creating the required infrastructure. Government

Figure 14 - Brazilian Options at the Pump 2009 shows Ethanol, Gasoline, Diesel and Natural Gas (EPRasheed)

legislation required 25% of all gasoline to be mixed with ethanol. Today, that percentage has fallen to 20% as demand (and exports) of ethanol rises. Ethanol does have its own supply volatility and liquidity limitations[26].

Successful usage in one country, however, does not mean that global roll-out can occur. As Brazil is one of the most advanced in energy diversification, what lessons can be drawn from its experience? First, government support was not enough; intervention was required. It was Brazil's dictatorship in the 1970s that issued the directives that led to today's usage. More than 30 years of government intervention, manufacturing incentives, infrastructure and retail outlets were needed to reach the current 'flex-fuel' conditions of 5% of all fuel consumed and 100% of all nationally manufactured cars. The main obstacle to worldwide roll-out is that the existing fleet of cars, buses, and boats around the world are configured for petroleum and diesel. This requires a phasing out or phasing in approach. Meanwhile, incentives or directives for new build vehicles should ensure that they are configured for flex-fuel renewables[27].

The Brazilian government has now applied the 5% minimum usage target to bio-diesel. This requirement has a number of transport fuel implications. First, it is likely to create more demand for petroleum replacements or 'unconventional fuels' as long as prices stay high. Second, more unconventional liquid fuels (GTLs, ethanol and biodiesel produced from alcohol or seeds) and natural gas (compressed or liquid) are likely to come onto the market and take up a larger share of overall demand for transportation petroleum liquids to 2030. Over the short run, this can be considered as a safety valve that eases off demand for traditional oil fuels (gasoline and diesel) in the transport demand component. In the long run, it can be considered as a partial exit scenario[28]. The major part of demand, however, resides within transportation and is highest in OECD countries such as the US, Canada and Western Europe. It is these countries that can help reduce demand by using more efficient vehicles as well as sharing transportation. A good idea would be to provide tax incentives for fuel efficient vehicles as well as car pooling.

Heating

Similar obstacles face the stock of domestic dwellings in that they cannot easily be configured to use oil or replacement gas. Greater acceptance of renewable energy sources (nuclear, solar, wind) can be expected in new-build residential usage. Natural gas (compressed or liquid) is also likely to take up a greater portion of total residential demand for petroleum. Over time, this can be considered another safety valve that eases off demand for traditional residential oil fuels (gas and diesel) in residential demand. Localised burning of any carbon-based fuel for residential heating creates considerable difficulties. Firstly, establishing an efficient distribution infrastructure to transport the fuel to the homes can be expensive, time-consuming and problematic. Secondly, the control and capture of CO_2 (or other GHGs) is virtually impossible at the house-to-house level. Better to

provide 100% electrification of communities, whereby carbon-based fuels are converted to electric energy at a few, centrally-located and controlled power stations where emissions can be controlled and GHGs sequestered. Electric power grids are relatively easy to establish, expand and maintain. Electric energy is a much more versatile form of energy, capable of providing many more services from heating to cooling, to illumination, to cooking and to powering appliances of all sizes. It is truly the world's cleanest and most easily-assimilated energy resource. Localised or dispersed burning sites would therefore be dramatically reduced, thus reducing the carbon footprint. More unconventional liquid fuels (GTLs, ethanol and biodiesel produced from alcohol or seeds respectively) and natural gas (compressed or liquid) are likely to come onto the market and take up a larger share of overall demand for commercial heating petroleum liquids to 2030. Over time, this can be considered a partial exit for traditional heating oil fuels (kerosene, diesel, heavy oil) in the commercial demand component[29].

Power Generation

What is important here is that each country's energy needs and resource profiles differ, and this affects how advanced (or not) their renewables uptake is and what size contribution it makes. It is clear to see that renewables offer a broad band of applications, concentrated in low-scale power generation, large scale gas turbine power generation or biomass co-generation applications. Choices exist, but they are tempered by the power generation facility type. Gas turbine or combustion turbines use natural gas, light fuel oil, diesel or biologically produced gas.

Still, many limitations exist; for example, power generating conditions for renewables do not always coincide with peak demands. Specific levels of sunshine or wind speed must exist at a given time to generate energy which must then be stored, creating a further challenge that must be resolved.

In the reference case, however, natural gas and renewable energy sources are predicted to increase in power generation markets. The natural gas share of world electricity markets increases from 19% in 2003 to 22% in 2030, and the renewable share rises from 18% in 2003 to 20% in 2010 before declining slightly to 19% in 2030. The relative environmental benefits and efficiency of natural gas make the fuel an attractive alternative to oil and coal-fired generation. Higher oil and gas prices enable renewable energy sources to compete more effectively in the electric power sector[30].

Petrochemical

High petrochemical feedstock demand is likely to create more demand for reformulated or 'synthetically' produced feedstocks. More synthetically produced alkenes and arenes will be created from gas, GTL and ethanol. As these products come onto the market, they will contribute to meeting higher levels of demand from the petrochemical sector. Over time, this will tend to a partial exit scenario with petrochemical-based hydrocarbon demand taking up to a 60% share of industrial demand up to 2030.

Lubricants and Surfacing

More synthetic lubricants (reformulated or vegetable seed based) and surfacing products (cement type) are likely to come onto the market and take up a larger share of overall demand for lubricants and surfacing. Over time, this can be considered an exit for traditional lubricants and surfacing (heavy oils, asphaltene) in the commercial demand component.

Price and Alternate Scenario

At any given point, the oil price is the closest, albeit imperfect indicator, due to delay of how the demand/supply equation is balanced. High oil and gas prices tend to indicate high demand and tight supply and vice versa. There is a complex inter-play, but clearly high oil and gas prices have three major implications. First, energy attracts investment. This is because high oil prices awaken demand for all types of energy sources, not just oil. This is double edged as not only does oil attract investment so do renewables. Exemplifying this is coal and ethanol which reached record prices during 2008. In the case of agriculturally produced ethanol, the price of other agricultural crops can also increase as arable land is used for ethanol production. Given that the uptake of renewables is very sensitive to oil and gas prices, a 1.5% increase per annum in renewables uptake can help stabilise energy demand with oil production staying constant. Second, large reserve holders do increase E & P but not relative to the oil price. As the absolute value of oil increases, these countries reduce domestic consumption, encourage substitutes and focus on maximising recovery from existing assets rather than producing from new finds. Third, high oil prices depress demand. Over time, all of this happens almost imperceptibly; pent up consumption for oil dissipates and demand for goods and services falls due to higher costs. It was incorrect thinking that suggested that high oil prices could be borne by economies without greatly affecting growth. This has been proven time and again to be the downfall of high oil prices and the precursor to a bust cycle[31].

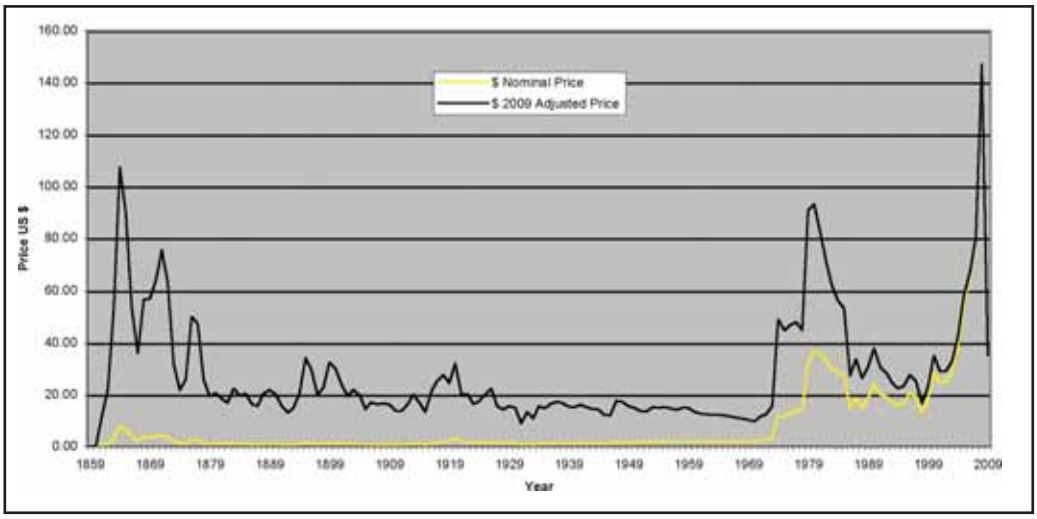

Figure 15 - Oil price 1861-2009. Source BP and EPRasheed (US, Arab Light and Brent Prices)

It is difficult to predict oil prices because oil price cycles tend to perform in a complex almost chaotic manner. Oil, however, is a commodity and obeys market rules or fundamentals despite the distortions. Research focused on commodities and, although not specifically designed for oil, shows how commodity cycles are affected by inventory, immediate production capacity and long-term production capacity. The combination of different timescales, time delays, different operators and human fallibility only adds to the complexity of the system. Although cycles (peaks and troughs) are not entirely random, we know that they will occur. The length of each cycle (say from peak to peak) is not entirely predictable as some last three years while others can last as long as ten years. There are, however, some telltale signs: economic conditions worldwide; extreme swings from a low to a high price or vice versa within a six month period; and, major geo-political tension. Prolonged periods of tightness in acquiring supply or services (or vice versa) also provide a good indication of where we are in the cycle.

The much touted increase in demand from China and India occurred in 2008 and is now slowing down. The growth in demand for energy is a much more gradual and long-term event linked to positive economic growth and consumption in developed countries. Combined demand from China and India exceeds North America by 2030, but not on a per capita energy usage basis. The bulk of Chinese and Indian industry and services are produced for end consumption by foreign customers mostly in Western countries and North America. Consumption has been transferred to China and India to reflect the industrial activity and production there. Endogenous demand for petroleum would be much lower without the energy consumption from traditionally high energy per capita users. The bulk of energy consumption, therefore, arises from the traditional users, i.e. in the US and Western Europe.

How long will the present recession last? Not even the world's best economists can say. Without getting too much into economic theory, we can say that there will be a market correction: a collapse or a period of depressed demand and lower oil and gas prices. We know that is certain because oil and gas are cyclical commodities that periodically experience peaks and troughs[32]. The problem is nobody knows when these will occur because the cycles are not entirely predictable; however, current market situations clearly seem to herald a low price cycle.

From a market perspective (putting government intervention aside), the troughs mean diminished demand for oil and gas and its applications, less cash for exploration and even less cash for renewable resources. Put simply, the return forecasts are lowered and the principal flow of capital from investors and speculators is diverted into markets other than energy and oil.

Nobody wants to talk about a collapse in prices. It frightens investors. Nobody wants to talk about a collapse when growth is strong, but ignoring a low price scenario is asking for trouble. This perhaps explains why oil companies want to stay cash rich. They have lived through the low price scenario—low revenues, poor utilisation and even lower returns. This is what some say keeps the cycle of under investment alive—fear of price collapse[33] (see Figure 15).

Our Legacy?

Our task is to lobby for investment, both in oil and gas and R & D in renewables and to understand there is no easy way out. We will all have to work to find an

Figure 16 - Future Options at the Pump; The Energy Express (EPRasheed)

exit. What about an energy revolution? It may happen, but my money is on the evolution: experimenting and tinkering with all energy sources. And what of global warming and energy? Simply put, we must reduce carbon emissions. There are new kids on the block (e.g. ethanol and wind farms) and there are some old-timers back as well (e.g. nuclear and coal). I believe that in the future, energy will become a new engineering discipline, along with mining, civil, mechanical, petroleum and nuclear and one that encompasses wind, solar and all other forms of energy.

Think legacy. Think future generations. Do we want to leave a mess of energy waste and environmental damage as a legacy for future generations? What does that say about us? Together, we need to apply our minds to exit the Hydrocarbon Highway without leaving a mess behind us. So how will things look in the future?

The narrowing base of opportunities for IOCs due to a changing E & P landscape means their activities will tend toward gas (GTL, LNG) and renewables. Here IOCs take a leadership position by differentiating themselves and adopting the 'Inclusive Energy Model' with project management, the know-how and capital. Gas becomes the fuel of choice from renewable streams, i.e. biomass as well as fossil fuel streams. Other applications are replaced, effectively relieving the major part of demand pressure on petroleum. Due to unreplaced applications, seasonal events and die-hards, the Hydrocarbon Highway runs on. Renewables increase over time but do not displace petroleum entirely creating an inclusive energy model. Petroleum remains a permanent feature, its demand increasing from time to time as ethanol crops fall short or rainfalls fall below hydro-electric dam requirements (and just as people still warm to a log-fire, people will always enjoy the thrill of gasoline powered revs).

Nuclear energy becomes a leading renewable energy source. Electricity prices rise, noticeably driven by the global rise in gas prices. As more nuclear energy plants come onstream, nuclear energy becomes more competitive and gas prices fall. Hydrocarbon demand is reduced by other factors too. Increasing GHGs and global warming becomes a reality. Companies are sued for producing emissions. The cases are defended, but companies become the champions of levying carbon taxes on the generation of GHGs. This is similar to the relationship between obesity and fast food chains. The fast food chains avoided direct responsibility in lawsuits and learned the lesson to offer 'healthy' alternatives. Aviation prices rise; the industry is thrown into disarray. Cheap airlines are forced to consolidate and stress on petroleum aviation demand is lowered further. Oil prices continue to fluctuate, yet a balance of residual demand keeps oil companies in business. A flourishing trade in carbon miles exist at the state, corporate and individual level. Worldwide, those who do not use their allowances sell the difference to high users. Electrically charged cars run globally.

Gasoline stations are still affectionately known as

petrol or gas stations as a throwback to when petroleum spirit was the dominant fuel, but they now offer biofuels, electricity, hydrogen and gasoline. The Hydrocarbon Highway has become the Energy Express. We have more choices than ever – the highway is still endless, but now there are many branching intersections one can take.

References

1. These are:
a) Power Generation [PGOil +PGGasTurbine (Non Ethanol/Brighton cycle) +PGGasSteam (Combustion)] (Gasoil/Fueloil) Gas & Oil (Methane, Heavy Oil)

b) Heating [H Industrial Process + H Construction +H Domestic Premises +H Commercial Premises] (Gas, Kerosene, Gasoil)

c) Transport [T Light Automotive Cars + T Aviation + T Marine Light T Marine T Military T Industrial + T Heavy Automotive Truck/Construction/Mining T Heavy Automotive Bus +T Train] (Gasoline, Diesel, Heavy Oil)

d) Petrochemicals [D Alkane Feedstocks (Naphthas) + D Arene Feedstocks (Pharmaceuticals) + D Alkene Feedstocks Plastics + D Foods + Resins & Waxes]

e) Lubricants [L GearOil + L IndustrialGrease], and

f) Surfacing [S Road+S Roof] Roofs, Cement.

2. Especially considering man-made Gas.

3. That make up the Oil and Gas Demand Equation: [PGGT+PGGS+PGO]+[HIP++HCon+HDP+HCP] +[TLAC+ TA + T M+ THAT+THAB+TT]+ [PCArF (Pharmaceuticals) + PC AlF PC AlkeneF + PC RW] + [LGO + LIG] + [SRd+SRf] 2007 World Demand (Consumption) Gas 2921.9 BCM and Oil 85.22 million bopd 2007 World Supply (Production) Gas: 2940 BCM and Oil 81.53 million.

Supply = [PGMethaneGT +PG MethaneGS+LPG,LNGGS + PG Oil] + [HGasOilIP+HGasDP Diesel, CNG,LPG] +[TLAC Gasoline+ Diesel + TA Compressed Natural Gas, Liquid Petroleum Gas + TM Diesel+ THAT Diesel+THAB Diesel+TT Heavy Oil] + [PCArF Naphtha (Pharmaceuticals) + PC AlF Naphtha PC AlkeneFNaphtha + PC RW Heavy Oil] +[LGOHeavy Oil + LIGHeavy Oil] + [SRdAsphalt+SRfBitumen].

4. This is our goal.

5. See EIA IEO 2008 Outlook.

6. See EIA IEO 2008 Outlook.

7. Idem.

8. Idem.

9. Certainly the EIA IEO 2008 Outlook thinks so.

10. EIA.

11. EIA.

12. EIA.

13. Idem.

14. Idem.

15. EIA.

16. EIA Footnote.

17. Increasing Feedstock Production for Biofuels: Economic Drivers, Environmental Implications, and the Role of Research. See also Options for Alternative Fuels and Advanced Vehicles in Greensburg, Kansas Harrow, G.

18. Further is the intrinsic volatility of the oil markets which complicates investment in renewables.

19. Exchange with EIA.

20. Exchange with EIA.

21. Brazil is a case in point hence why it was chosen.

22. BP Statistical Review 2008.

23. Idem.

24. Idem.

25. Gasoline and Ethanol Prices Fall" (in Portuguese). Folha Online 18 09 2008.

26. US DOE Flexible Fuel Vehicles: Providing a Renewable Fuel Choice. Again no single source of energy is universally applicable.

27. See also The Methanol Story: A Sustainable Fuel for the Future Roberta J Nichols.

28. US DOE Flexible Fuel Vehicles: Providing a Renewable Fuel Choice.

29. In many ways this is more elastic than transportation demand.

30. It is the backdrop of high oil prices that makes renewables viable.

31. The trends for continued economic and population growth will create further demand on oil and gas in the medium and long term.

32. The problem is that not even the world's foremost thinkers can satisfactorily predict the cycles.

33. Due to the vicious cycle involved it is likely that change will be slow and steady.

Saudi Arabia oil & gas

www.saudiarabiaoilandgas.com

Contribute to Saudi Arabia Oil & Gas during 2011

EPRasheed is looking for editorial submissions on the topics outlined in the editorial calendar. This can provide your company with the opportunity to communicate EP technology to the wider oil and gas community.

Please send abstracts or ideas for editorial to **wajid.rasheed@eprasheed.com**

Preference is given to articles that are Oil Company co-authored, peer reviewed or those based on Academic research.

Editorial 2011 Calendar

Jan/Feb	Mar/Apr	May/Jun	Jul/Aug	Sep/Oct	Nov/Dec
Ad Closing: 4 Jan 2011 **Materials Closing:** 11 Jan 2011	**Ad Closing:** 1 March 2011 **Materials Closing:** 4 March 2011	**Ad Closing:** 22 April 2011 **Materials Closing:** 29 April 2011	**Ad Closing:** 5 July 2011 **Materials Closing:** 12 July 2011	**Ad Closing:** 29 August 2010 **Materials Closing:** 30 August 2011	**Ad Closing:** 8 October 2011 **Materials Closing:** 15 October 2011
• Saudi Aramco RTOC • Digitalization • While Drilling Technology • Telemetry • Production • OGEP II Review	• Khurais • Near Surface Modelling • Rotary Steerable & Motor Systems • Drill Bits and Under-reamers • Complex Wells • Geophysical • Drill Pipe Integrity	• Manifa • Remote Operation Centre • Drill-Bit Tech • Inflow Control Devices • Zonal Isolation (incl. Packers,Multi-Zone Completions) • Carbonate Reservoir Heterogenity • Exploration Rub Al Khali	• Formation Evaluation • Wellbore Intervention • Casing While Drilling • Multi-Laterals • Lowering Drilling Costs in Tight Gas • Evaluating Tight Gas Formations •Increasing Productivity of Tight and Shale Gas	• Khursaniyah • Expandable Completions • Tubulars • Logging and Measurement WD • Electrical Submersible Pumps • Progressive Cavity Pumps • Novel Tight Gas Technologies	• Hawiyah • Smart Completions • I field • Geosteering • GOSP • Extended Seismic Feature (4D, OBC, Wide Azimuth)
Issue 18 *'OGEP II Review'*	**Issue 19** *'Innovation, IOC, NOC and Service Company Alliances'*	**Issue 20** *'Upstream Challenges'*	**Issue 21** *'Tight Gas Lowering Costs and Increasing Productivity'*	**Issue 22** *'Cost Effective Drilling and Completions'*	**Issue 23** *'Cooperation, Innovation and Investment'*
BONUS CIRCULATION					
SPE/IADC Drilling Conference 1-3 March 2011 Amsterdam The Netherlands **Royal Commission for Yanbu and Jubail Saudi Downstream*** 8-9 March 2011 **YP Symposium**** 14-16 March 2011	**Middle East Oil and Gas Show and Conference*** 20-23 March 2011 Manama Bahrain **9th Meeting of the Saudi Society for Geosciences**** 26-28 April, 2011 King Saud University Campus, Riyadh	**Offshore Technology Conference** 2-5 May 2011 Houston,Texas, USA **SPE/DGS Annual Technical Symposium & Exhibition*** 15-18 May 2011 Khobar, Saudi Arabia **73rd EAGE Conference & Exhibition/SPE EUROPEC** 23-26 May 2011 Vienna,Austria **Brasil Offshore Exhibition Conference** 14-17 June 2011 Macae, Brazil		**Offshore Europe*** 6-8 Sept 2011 Aberdeen, UK **SPE/EAGE Reservoir Characterization and Simulation Conference** 26-28 Sept 2011 Abu Dhabi, UAE **OTC Brasil** 4-6 Oct 2011 Rio de Janeiro, Brazil **Middle East Drilling Technology Conference and Exhibition** 24-26 Oct 2011 Muscat, Oman	**SPE Annual Technical Conference and Exhibition** 30 Oct - 2 Nov 2011 Denver Colorado, USA **International Petroleum Technology Conference** 15-17 Nov 2011 Bangkok,Thailand **20th World Petroleum Congress*** 4-8 December 2011 Doha, Qatar
SPECIAL PUBLICATIONS					
* Official Saudi Magazine ** Official Magazine	* Media Partner ** Official Technical Magazine	* Official Technical Magazine		* Saudi Aramco Supplement	* Media Partner

Experience **infinite** fracture conductivity

HiWAY

FLOW-CHANNEL
HYDRAULIC FRACTURING
TECHNIQUE

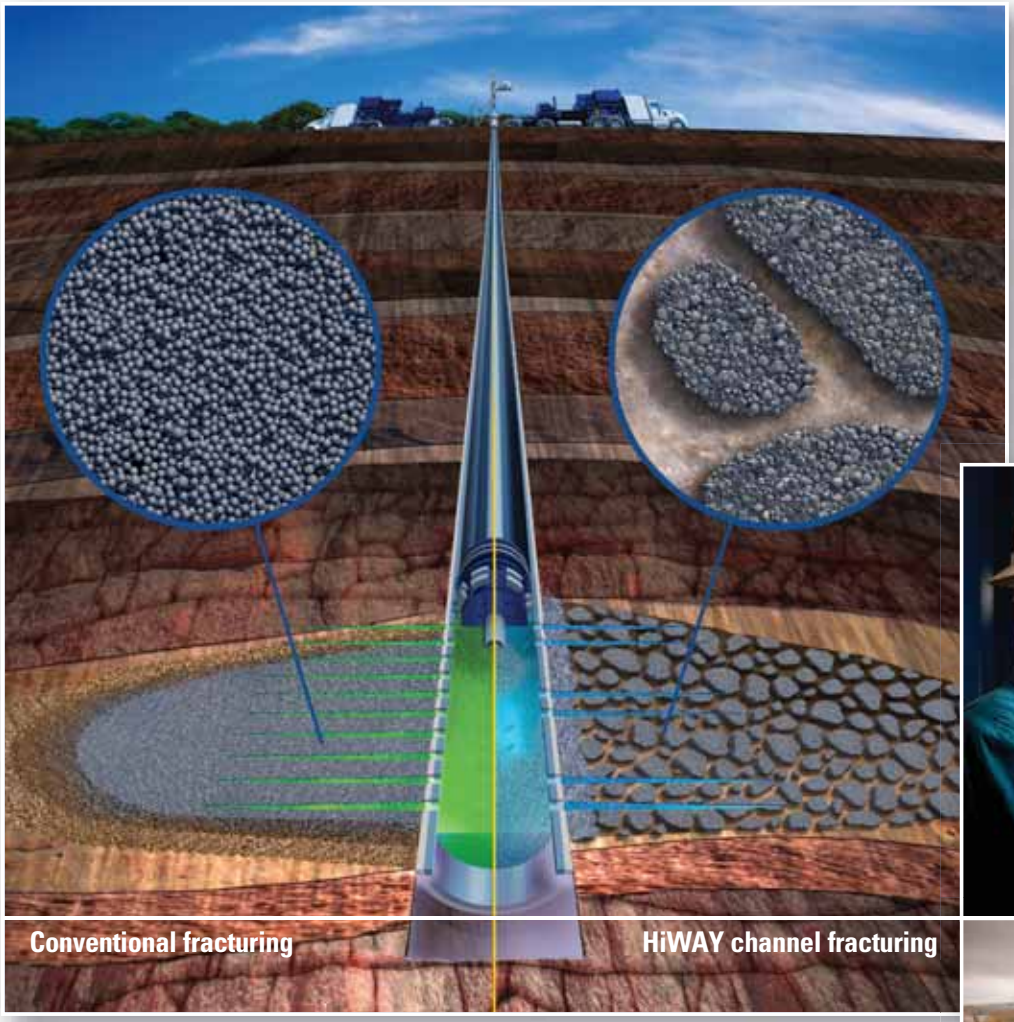

Introducing HiWAY* channel fracturing—

A new hydraulic fracturing technique that creates flow channels to maximize the deliverability of the reservoir.

With this technique, there's nothing between the reservoir and the well, so reservoir pressure alone determines flow.

Open up. No speed limits.

www.slb.com/HiWAY

Global Expertise | Innovative Technology | **Measurable Impact**

Schlumberger